KLOE NOTE n^{o}218
November 2007

Measurement of charged kaon lifetime

F. Ambrosino, P. Massarotti

Dipartimento di Scienze Fisiche dell'Università "Federico II" e sezione INFN Napoli

Abstract

We have measured the charged kaon lifetime using a sample of 15×10^{6} tagged $K^{\pm} \to \mu^{\pm} \overset{(-)}{\nu}_{\mu}$ from an integrated luminosity of $\sim$ 210 pb^{-1}. We have obtained for both charges the decay time distribution from measurements of both the decay length and the decay time. From fits to the four distributions we find
$\tau = (12.347\pm\ 0.030)$ ns.

Contents

1 Introduction

In the following we describe a new precise measurement of the charged kaon lifetime. This quantity is a fundamental parameter for the extraction of the V_{us} element of the CKM matrix, together with all the other inputs already measured at KLOE, namely the semileptonic branching ratios and the form factor slopes. Moreover a comparison of the lifetime for the two charges can provide a test of CPT invariance. The PDG [1] average reports an error of about 25 ps, corresponding to a precision of $\simeq 0.2\%$. However this average stems from five measurements which are not in agreement between each other, and whose errors must be multiplied by a factor 2.1 in order to give an acceptable chisquare. The discrepancies between the only "in-flight" [2] measurement and the "at-rest"[3],[4],[5] measurements calls for a new "in flight" determination of this quantity. This new measurement is thus necessary in order to clarify the present experimental scenario.
The statistical error on the lifetime measurements depends on the numbers of events collected and on the time interval covered in the measurement [6]:

$$\frac{\delta\tau}{\tau} = \frac{1}{\sqrt{N}} \times \left[\frac{e^{3T} - 1 + (e^{T} - e^{2T})(3 + T^2)}{(e^{T} - 1)^3}\right]^{-0.5} \tag{1}$$

where T = Δ/τ is the fitted time interval in K$^{\pm}$-lifetime units. With $T \approx 2$ and about $N \approx 4 \times 10^6$ the best statistical accuracy reachable in our case is 0.1%, if no other sources of statistical error were present. We note in passing that the most precise measurement used in PDG average (namely [4]) quotes a statistical error smaller than the best one obtainable with eq. 1.
In order to cross check systematic effects we developed two different analysis methods: the kaon decay length and the kaon decay time measurement.
The measurement of the charged kaon decay length requires the reconstruction of the kaon decay vertex using only Drift Chamber, DC [7], information while the efficiency of reconstruct the kaon decay vertex is evaluated using a control sample given by ElectroMagnetic Calorimeter, EMC [8], information only.
The second method relies on the measurement of the kaon decay time using EMC information only. We consider events with a π^0 in the final state only:

$$K^{\pm} \to X + \pi^0 \to X + \gamma\gamma \tag{2}$$

In this case the efficiency of reconstruct the kaon decay vertex is evaluated using a control sample given by DC information only.

2 Analysis scheme

The procedure of this analysis can be summarized as follows:

1. Selection of a pure "$K^{\pm}$ beam" using the tag algorithm (see section 4).

2. Definition of the two methods and for each method:

   (a) determination of the charged kaon proper time distribution (see sections 5.1.1 and 5.2.1), evaluation of the background events and background rejection, (see sections 5.1.2 and 5.2.2),

   (b) evaluation of the efficiency to reconstruct the charged kaon decay vertex on data. The efficiency is corrected to take in account a small discrepancy between the true and the reconstructed MC efficiencies (see sections 6.1 and 6.2),

   (c) measurement of the resolution curves as a function of the charged kaon proper time (see sections 7.1 and 7.2).

   (d) fit of the proper time distribution, taking into account the correction given by the kaon decay vertex reconstruction efficiency and the resolution effects (see sections 8.1 and 8.2),

   (e) evaluation of the systematics on the measurement. (see sections 9.1 and 9.3).

3. Evaluation of the correlation between the two different methods and of their weighted mean (see sections 10).

3 Data sample

The sample used for this analysis has been collected during 2002 data taking, processed and filtered with the KLOE standard reconstruction software and the event classification procedure [9]. We used about 210 pb^{-1} of data to evaluate the charged kaon decay vertex reconstruction efficiency as a function of the charged kaon proper time; we used 210 pb^{-1}of data to measure the charged kaon proper time distribution and the resolution curves.
We have produced about 175 pb^{-1} of MonteCarlo Which were used to evaluate the charged kaon decay vertex reconstruction efficiency as a function of the charged kaon proper time and to measure the charged kaon proper time distribution and the resolution curves.

4 Selection of the self-triggering tag events

The peculiarity of a ϕ-factory is that kaons are produced in pairs, namely K^+K^- and K_LK_S. Therefore the detection of a K guarantees the presence of a $\bar{K}$ on the other side with known momentum and direction. This feature allows the measurement of absolute branching ratios. The decay products of the $K^{\pm}$ pair define two ideally separated regions called hereafter the tag and the signal hemispheres.
To measure the charged kaon lifetime we consider the subsample of events selected

by the TAG algorithm (see section 4.1). Once the algorithm has found a $K^{\mp}$ tag decay, it can be used as reference normalization and the kaons in the other hemisphere can be considered as a pure $K^{\pm}$ beam. In the two-body decays the secondary tracks have a well defined momentum in the kaon rest frame and this allows a good particle identification. To minimize the impact of the trigger efficiency on the signal side, we look for a tag decay which also provided by itself the EMC trigger of the event.
Even if the analyzed events already belong to the charged kaons stream, it is necessary to reprocess them for the following reasons: to tighten the requirements on the tag decay, cleaning the data sample, and to select a specific charge for the self-triggering tags (see section 4.2).
Hereafter we use a coordinate system with the z-axis defined as the bisectrix of the beams, the y-axis vertical and the x-axis toward the center of the collider rings.

4.1 The TAG algorithm

The TAG algorithm identifies the two-body decays $K \to \mu\nu$ or $K \to \pi\pi^0$, which are about 85% of charged kaon decays. It is based on the presence of a two-tracks vertex in the DC which defines the $K^{\pm}$ decay.
The first requirement is the existence of a track (kaon candidate) with the point of closest approach to the IP smaller than $d_0 = 10$ cm ($z_0 = 20$ cm) along the radial (longitudinal) axis. Then the radial distance between the kaon candidate decay vertex and the beam axis, R_V, has to fulfill $40 < R_V < 150$ cm. The kaon candidate must also have $70 < |\overrightarrow{p}| < 130$ MeV/c.
Once the kaon candidate has been identified:

- the candidate track associated to the charged decay particle (secondary) must have the same charge of the kaon;
- the momentum difference between the kaon and the secondary must fulfill $-320 < \Delta p = |\overrightarrow{p}_K| - |\overrightarrow{p}_{sec}| < -120$ MeV/c;
- the secondary charged particle momentum in the kaon rest frame, p^*, using the $\pi^{\pm}$ mass hypothesis, must be in the range $180 < p^* < 270$ MeV/c.

The following cuts are applied to distinguish between K_{μ} and $K_{\pi\pi^0}$ decays:

$$225 < p^* < 245 \text{ MeV/c} \quad \Rightarrow \quad K_{\mu}\text{-tag} \tag{3}$$
$$195.5 < p^* < 213.5 \text{ MeV/c} \quad \Rightarrow \quad K_{\pi\pi^0}\text{-tag.} \tag{4}$$

4.2 Self-triggering conditions

The particles on the tagging side are required to deposit enough energy in the calorimeter to trigger the data acquisition (self-triggering tag). The EMC trigger

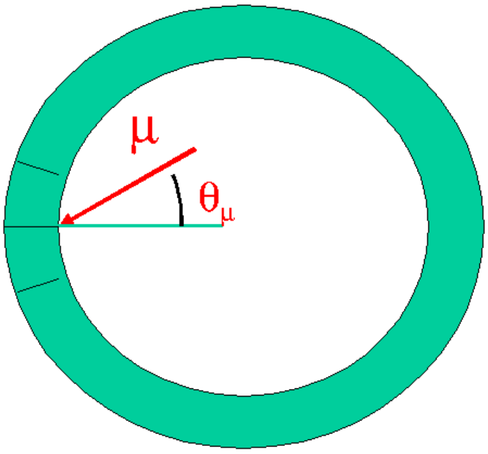

Figure 1: Schematic geometrical overview of a K_μ self-triggering event. Depending on the incidence angle θ_μ, the muon can cross two trigger sectors and then self-trigger the event.

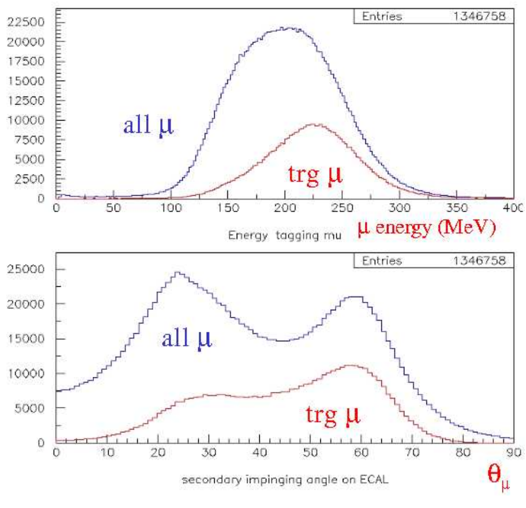

Figure 2: Above: distribution of self-triggering muon as function of the energy released by the muon in the calorimeter. Below: distribution of self-triggering muon as function of its impinging angle on the EMC.

is given by two energy deposits in two trigger sectors which overcome the LET threshold [10], whose average values corresponds to about 50 MeV in the barrel and about 150 MeV in the endcaps.
The possibility for a K_μ decay to self-trigger the event is due to the cluster associated to the secondary $\mu^\pm$ track. The trajectory of the $\mu^\pm$ in the EMC can cross two adjacent trigger sectors. If the two energy deposits are over threshold we have a self-triggering K_μ decay event. The self-triggering request reduces the analysis sample. The yield has been evaluated on a 4.85 pb^{-1} data sample. The results are reported in table 1. The amount of self-triggering K_μ tag decays is about 35%.
In the case of $K_{\pi\pi^0}$ tag decay the amount of self-triggering event is about 75%; this is due to the fact that either the charged pion or the photons from the π^0 decay can overcome the calorimeter energy threshold.

Kind of tag	Number of tags/pb^{-1}	Number of self-trigger/pb^{-1}
$K^- \rightarrow \mu^- \bar{\nu}$	279×10^3	95×10^3
$K^- \rightarrow \pi^- \pi^0$	95×10^3	73×10^3

Table 1: Number of self-triggering tag events per pb^{-1}, evaluated using a data sample of about 4.85 pb^{-1}

For the measurement we require self-triggering tags. It must be stressed that after the self-triggering tag request, we end up on the opposite hemisphere with a pure $K^\pm$ beam.

4.3 Why self-triggering request?

Before entering in the details of the analysis, we should comment on the self-triggering request. As shown in the previous section this request reduces the analysis sample, in fact the amount of self-triggering K_μ tag decays is about 35%. To understand the reason of this choice we have to study, on MonteCarlo simulation, the trigger efficiency, the tag efficiency given the trigger and the self-triggering tag efficiency as functions of the signal kaon *true* proper time which is the proper time given by the MonteCarlo simulation. It is defined as:

$$t^*_{true} = tof^K_{true} \cdot \sqrt{1-\beta^2_{true}} \qquad \text{where} \quad \beta_{true} = (\beta^{IP}_{true} + \beta^{VTX}_{true})/2, \tag{5}$$

tof^K_{true} is signal kaon time of flight, in the laboratory frame, given by the MonteCarlo simulation while $\beta^{\rm IP}_{\rm true}$ and $\beta^{\rm VTX}_{\rm true}$ are the β values of the signal kaon at the Interaction Point, IP, and at the decay vertex, respectively. The energy loss in the DC decreases the beta of the kaon. This effect leads to an underestimate of about 0.65% of the true proper time. A correction has been introduced to take into account this effect.
The trigger efficiency is defined as the ratio of the events K^+K^- with a trigger signal over threshold over the total number of K^+K^- events, as a function of the *true* proper time:

$$\varepsilon_{\text{Trig}} = \frac{\text{N}_{\text{Trig}_{\text{K+K-}}}}{\text{N}_{\text{K+K-}}}. \tag{6}$$

The tag efficiency is defined as the ratio of triggered events with a tagging kaon over all the triggered K^+K^- events, as a function of the *true* proper time:

$$\varepsilon_{\text{Tag}} = \frac{\text{N}_{\text{TrigTag}}}{\text{N}_{\text{Trig}_{\text{K+K-}}}}. \tag{7}$$

The self-triggering tag efficiency is defined as the ratio of the events K^+K^- in which we reconstruct a self-trigger tag over all the events K^+K^-, as a function of the true proper time

$$\varepsilon_{\text{StrTag}} = \frac{\text{N}_{\text{StrTag}}}{\text{N}_{\text{K+K-}}} \tag{8}$$

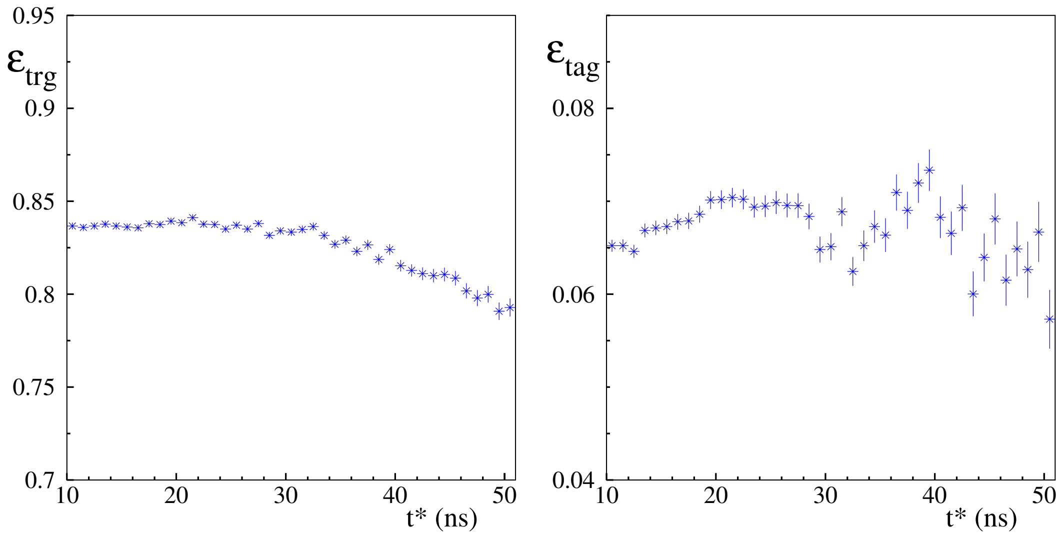

Figure 3: Left. Trigger efficiency as a function of the charged kaon proper time. Right. Tag efficiency, given the trigger, as a function of the signal kaon proper time.

As shown in figure 3, the trigger and moreover tag efficiencies behavior with respect to the kaon proper time are not flat. Therefore we should correct for these effects relying blindly in the MC. Instead, the self-triggering tag efficiency is constant for a wide range, between 12 and 35 ns and therefore we will use the self-triggering request, see figure 4.

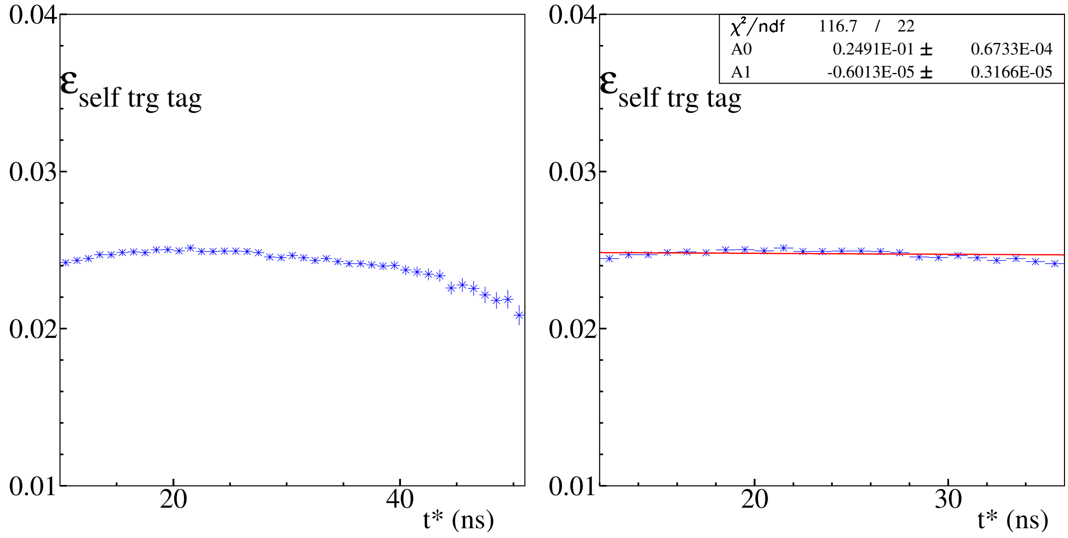

Figure 4: Left. Self-triggering tag efficiency as a function of the signal kaon proper time. Right. Zoom of the region between 12 and 35 ns.

In order to check the goodness of the MonteCarlo simulation we use the double tag events, events in which both the charged kaons are reconstructed and tagged, to compare on data and on MonteCarlo datalike the self trigger tag efficiency. This procedure has been used only to assess the systematic uncertainty on the MonteCarlo self-triggering tag efficiency used in our fit.
The self-triggering tag efficiency, evaluated with the double tag events, is defined, bin by bin, as:

$$\varepsilon_{\mathrm{StrTag(double\ \ tag)}} = \frac{\mathrm{N}_{\mathrm{StrTag2}(\mu_2)}}{\mathrm{N}_{\mathrm{StrTag1}}} \tag{9}$$

where $\mathrm{N}_{\mathrm{StrTag1}}$ is the number of events in which a $K^{\mp}$ tags the event as a K^+K^- event and fires the trigger, while $\mathrm{N}_{\mathrm{StrTag2}(\mu_2)}$ is the number of events in which a $K^{\pm} \to \mu^{\pm}\overset{(-)}{\nu}_{\mu}$ independentelly tags the event as a K^+K^- event and fires the trigger. This efficiency is function of the reconstructed proper time. As it can be seen in the fig. 5 the agreement between the self-triggering tag efficiency evaluated using the double tag events on data and on MC datalike is good.

5 The event selection

5.1 First method: charged kaon decay length

For the first method we measure the kaon decay length, from the IP to the kaon decay vertex, reconstructed in the DC. The reconstruction efficiency of the kaon

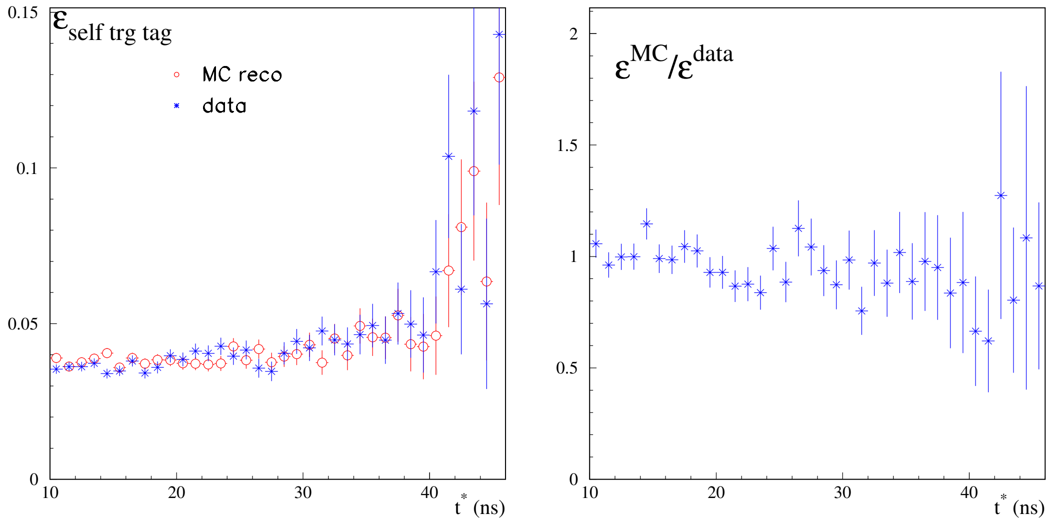

Figure 5: Left. Self-triggering tag efficiency evaluated using the double tag events on data (blue) and on MC datalike (red). Right. Ratio of the self-triggering tag efficiency evaluated and data over the one evaluated on MC datalike, using the double tag events.

decay path is evaluated using a control sample selected with EMC information only.

5.1.1 Charged kaon proper time distribution

Given a charged kaon fulfilling the self-triggering tag requirements, our signal is given by an opposite charged kaon which decayed in the DC. This signal is selected looking for a charged kaon track, the signal kaon track, defined by the following requests:

$$R_{PCA} < 10 \text{ cm} \qquad \text{where} \quad R_{PCA} = \sqrt{x_{PCA}^2 + y_{PCA}^2}, \tag{10}$$

$$|Z_{PCA}| < 20 \text{ cm}, \tag{11}$$

$$70 < P_K < 130 \text{ MeV/c}. \tag{12}$$

where $X_{PCA}, Y_{PCA}, Z_{PCA}$ are the coordinates of the Point of Closest Approach of the kaon track to the IP. Using the extrapolation of the tagging kaon track to the IP, the $\phi-$meson momentum measured from Bhabha scattering events and imposing momentum conservation, we can evaluate the momentum of the signal kaon at the IP and build the path of the signal kaon up to the DC (helix reconstruction). This allows us to apply further cuts on differences between the signal kaon track and the signal kaon helix, namely:

- the difference between the momenta evaluated at the first hit has to be less than 20 MeV/c;

- the distance between the signal kaon track and the signal kaon path, extrapolated until the first hit, has to be less than 20 cm, see figure 6.

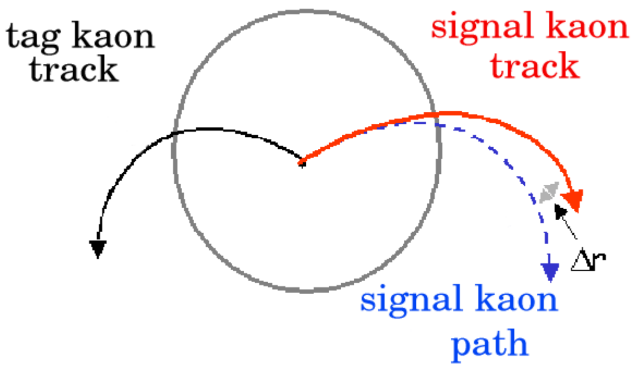

Figure 6: Exempli of the difference between signal kaon track and the reconstructed kaon path.

The next step is to look for the charged kaon decay vertex. We select the vertex which connects the signal kaon track with another track different from the tag kaon track. The vertex coordinates have to satisfy the following request:

$$40\ \text{cm} < R_{VTX} < 150\ \text{cm} \qquad \text{where} \quad R_{VTX} = \sqrt{x_{VTX}^2 + y_{VTX}^2}, \tag{13}$$

$$|Z_{VTX}| \leq 150\ \text{cm}, \tag{14}$$

The charged kaon proper time, t^*, for a kaon with path length l is defined as:

$$t^* = \frac{\sqrt{1-\beta^2}}{\beta} l. \tag{15}$$

Therefore we have to account for the changes of the β value of the kaon due to energy losses in the DC. For this reason we divide the signal kaon track in small steps of 5 mm, Δl_i, and we evaluate the energy loss and each step using the Bethe-Bloch formula. We calculate the charged kaon β and obtain the proper time of the kaon for every step:

$$\Delta t_i^* = \frac{\sqrt{1-\beta^2}}{\beta} \Delta l_i. \tag{16}$$

The sum of Δt_i^* gives the charged kaon proper time:

$$t^* = \sum_i \Delta t_i^*, \tag{17}$$

its distribution is shown in figure 7. This distribution has to be corrected, bin by bin,

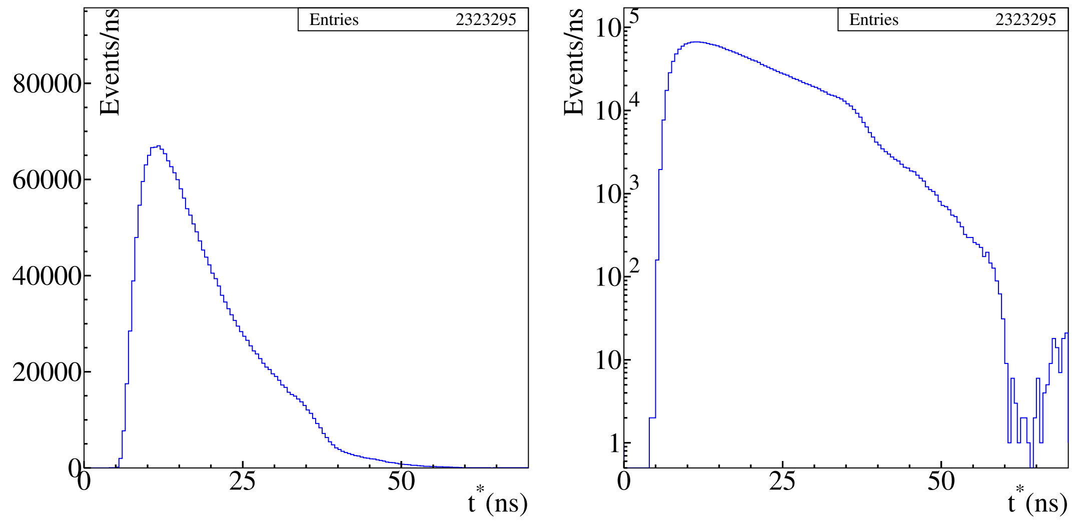

Figure 7: Charged kaon proper time distribution in linear and logarithmic scale evaluated on data, for the first method.

for its reconstruction efficiency and for its resolution effects. The shoulder visible in the region between 30 and 40 ns is due to events in which the kaon decay vertex has been wrongly reconstructed. This background has been evaluated and studied using the MonteCarlo simulation.

5.1.2 Background evaluation

The charged kaon proper time distribution shown in figure 7 is composed by four families:

1. correctly reconstructed vertices, about 69.1%,
2. kaon decays in pion which early decays in muons; the pions hits are associated to the muon track, about 1.4%,
3. wrongly reconstructed vertices, in which some hits of the kaon track are associated to the secondary track, about 20.6%,
4. wrongly reconstructed vertices, in which some hits of the secondary track are associated to the kaon track, about 5.2%,
5. vertices obtained from kaon broken tracks, about 3.7%, see figure 8.

The vertices not obtained from kaon track are less than 0.02% and are given by electron, muon or pion tracks reconstructed as kaon tracks.
In figure 9 the different contributions to the proper time distribution given by the above listed families are shown.

Figure 8: Vertex obtained by a kaon broken track.

.

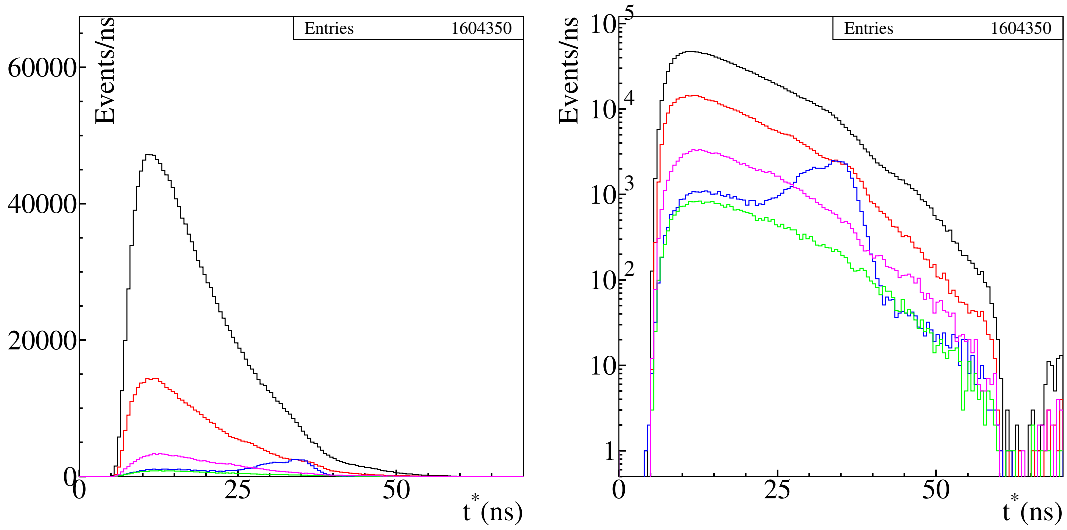

Figure 9: Different contributions to the proper time distribution in linear and logarithmic scale. Five families are described and listed in the text: 1. (black); 2. (green); 3. (red); 4. (pink); 5. (blue).

It is possible to see, in logarithmic scale, that the first four families have the same slope and that the last one has a peak in the region between 30 and 40 ns. In figure 10 the distributions of the resolution on the charged kaon proper time for the different families, evaluated using MonteCarlo, are shown.
The measured proper times for the first four families have a small shifts with respect to the "true" proper time (and much smaller than the bin size we use in the fit, 1 ns). These effects can thus just be taken into account by measuring the resolution function. The fifth family must be rejected in order to not spoil the lifetime measurement.

5.1.3 Background rejection

In order to cut this background we can use the momentum of the charged secondary particle (p^*_K) evaluated in the kaon rest frame, using the kaon mass hypothesis. For the vertices obtained from kaon broken tracks, we expect this variable to be very small, of the order of a few MeV/c.
The distribution of p^*_K is shown in figure 11. The peak in blue is given by the events in which the decay vertices come from kaon broken tracks.
Using the cut $p^*_K > 100$ MeV/c we lose about 5.6% of signal but we discard about 73.5% of this background. The charged kaon proper time distribution obtained applying this cut is shown in figure 12: the shoulder between 30 and 40 ns disappeared.

5.2 Second method: charged kaon decay time

For the second method we measure the kaon decay time obtained using EMC information. The kaon decay time reconstruction efficiency is evaluated using a control sample given by DC information only.

5.2.1 Charged kaon proper time distribution

Given a charged kaon fulfilling the self-triggering tag requirements our signal is given by an opposite charged kaon decay reconstructed using EMC information only.
To do this we have developed the $\pi^0 \to \gamma\gamma$ vertex technique [11] based on events in which the kaon has a π^0 in the final state:

$$K^{\pm} \to \pi^0 X^{\pm}. \tag{18}$$

The π^0 is identified using the $\pi^0 \to \gamma\gamma$ decay vertex and the calorimetric information of the photon clusters. The kaon decay vertex coincides with the decay vertex of the π^0, the $\pi^0 \to \gamma\gamma$ vertex.
First of all we build the helix of the signal kaon as previously described in 5.1.1. In the EMC we look for clusters not associated to tracks in the DC, according to the

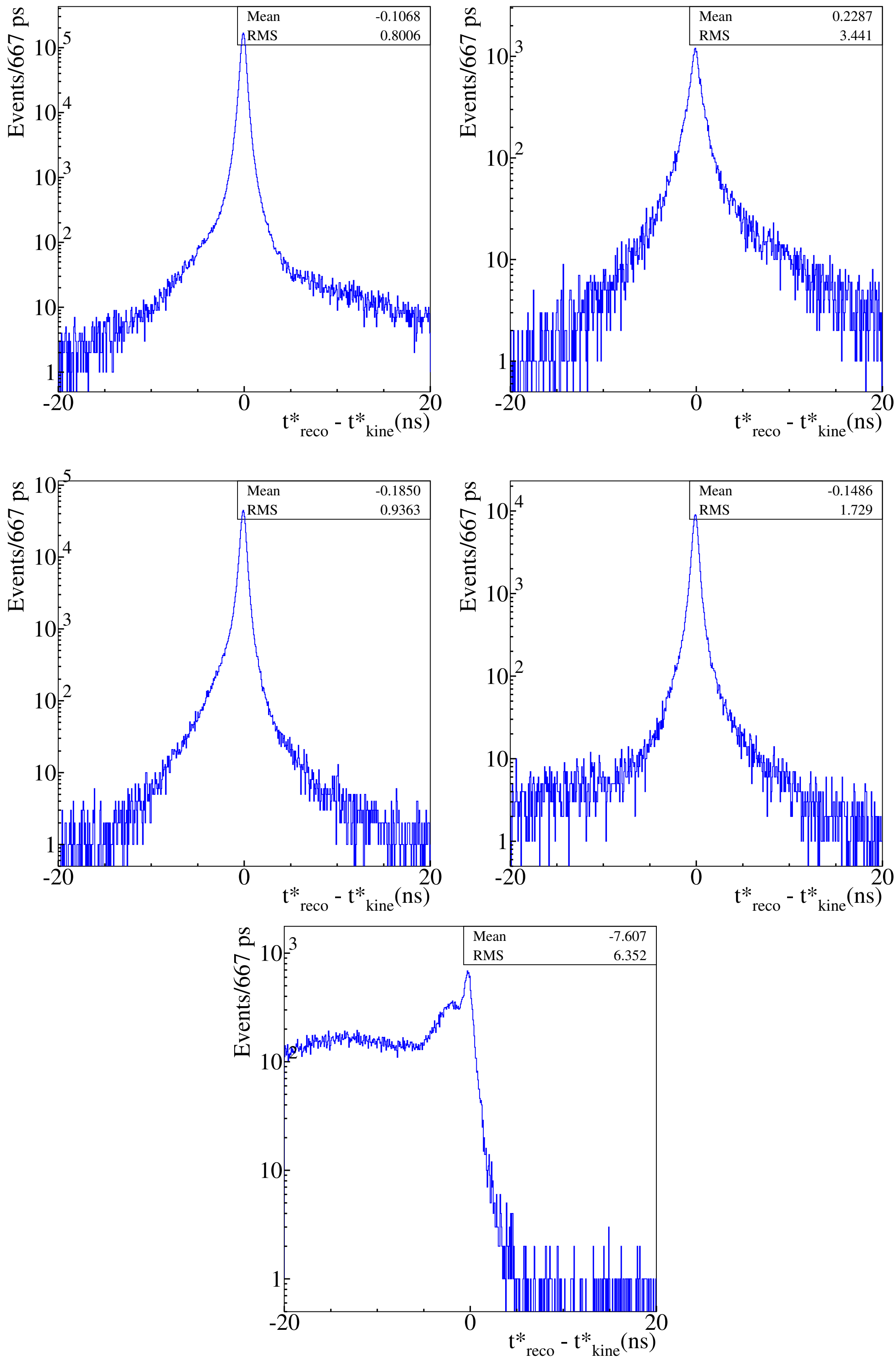

Figure 10: From top left, to bottom: resolution curves for the five families described in the text.

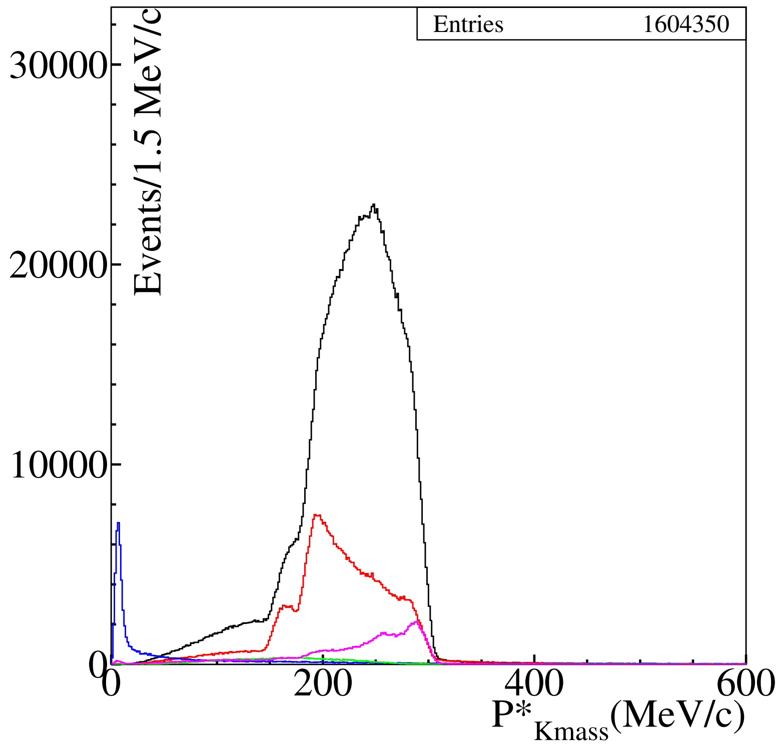

Figure 11: P_K^* for the five families described in the text. Colors are the same as in fig. (9).

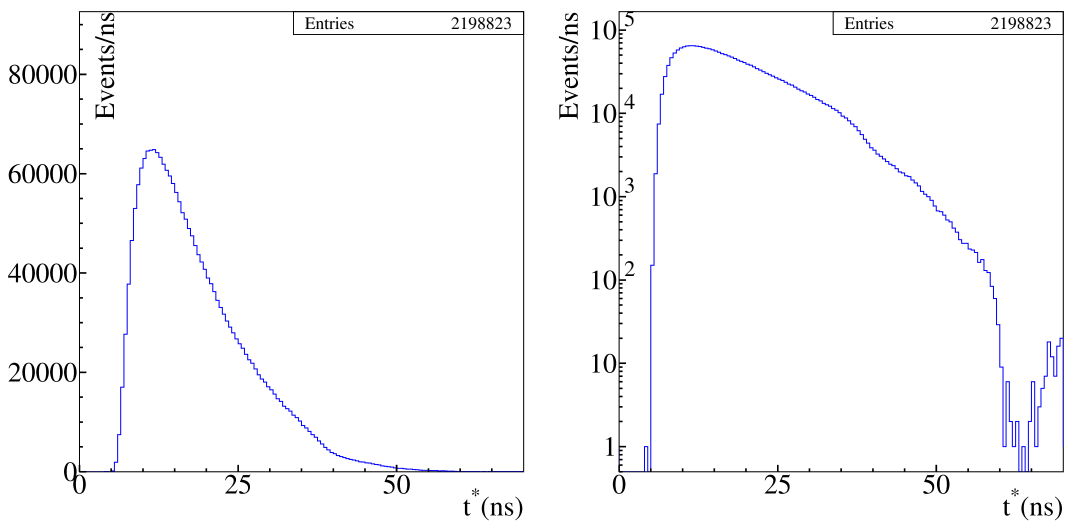

Figure 12: Charged kaon proper time distribution, in linear and in logarithmic scale, after the cut on p_K^*.

KLOE track-to-cluster algorithm [9]. Among these we select the two (or three, if there are) most energetic clusters with:

$$24^\circ < \alpha_{cl} < 156^\circ \tag{19}$$

$$t_\phi < t_{cl} < t_\phi + 70 \text{ ns} \tag{20}$$

where α_{cl} is the polar angle, the angle between the direction of the cluster and the z axis, t_{cl} is the time of the cluster, and t_ϕ is the ϕ decay time evaluated considering the $K_{\mu 2}$ decay chain on the tagging side. These cuts are used to remove the machine background. The request of three neutral clusters allows us to select also the events with the track of the charged decay particle not associated to its calorimeter clusters. Then we move along the path of the signal kaon helix with a step of 5 mm and we look for $\pi^0 \to \gamma\gamma$ decay vertex identified by minimizing a least square function obtained using the following quantities:

1. $$(\Delta M_{\pi^0})^2 = (\sqrt{2E_{cl1}E_{cl2}(1-cos\theta)} - m_{\pi^0})^2 \tag{21}$$

   where θ is the angle between the directions of the two photons given by π^0 decay, E_{cl1} and E_{cl2} are the energies of the neutral clusters fired by the photons and m_{π^0} is the π^0 mass (134.98 MeV). The direction of the photons is defined as the vector going from the candidate kaon decay vertex to the centroid of the selected neutral cluster in the EMC.

2. $$(\Delta t)^2 = [(t_{cl_1} - \frac{\Delta x_1}{c}) - (t_{cl_2} - \frac{\Delta x_2}{c})]^2. \tag{22}$$

   where t_{cl_i} is the time of the i-th cluster and Δx_i is the distance between the neutral cluster and the candidate kaon decay vertex.

3. The difference between the time of flight of the charged kaon, measured along the kaon trajectory, tof_K^{decay}, and the time of flight of the charged kaon measured using the EMC information of the two neutral clusters, tof_{cl}^{decay}:

   $$(\Delta tof)^2 = (tof_K^{decay} - tof_{cl}^{decay})^2 \tag{23}$$

   The first one, tof_K^{decay}, is measured taking into account the energy loss in the different materials given by the Bethe-Bloch formula;
   the second one, tof_{cl}^{decay}, is obtained from the selected neutral clusters weighting their time differences $(t_{cl_i} - \frac{\Delta x_i}{c})$ with the time resolution $\sigma_{t_{cl_i}}$:

   $$\sigma_{t_{cl_i}} = 140\ ps \oplus \frac{57\ ps}{\sqrt{E_{cl_i}(GeV)}}. \tag{24}$$

We define a χ^2-like variable which is:

$$\chi^2 = \frac{(\Delta M_{\pi^0})^2}{\sigma^2_{M_{\pi^0}}} + \frac{\Delta t^2}{(\sigma_{\Delta t})^2} + \frac{(\Delta tof)^2}{\sigma^2_{t_{decay}}} \tag{25}$$

where $\sigma_{M_{\pi^0}}$ is the resolution on the π^0 mass, of about of 17 MeV. $\sigma_{t_{decay}}$ is the uncertainty on the kaon decay time obtained from the selected neutral clusters and on the kaon decay time obtained from the kaon path, of the order of few hundreds ps.
In case three clusters have been selected we choose the pair with the best χ^2. The position along the signal kaon helix that gives the minimum value of the χ^2 defines the $\pi^0 \to \gamma\gamma$ vertex position. It is also required:

$$\chi^2 < 30, \tag{26}$$

$$80MeV/c^2 < M_{\pi^0} < 200MeV/c^2, \tag{27}$$

$$\left|\frac{\Delta t}{\sqrt{\sigma^2_{t_{cl_1}} + \sigma^2_{t_{cl_2}}}}\right| < 5, \tag{28}$$

$$40(cm) < R_{\pi^0} < 150\text{cm} \qquad \text{where} \quad R_{\pi^0} = \sqrt{x^2_{\pi^0} + y^2_{\pi^0}}, \tag{29}$$

$$|Z_{\pi^0}| \leq 150 \text{ cm}, \tag{30}$$

where $X_{\pi^0}, Y_{\pi^0}, Z_{\pi^0}$ are the coordinates of the $\pi^0 \to \gamma\gamma$ vertex. Using this procedure

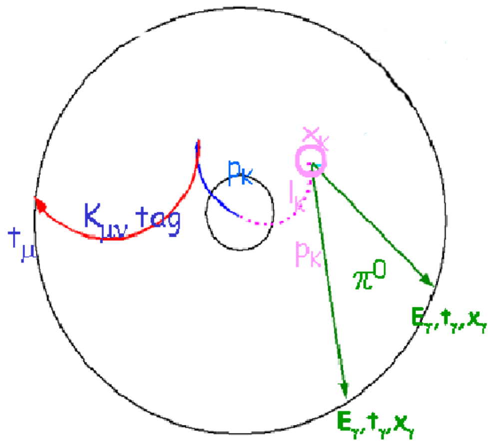

Figure 13: The procedure to search the $\pi^0 \to \gamma\gamma$ vertex along the signal kaon path.

we obtain the χ^2 distribution shown in figure 14. Once the charged kaon decay vertex has been found we can estimate the kaon proper time:

$$t^* = tof^{decay}_{cl} \cdot \sqrt{1-\beta^2} \qquad \text{where} \quad \beta = (\beta^{IP} + \beta^{VTX})/2 \tag{31}$$

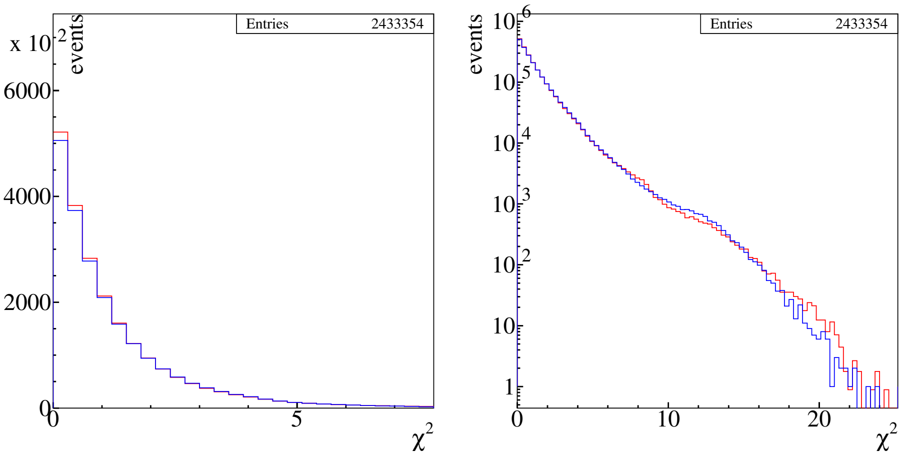

Figure 14: χ^2 distribution for data (blue) and for MonteCarlo (red) in linear and in logarithmic scale.

where tof_{cl}^{decay} is signal kaon time of flight, obtained from the selected neutral clusters in the laboratory frame, while β^{IP} and β^{VTX} are the β values of the signal kaon at the interaction point and at the decay vertex, respectively. The kaon β changes due to the energy loss in the different materials and we have estimated that, with the approximation in equation(31), we have a systematic underestimate of the order of .65% on the proper time. The beta of the kaon is scaled by a factor 1.0065 according to what has been said in section 4.3

We obtain the distribution shown in the figures 15 and 16. It has to be corrected bin by bin for its reconstruction efficiency and for resolution effects.

5.2.2 Background evaluation

The events used for the evaluation of the charged kaon proper time distribution belong to four families:

1. correctly reconstructed vertices, about 95.5%,
2. vertices reconstructed using photons from different π^0's, ($K^\pm \to$ X π^0 π^0 events), about 2.6%,
3. vertices reconstructed with at least one cluster from a charged particle, about 1.3%,
4. vertices reconstructed with one photon which doesn't come form π^0 decay, about 0.6%.

In figure 17 the distributions of the resolution on the charged kaon proper time for the different families, evaluated using MonteCarlo simulation are shown. The main effect of the "backgrounds" is taken into account by properly correcting for the smearing in to the fit.

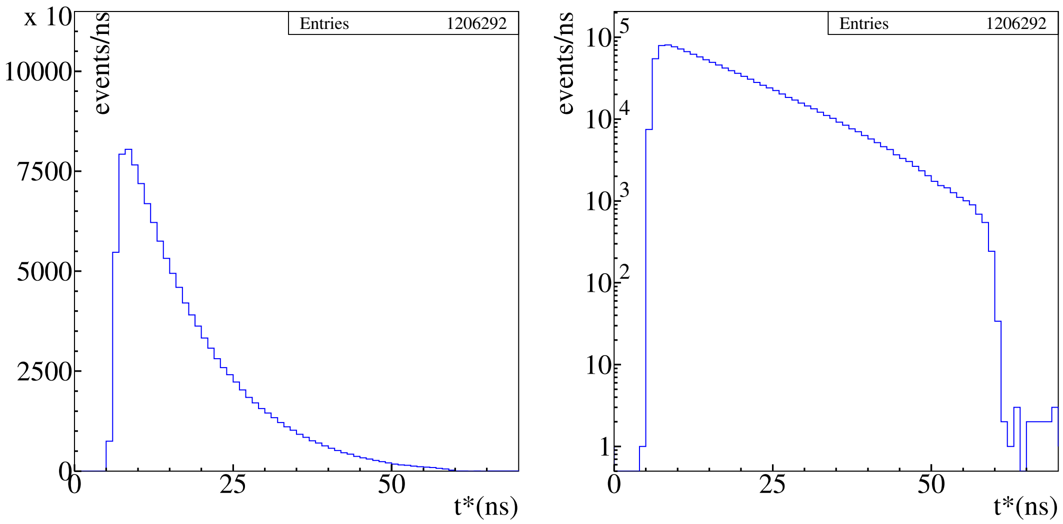

Figure 15: Charged kaon proper time distribution in linear and in logarithmic scale, evaluated on MonteCarlo, for the second method.

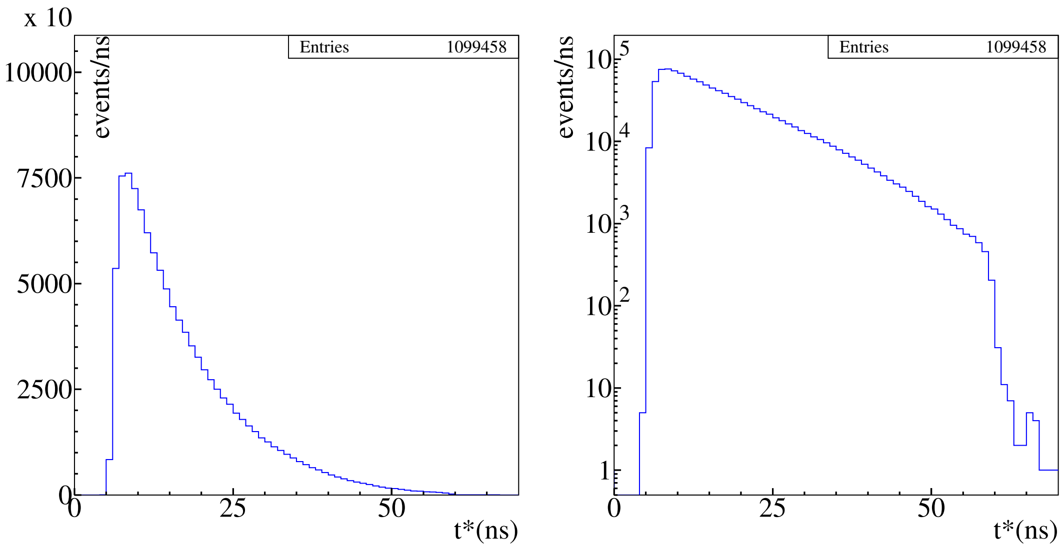

Figure 16: Charged kaon proper time distribution in linear and in logarithmic scale, evaluated on data, for the second method.

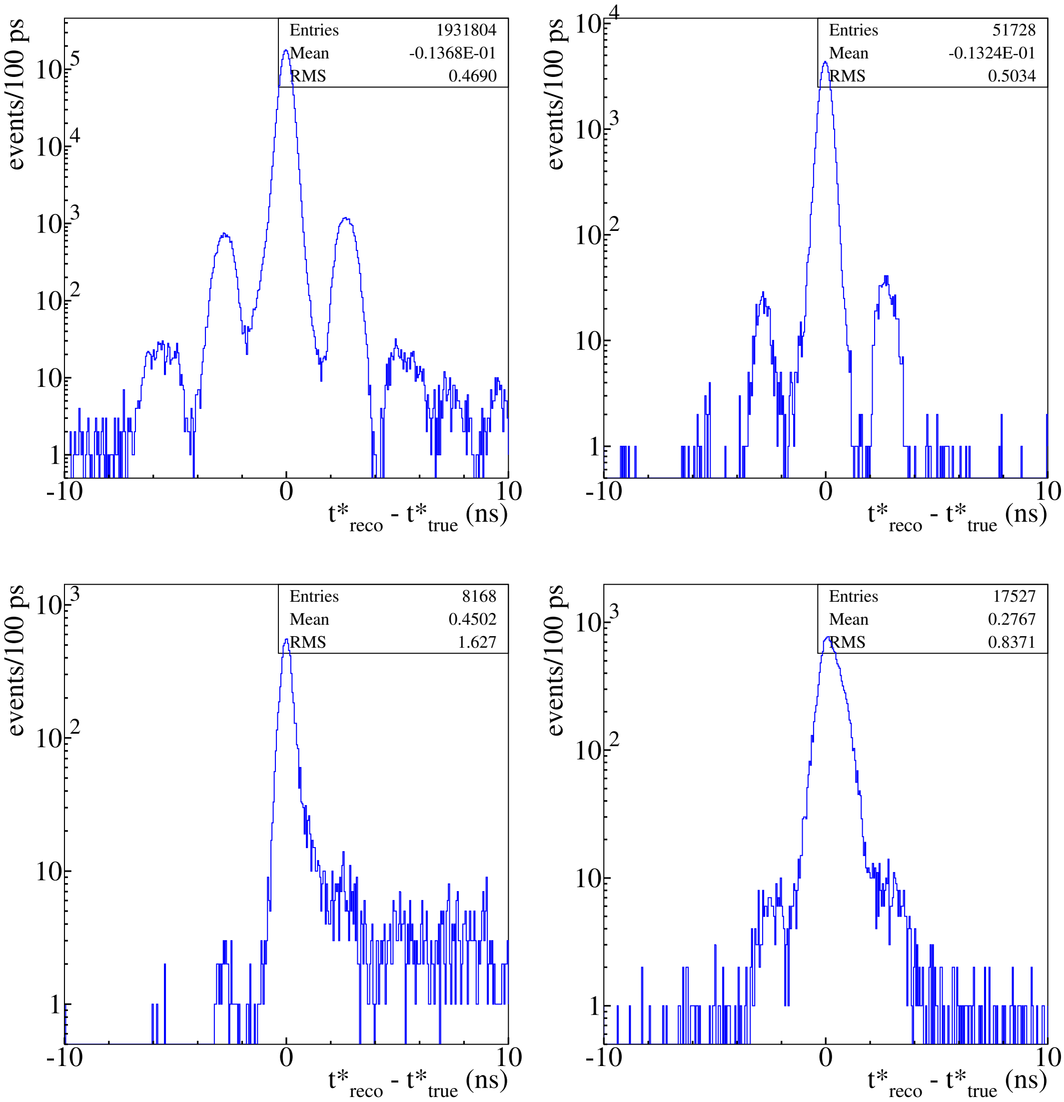

Figure 17: Resolution functions for the four families. Above on the left: correctly reconstructed vertices. Above on the right vertices reconstructed using photons from different π^0. Below on the left vertices reconstructed with at least one cluster from a charged particle. Below on the right vertices reconstructed with one photon which doesn't come form π^0 decay.

6 Efficiency evaluation

Our purpose is to measure directly on data the reconstruction efficiency of the kaon decay (vertex), as a function of the charged kaon proper time, for both the techniques. In order to do this, as control sample, we use for the first method, in which the signal is given by events obtained by DC information only, the signal of the second method, obtained using EMC information only; for the second method, in which the signal is given by events obtained by EMC information only, our control sample is given by the signal of the first method.

6.1 First method: DC efficiency evaluation

The total reconstruction efficiency of the kaon decay vertex in the DC is given by the product of the reconstruction efficiencies of the charged kaon track, of the charged secondary particle track and of the decay vertex given the two tracks.
Two techniques to evaluate the total reconstruction efficiency can be used. The reconstruction efficiency can be obtained either evaluating the global efficiency (kaon track + secondary track + vertex), or evaluating each separately and then multiplying them. In any case only information from the EMC and from the tagging hemisphere are used and the normalization sample is given by events with a $\pi^0 \to \gamma\gamma$ vertex.

6.1.1 *Global* kaon decay vertex efficiency

The *global* kaon decay reconstruction efficiency, the global reco efficiency, is defined as:

$$\varepsilon_{\mathrm{reco}}^{\mathrm{G}} = \frac{N_{\pi^0\&\mathrm{cv}}}{N_{\pi^0}}. \tag{32}$$

where N_{π^0} are the events in which a $\pi^0 \to \gamma\gamma$ vertex has been reconstructed and $N_{\pi^0\&\mathrm{cv}}$ are the events in which a $\pi^0 \to \gamma\gamma$ vertex and a charged vertex, a vertex in the DC, have been reconstructed.
The procedure used to select the normalization sample has been described in the section 5.2.1.
Within the normalization sample we look for a signal kaon track and its decay vertex applying p_K^* cut the previously discussed, see sec 5.1.3.
The efficiency has to be evaluated as a function of the signal kaon proper time, measured along the signal kaon path going from the IP to the $\pi^0 \to \gamma\gamma$ vertex position and accounting for the energy loss in the beam pipe, in the air, in the DC wall and in the DC.
This has been done measuring the efficiency on a MonteCarlo sample treated like data (data-like) of about 175 pb^{-1} and using a bin size of 1 ns, see picture 18.

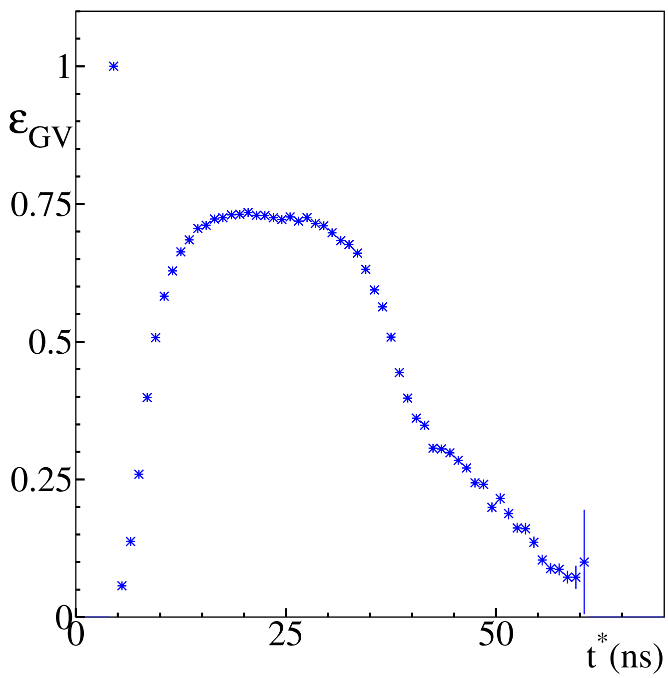

Figure 18: Global reco reconstruction efficiency as function of the charged kaon proper time.

In order to check the reliability of the method, the efficiency has to be compared with the one obtained using the MonteCarlo simulation, the global true efficiency:

$$\varepsilon^{\mathrm{G}}_{\mathrm{true}} = \frac{\mathrm{N_{cv}}}{\mathrm{N_{Tag}}}. \tag{33}$$

where $\mathrm{N_{Tag}}$ are the $\phi \rightarrow K^+K^-$ self-triggering tag events and N_{cv} are the events with a reconstructed charged vertex.
In this case the efficiency is measured as a function of the true proper time, defined in section 4.3 The distributions of the two efficiencies as a function of the proper time of the kaon are shown in figure 19. There is a good agreement between the two distributions. The ratio of the two efficiencies is flat (see fig. 20). A linear fit to this ratio, in the region between 12 and 40 ns, gives the following values for the intercept, a_G, and slope, b_G:

$$a_G = (104.4 \pm 0.3) \times 10^{-2}, \tag{34}$$
$$b_G = (2.7 \pm 1.4) \times 10^{-4}. \tag{35}$$

These two values show an agreement with a residual slope of the order of 10^{-4} for a region of about 30 ns, corresponding to two lifetimes

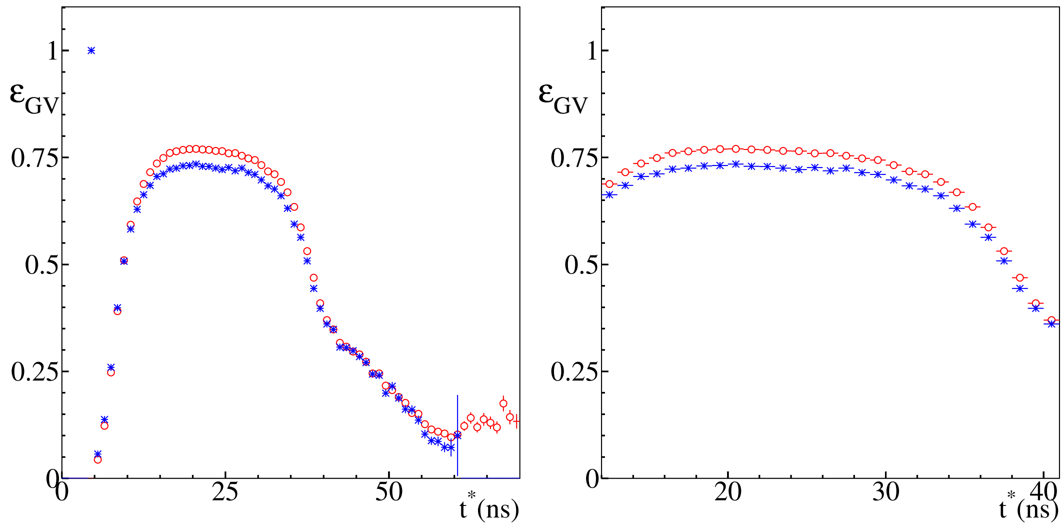

Figure 19: Comparison the global reco efficiency (blue) and the global true efficiency (red) as function of the charged kaon proper time.

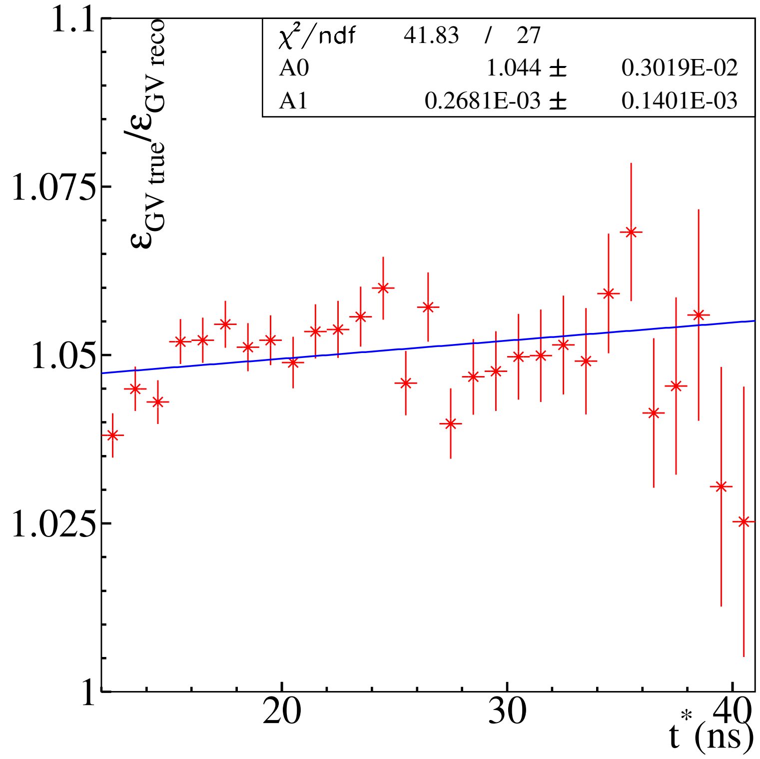

Figure 20: Ratio of the global true efficiency over the global reco efficiency as function of the charged kaon proper time between 12 and 40 ns.

If we make a linear fit in the region between 15 and 35 ns we obtain the following values (see figure 21):

$$a_G = (105.4 \pm 0.4) \times 10^{-2}, \tag{36}$$
$$b_G = (-0.8 \pm 1.9) \times 10^{-4}. \tag{37}$$

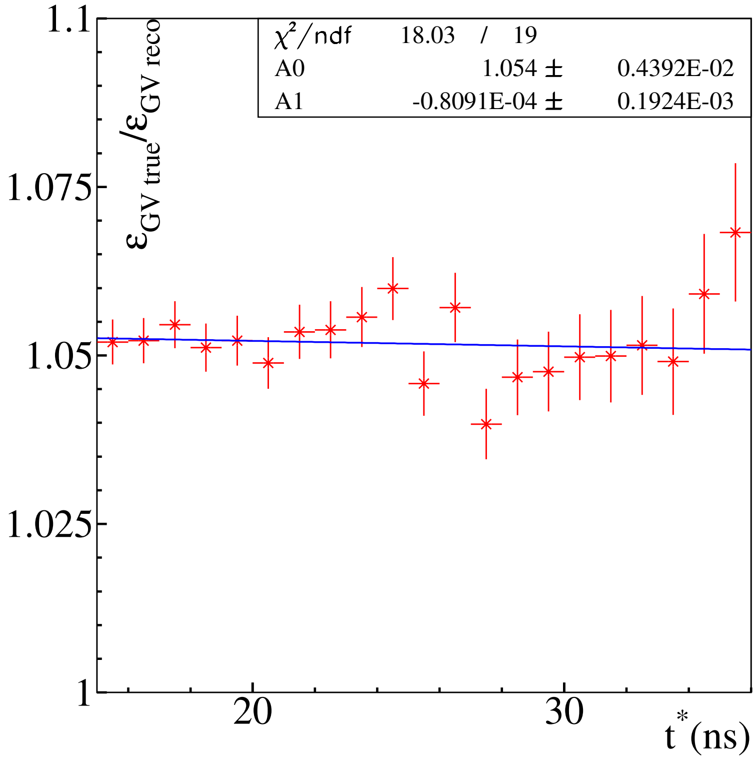

Figure 21: Ratio of the global true efficiency over the global reco efficiency, as function of the charged kaon proper time, between 15 and 35 ns.

The 5% underestimate of the reconstruction efficiency is due to the cut in p^*_K; its effect on $K^\pm \to \mu^\pm \overset{(-)}{\nu}_\mu$ events is not properly evaluated using the $\pi^0 \to \gamma\gamma$ vertex technique. Restricting ourselves to events with a π^0 in the final state the two efficiency are in perfect agreement see fig. 22 and 23. Anyhow the ratio of the efficiencies is important for the measurement because only the shape of the efficiency is relevant.
Once the reliability of this method has been checked on MC, it is possible to measure the efficiency on data. Using a sample of about of 210 pb^{-1} we obtain the distribution shown in figure 24.
The agreement between the efficiency evaluated on data and the efficiency evaluated on MonteCarlo data-like is good except for the region between 8 and 20 ns. This is

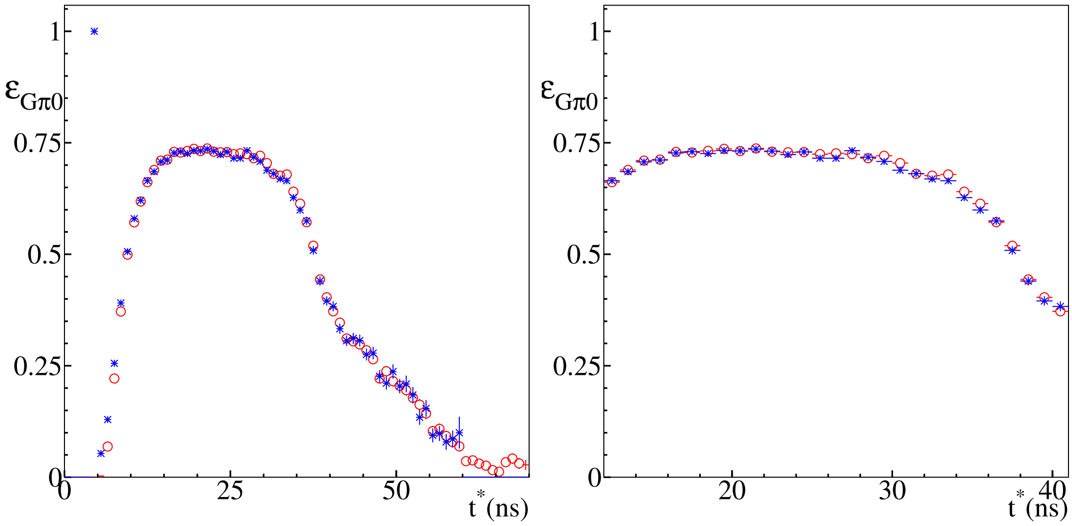

Figure 22: Comparison the global reco efficiency (blue) and the global true efficiency (red) as function of the charged kaon proper time, normalized to events in which the kaon decay with a π^0 in the final state.

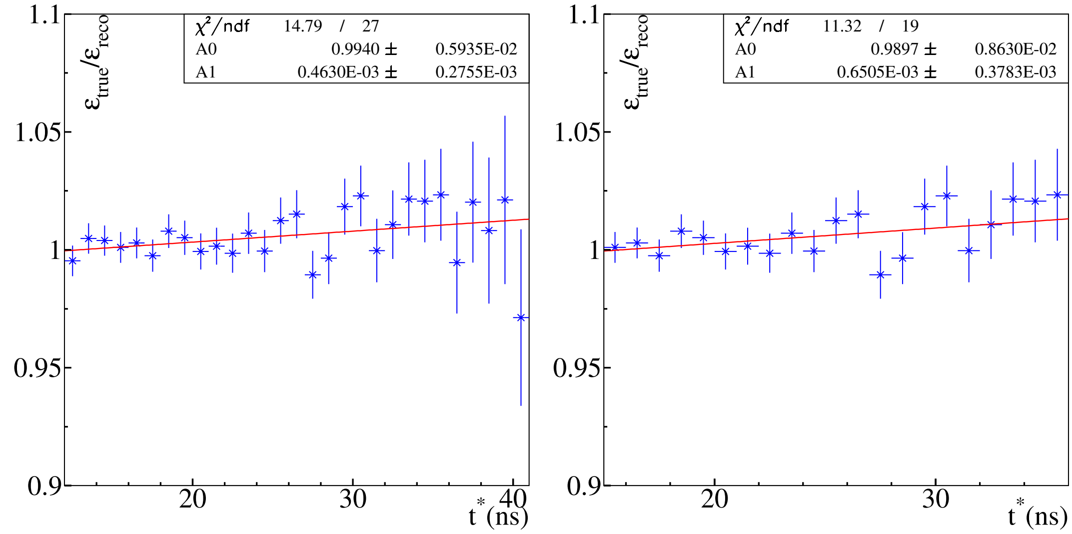

Figure 23: Ratio of the global true efficiency over the global reco efficiency of reconstructing the decay vertex of the charged kaon, as function of the charged kaon proper time, normalized to events in which the kaon decay with a π^0 in the final state.

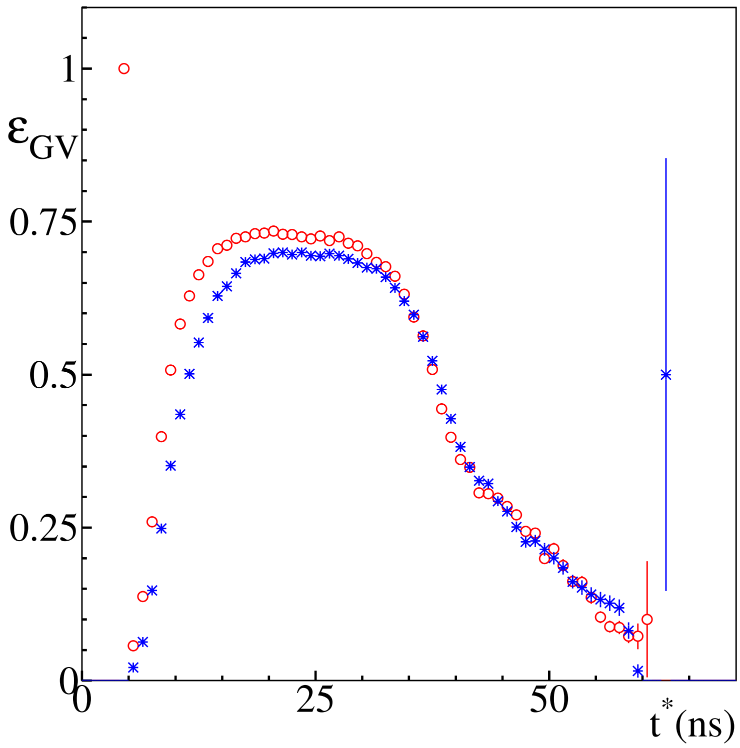

Figure 24: Comparison between the global reco efficiency of reconstructing the decay vertex of the charged kaon evaluated on data (blue) and on MonteCarlo data-like (red) as function of the charged kaon proper time.

due to imperfect simulation of the so-called correlated background in the first cells of the DC. In the first 12 layers of the DC a charged kaon loses so much energy that it fires more than a single cell. This sort of background is not well simulated and gives problems in the measurement of the reconstruction efficiency of the kaon track. This effect is shown when we measure the efficiency of reconstruct the track of the charged kaon, see section 6.1.3.

6.1.2 Separated *tracking* and *vertexing* efficiency

The second technique is based on the evaluation of each efficiency (the reconstruction efficiency of the charged kaon track, *tracking* efficiency, and the reconstruction efficiency of the charged kaon decay vertex given the kaon track, *vertexing* efficiency) separately. The product of these two efficiencies gives the reconstruction efficiency of the charged kaon decay vertex.

6.1.3 *Tracking* efficiency

The kaon *tracking* efficiency, the tracking reco efficiency, is defined as:

$$\varepsilon_{\text{reco}}^{\text{Trk}} = \frac{N_{\pi^0\&\text{Trk}}}{N_{\pi^0}}. \tag{38}$$

where $N_{\pi^0\&\text{Trk}}$ are the events in which a $\pi^0 \to \gamma\gamma$ vertex and the signal kaon track have been reconstructed.
The π^0 decay is identified as described in section 5.2.1. The signal kaon track is identified as described is section 5.1.1.
The tracking efficiency is evaluated on a MC data-like sample of about 175 pb^{-1} using a bin size of 1 ns.
Also the method has been validated after the comparison with the true tracking efficiency, defined as:

$$\varepsilon_{\text{true}}^{\text{Trk}} = \frac{\mathrm{N_{Trk}}}{\mathrm{N_{TAG}}}. \tag{39}$$

where N_{Trk} are the events in which the kaon track has been reconstructed. The agreement between these two efficiencies is remarkable (see fig. 25) as can be seen also in the ratio of the true and reco efficiencies (see fig. 26). A linear fit to the ratio, in the region between 12 and 40 ns, gives the following values for the intercept, a_{Trk}, and slope, b_{Trk}:

$$a_{Trk} = (99.62 \pm 0.13) \times 10^{-2}, \tag{40}$$

$$b_{Trk} = (-0.3 \pm 5.4) \times 10^{-5}. \tag{41}$$

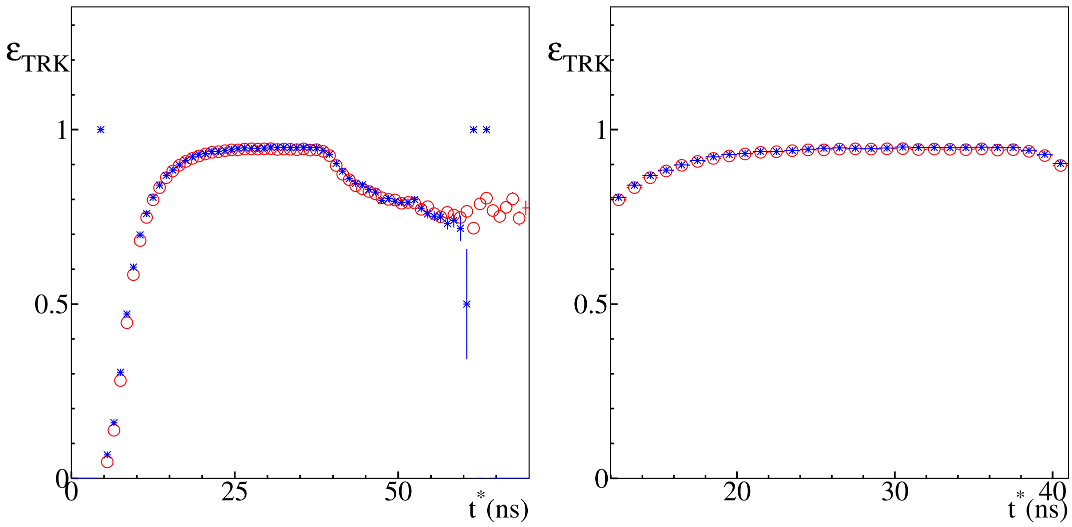

Figure 25: Comparison the tracking reco efficiency (blue) and the tracking true efficiency (red) as function of the charged kaon proper time.

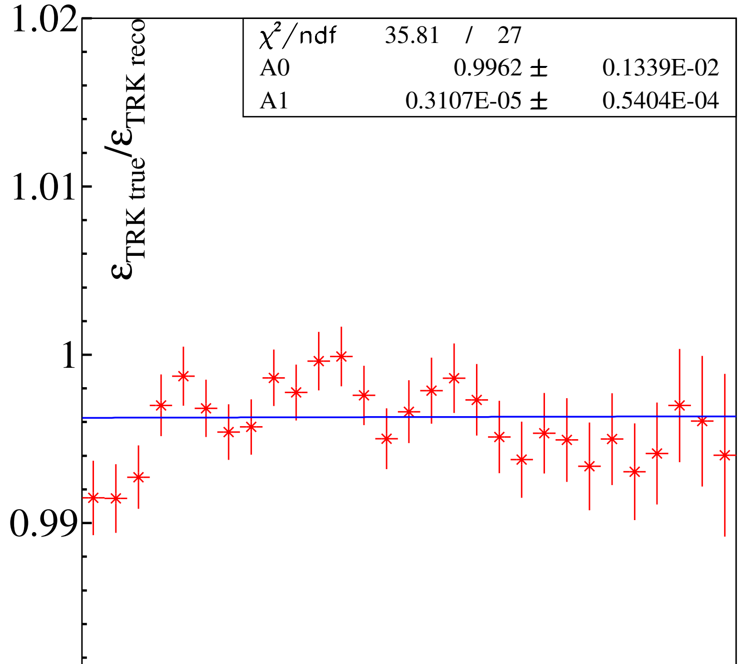

Figure 26: Ratio of the tracking true efficiency over the tracking reco efficiency, as function of the charged kaon proper time, between 12 and 40 ns.

The agreement is very good with a residual slope of the order of 10^{-5} for a region of 30 ns (more than two lifetimes). In the region between 15 and 35 ns we obtain (see figure 27):

$$a_{Trk} = (100.0 \pm 0.2) \times 10^{-2}, \tag{42}$$
$$b_{Trk} = (-0.13 \pm 0.08) \times 10^{-3}. \tag{43}$$

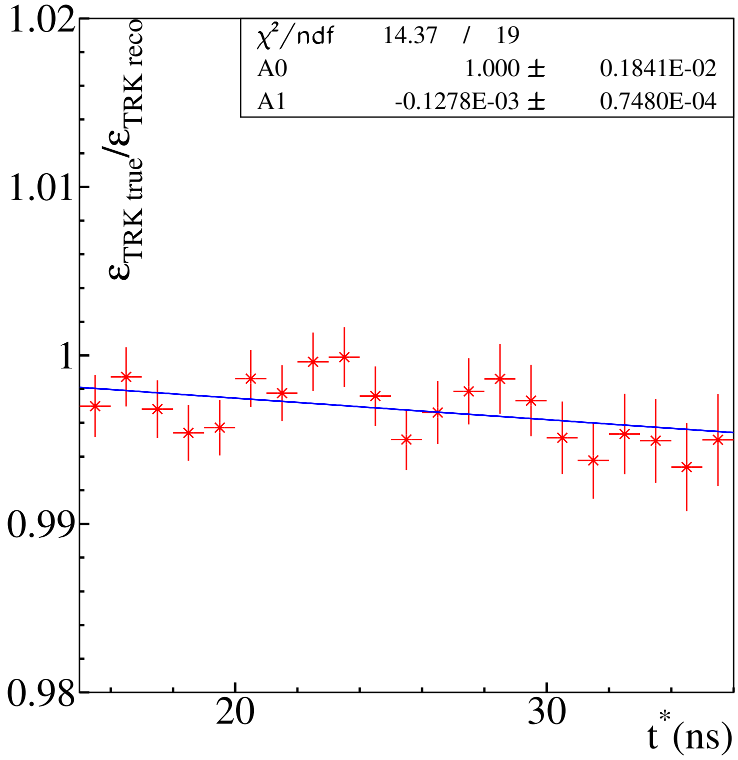

Figure 27: Ratio of the tracking true efficiency over the tracking reco efficiency, as function of the charged kaon proper time, between 15 and 35 ns.

This garantees the reliability of the method, and allows its use on data.
Using a sample of about 210 pb^{-1} we obtain the distribution shown in figure 28. The agreement between the efficiency evaluated on data and the efficiency evaluated on MonteCarlo data-like is good, except for the region between 8 and 20 ns. The reason for this discrepancy is the same of the analogous discrepancy for the global efficiency and has been discussed at the end of section 6.1.1.

6.1.4 *Vertexing* efficiency

For the measurement of the reconstruction efficiency of the kaon decay vertex we have to relay on the DC for the determination of the kaon track. This is the main

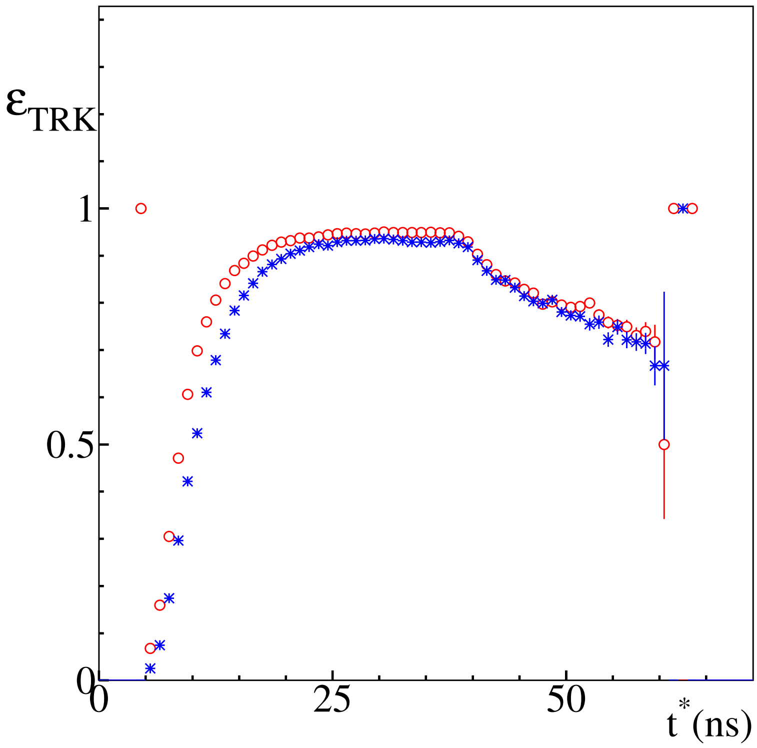

Figure 28: Comparison between tracking reco efficiency evaluated on data (blue) and on Monte-Carlo data-like (red) as function of the charged kaon proper time.

difference with respect to the other technique.
The vertexing reco efficiency is defined as:

$$\varepsilon^{\rm Vtx}_{\rm reco} = \frac{\rm N_{\pi^0\&cv}}{\rm N_{Trk\&\pi^0}}. \tag{44}$$

where $N_{\pi^0\&\rm cv}$ are the events in which a $\pi^0 \to \gamma\gamma$ vertex and a charged vertex have been reconstructed and $N_{\rm Trk\&\pi^0}$ are the events in which a $\pi^0 \to \gamma\gamma$ vertex and a charged kaon track have been reconstructed.
For the reconstruction of the $\pi^0 \to \gamma\gamma$ vertex we use the same procedure described in the section 5.2.1, but we start from the Last Hit of the reconstructed kaon track instead of starting from the IP. The DC information we use are then the kaon position and momentum at the Last Hit. We have also to measure the $\mathrm{tof}_K^{\rm decay}$ for the π^0 decay reconstruction, then we measure the time of flight of the charged kaon along the track, from the IP to the Last Hit, $\rm tof_{F_hL_h}$. Then we extrapolate the signal kaon track up to a maximum value of one meter, backward and forward, looking for the π^0 decay vertex and using the following relations:

$$tof_K^{decay} = tof_{F_hL_h} - tof_{bwd} \tag{45}$$

or

$$tof_K^{decay} = tof_{F_hL_h} + tof_{fwd}. \tag{46}$$

We use this $\rm tof_K^{decay}$ in eq 23 for the search of the $\pi^0 \to \gamma\gamma$ vertex. Since the efficiency has to be function of the charged kaon proper time, we have to measure the kaon proper time along the track, from the IP to the Last Hit, $t^*_{F_hL_h}$. Therefore if we extrapolate the signal kaon track backward or forward, looking for the $\pi^0 \to \gamma\gamma$ vertex, we have:

$$t^* = t^*_{F_hL_h} - t^*_{bwd} \tag{47}$$

or

$$t^* = t^*_{F_hL_h} + t^*_{fwd}. \tag{48}$$

To evaluate the *vertexing* efficiency we have used a MonteCarlo data-like sample of about 175 pb^{-1}, using a bin size of 1 ns. As usual the efficiency is compared with the one obtained on MC truth.
This is defined as the ratio of the events in which the kaon decay vertex has been reconstructed (N_{Vtx}) over the events in which the kaon track has been reconstructed (N_{Trk}):

$$\varepsilon^{\rm Vtx}_{\rm true} = \frac{\rm N_{Vtx}}{\rm N_{Trk}}. \tag{49}$$

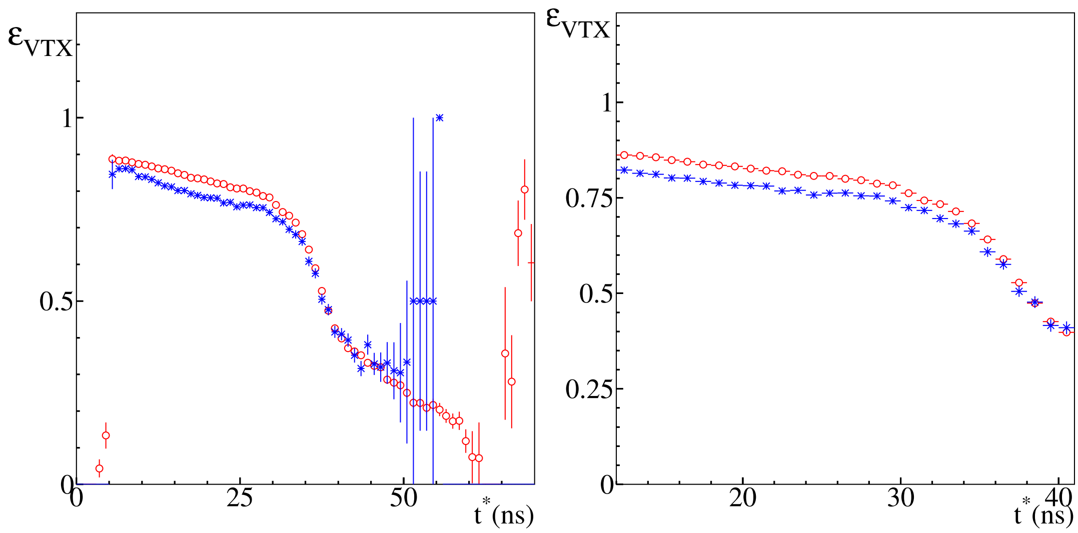

Figure 29: Comparison between the vertexing reco efficiency (blue) and the vertexing true efficiency (red) as function of the charged kaon proper time.

In this case we have evaluated the efficiency as a function of the proper time given by the MonteCarlo simulation, the true proper time.
The comparison between these two efficiencies is shown in figure 29. As can be seen from the ratio of these efficiencies, shown in figure 30, there is a very satisfactory agreement between the two. Making a linear fit in the region between 12 and 40 ns, the values for the intercept, a_{Vtx}, and slope, b_{Vtx}, are:

$$a_{Vtx} = (106.2 \pm 0.6) \times 10^{-2}, \tag{50}$$
$$b_{Vtx} = (-4. \pm 3.) \times 10^{-4}. \tag{51}$$

The agreement is fine with a residual slope of the order of 10^{-4} for a region of 30 ns, more than two lifetimes.
Restricting the linear fit to the region between 15 and 35 ns we obtain (see figure 31):

$$a_{Vtx} = (106.8 \pm 1.0) \times 10^{-2}, \tag{52}$$
$$b_{Vtx} = (-6. \pm 4.) \times 10^{-4}. \tag{53}$$

The next step is the measurement of the vertex efficiency on the data sample. We use a sample of about of 210 pb^{-1} and we obtain the distribution shown in figure 32.
The agreement between the efficiency evaluated on data and the efficiency evaluated on MonteCarlo data-like is very good, see figure 32.

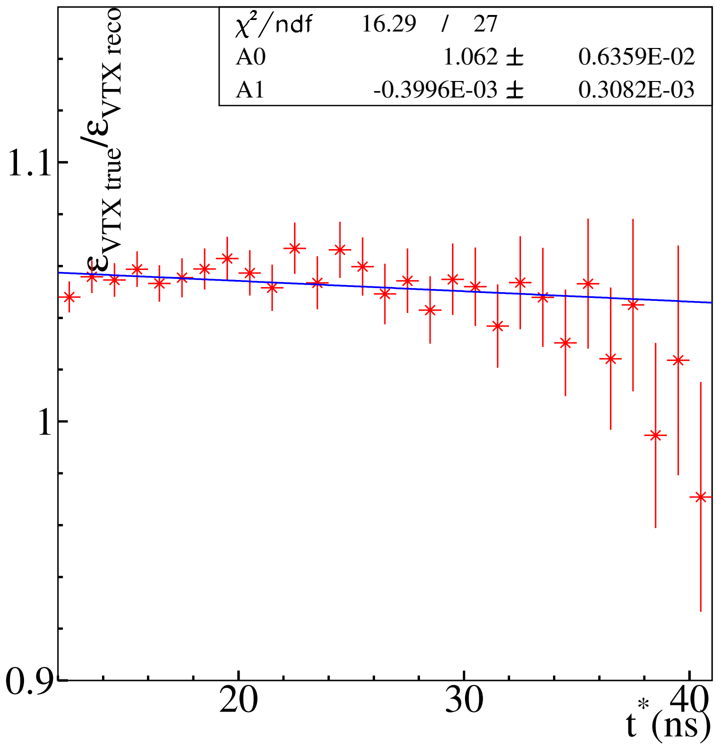

Figure 30: Ratio of the vertexing true efficiency over the vertexing reco efficiency, as function of the charged kaon proper time, between 12 and 40 ns.

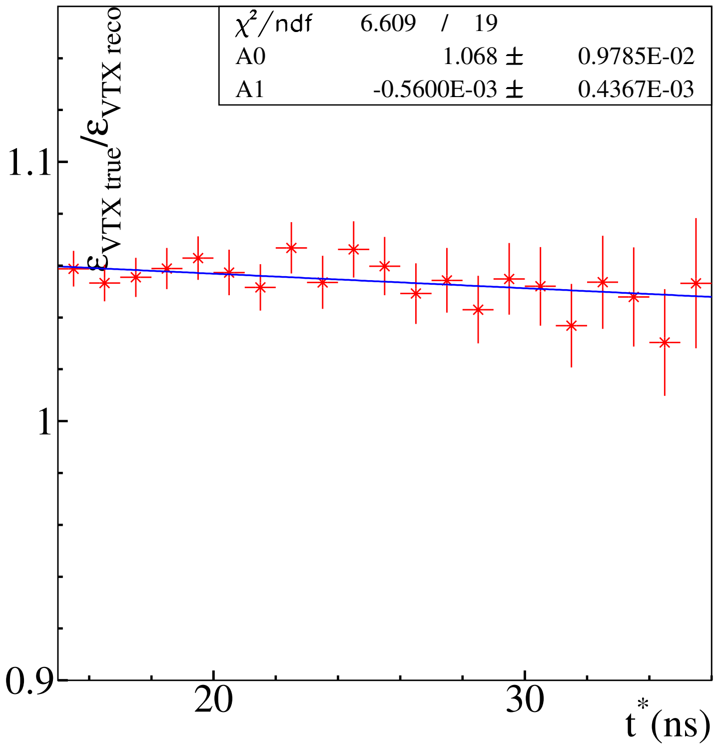

Figure 31: Ratio of the vertexing true efficiency over the vertexing reco efficiency, as function of the charged kaon proper time, between 15 and 35 ns.

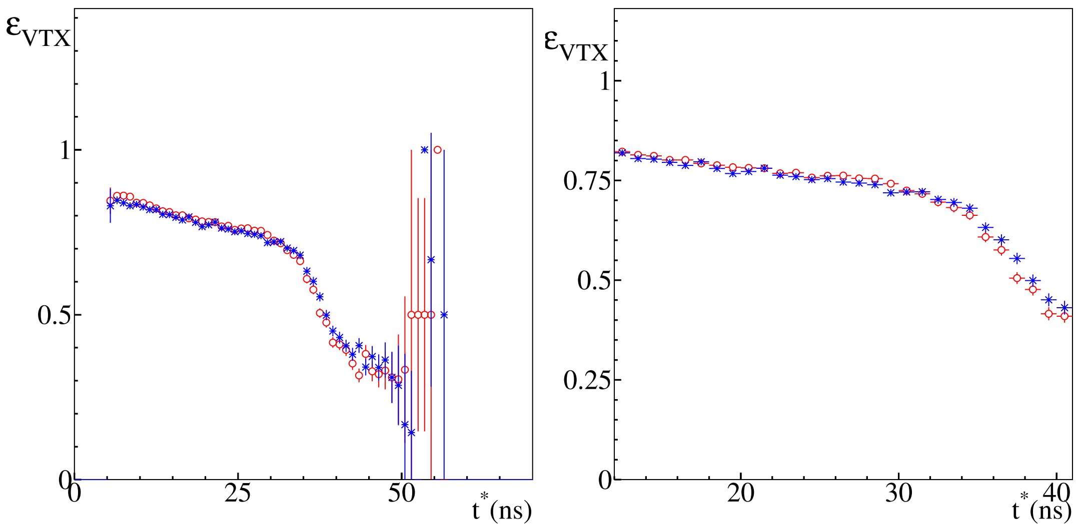

Figure 32: Comparison the vertexing reco efficiency evaluated on data (blue) and on MonteCarlo data-like (red) as function of the charged kaon proper time.

We also made a background analysis with the MonteCarlo simulation and we have estimated that there is a $K^{\pm} \to \mu^{\pm}\overset{(-)}{\nu}_{\mu}$ background in our $\pi^{o} \to \gamma\gamma$ technique of the order of 0.2%. In these events the two clusters selected are due to the machine background. These events do not represent a significant bias for our efficiency measurement.

6.1.5 Two techniques compared

We compared, on the MonteCarlo data-like sample, the efficiency obtained in the section 6.1.1, the *global* kaon decay vertex efficiency, and the efficiency given by the product of the kaon *tracking* efficiency and kaon *vertexing* efficiency, obtained in section 6.1.3 and 6.1.4 Although the two methods are not completely independent,

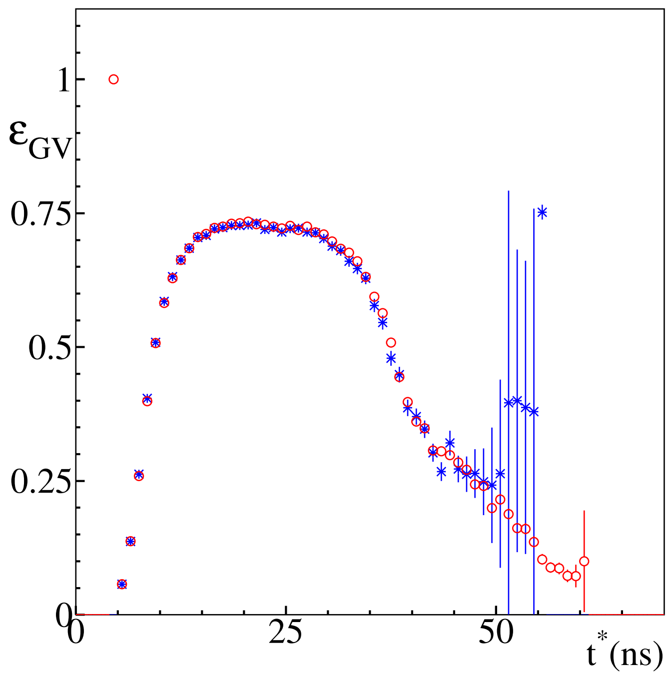

Figure 33: Comparison the *global* reco efficiency (blue) and efficiency given by the product of the kaon *tracking* efficiency and kaon *vertexing* efficiency (red) as function of the charged kaon proper time, on MonteCarlo.

since both rely on the $\pi^0 \to \gamma\gamma$ technique, it is worth to compare the overall efficiency obtained in the two approaches. For the *global* approach we used only extrapolation of the tagging information in finding the π^0 decay vertex; for the second approach we used the measured track in finding the π^0 decay vertex, and is expected to have a better resolution. The agreement between the two efficiencies is exccelent. This is confirmed by the bin by bin ratio of the two (fig. 34) and the result of a linear fit to this ratio in the region between 12 and 42 ns, giving the following values for the intercept, a_G, and slope, b_G:

$$a_G = (99.3 \pm 0.6) \times 10^{-2}, \tag{54}$$
$$b_G = (6 \pm .3) \times 10^{-4}. \tag{55}$$

Restricting the linear fit to the region between 15 and 35 ns we obtain the following values (see figure 34):

$$a_G = (99.4 \pm 1.0) \times 10^{-2}, \tag{56}$$
$$b_G = (5. \pm 4.) \times 10^{-4}. \tag{57}$$

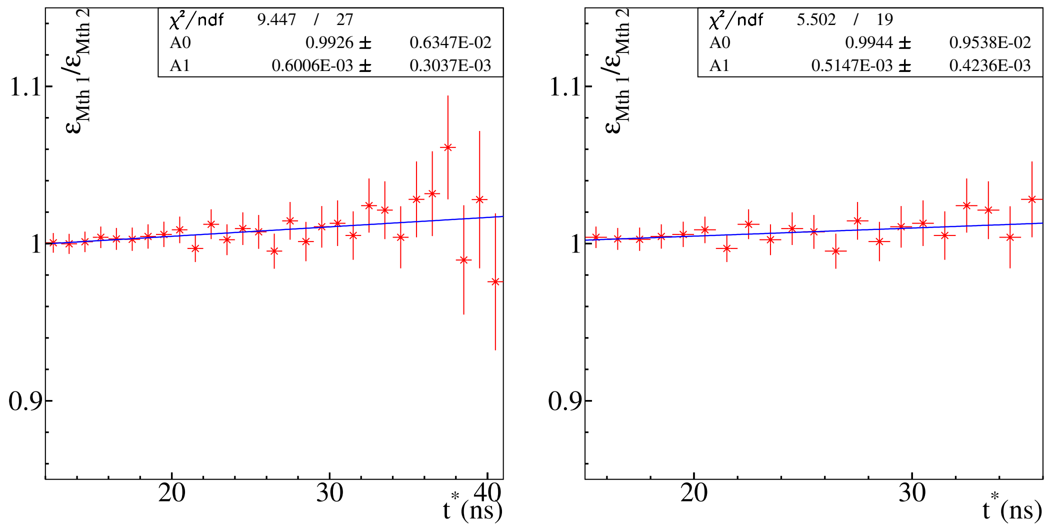

Figure 34: Ratio of the global reco efficiency over the efficiency given by the product of the kaon tracking efficiency and kaon vertexing efficiency, as function of the charged kaon proper time, evaluated on MonteCarlo.

We obtained good result also on the data sample, as shown in figure 35. It is confirmed by the bin by bin ratio of the two (fig. 36) and by the result of a linear fit to this ratio in the region between 12 and 40 ns. The linear fit gives the following values for the intercept, a_G, and slope, b_G:

$$a_G = (99.3 \pm 0.7) \times 10^{-2}, \tag{58}$$
$$b_G = (2. \pm 3.) \times 10^{-4}. \tag{59}$$

While if we make a linear fit in the region between 15 and 35 ns we obtain the following values (see figure 35):

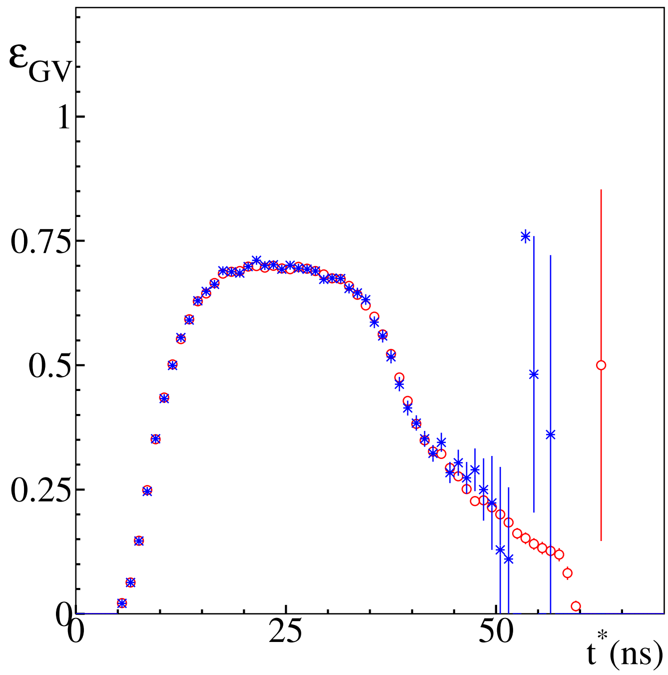

Figure 35: Comparison the *global* reco kaon efficiency (blue) and the efficiency given by the product of the kaon *tracking* efficiency and kaon *vertexing* efficiency (red) as function of the charged kaon proper time, on data.

$$a_G = (99.3 \pm 1.0) \times 10^{-2}, \tag{60}$$
$$b_G = (2 \pm 4.) \times 10^{-4}. \tag{61}$$

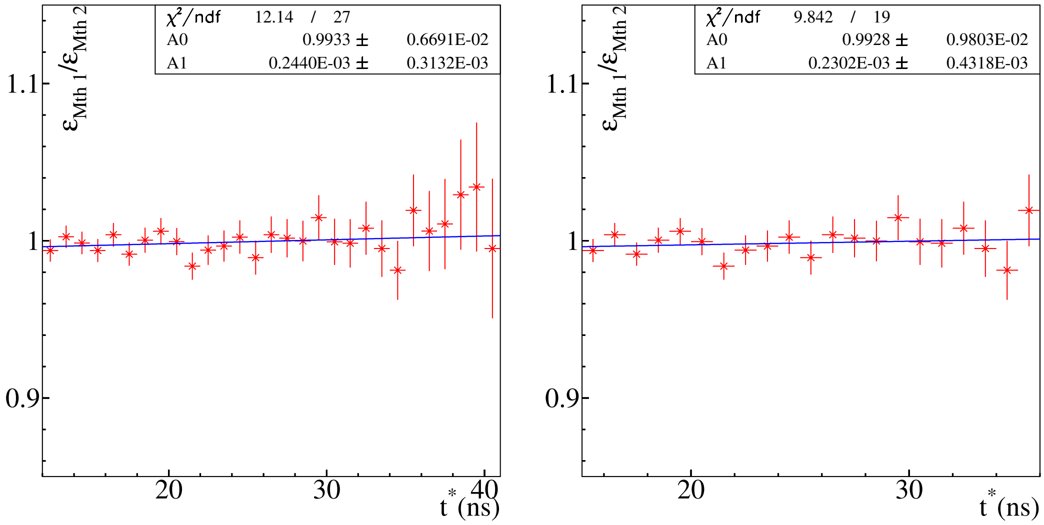

Figure 36: Ratio of the global reco efficiency of reconstructing the decay vertex of the charged kaon and efficiency given by the product of the kaon tracking efficiency and kaon vertexing efficiency, as function of the charged kaon proper time, evaluated on the data sample.

6.2 Second method: $\pi^0 \to \gamma\gamma$ vertex efficiency evaluation

In order to measure the kaon decay vertex reconstruction efficiency, using EMC information only, the π^0 reco efficiency, we have used as normalization sample the events in which the charged decay vertex, the vertex given by two tracks in the DC, has been reconstructed. The normalization sample is given by the signal sample for the first method, see section (5.1.1).
The π^0 reco efficiency is defined, bin by bin, as the ratio between the number of events with the kaon charged decay vertex ($\mathrm{N_{cv}}$) as denominator and the number of events in which the $\pi^0 \to \gamma\gamma$ vertex has been reconstructed, given the existence of the *charged* vertex, ($\mathrm{N_{cv\&\pi^0}}$), as numerator:

$$\varepsilon^{\pi^0}_{\mathrm{reco}} = \frac{\mathrm{N_{\&cv\&\pi^0}}}{\mathrm{N_{cv}}}. \tag{62}$$

In order to check the reliability of the described method, this efficiency has to be compared with the true one defined as the ratio of the events with a reconstructed $\pi^0 \to \gamma\gamma$ vertex, ($\mathrm{N_{\pi^0}}$) over the $\phi \to K^+K^-$ self-triggering tag events:

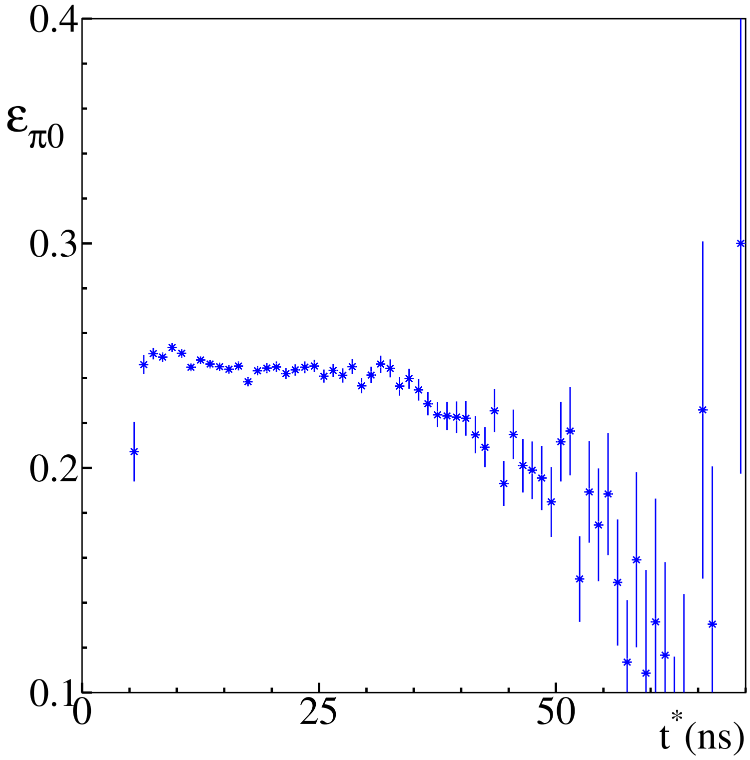

Figure 37: π^0 reco efficiency as a function of the charged kaon proper time.

$$\varepsilon^{\pi^0}_{\text{true}} = \frac{\text{N}_{\pi^0}}{\text{N}_{\text{Tag}}}. \tag{63}$$

In this case the efficiency is measured as a function of the true proper time, the proper time given by the MonteCarlo simulation. We measured the $\pi^0 \to \gamma\gamma$ efficiency on a MonteCarlo data-like sample of about 175 pb^{-1} using a bin size of 1 ns. The distributions of the expected and measured efficiencies as a function of the proper time of the kaon are shown in figure 38. There is a good agreement between

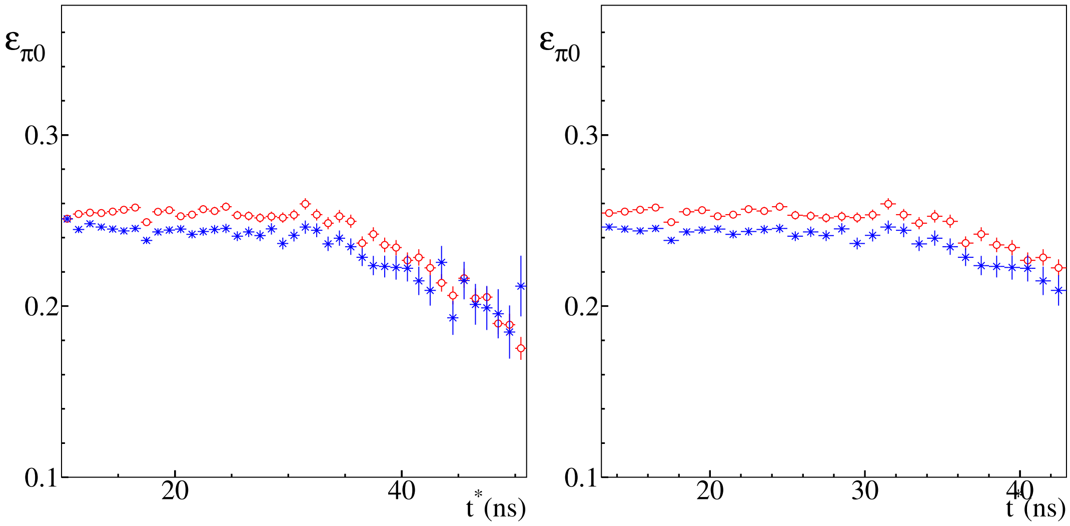

Figure 38: Comparison the π^0 reco efficiency of reconstructing the $\pi^0 \to \gamma\gamma$ vertex of the charged kaon (blue) and the π^0 true efficiency of reconstructing the $\pi^0 \to \gamma\gamma$ vertex of the charged kaon (red) as function of the charged kaon proper time. In the figure on the left the two efficiencies are normalized to the unity in the region between 10 and 50 ns, in the figure on the right the two efficiencies are normalized to the unity in the region between 12 and 43 ns

the two efficiencies. It is confirmed by the bin by bin ratio of the two (fig. 39) and by the result of a linear fit to this ratio in the region between 10 and 50 ns:

$$a_{\pi^0} = (102.6 \pm 0.7) \times 10^{-2}, \tag{64}$$
$$b_{\pi^0} = (7. \pm 3.) \times 10^{-4}. \tag{65}$$

The agreement is fine with a residual slope of the order of 10^{-4} for a region of 40 ns, about three lifetimes.
Doing a linear fit between 13 and 42 ns (fig 40) we obtain:

$$a_{\pi^0} = (103.7 \pm 1.0) \times 10^{-2}, \tag{66}$$
$$b_{\pi^0} = (4. \pm 4.) \times 10^{-4}. \tag{67}$$

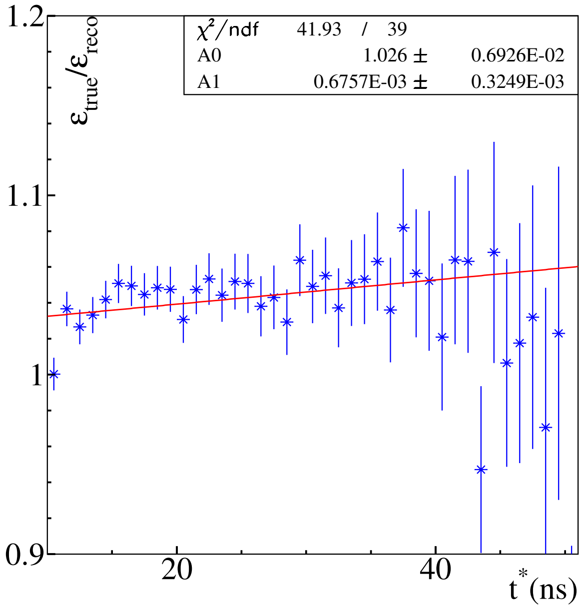

Figure 39: Ration of the π^0 true efficiency over the π^0 reco efficiency of reconstructing $\pi^0 \to \gamma\gamma$ decay vertex, as function of the charged kaon proper time, between 10 and 50 ns.

The agreement is very good with a residual slope of the order of 10^{-4} for a region of about 30 ns, about two lifetime, see figure 40. The reason for overestimate

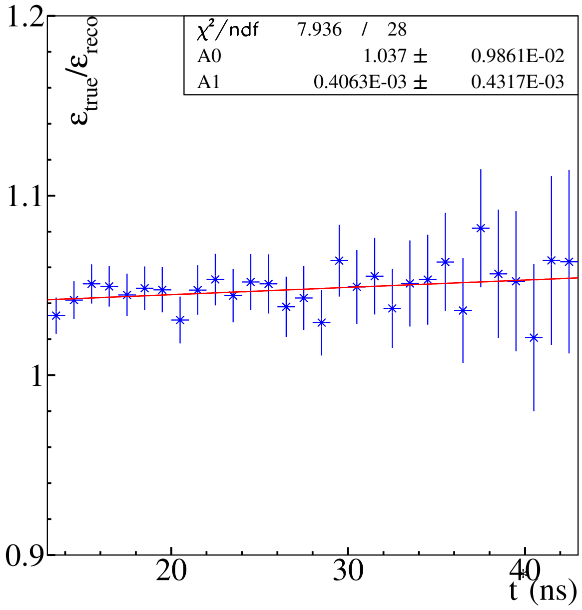

Figure 40: Ratio of the π^0 true efficiency over the π^0 reco efficiency of reconstructing the $\pi^0 \to \gamma\gamma$ vertex, as function of the charged kaon proper time, between 13 and 42 ns.

of the efficiency is in the normalization used for the reconstructed efficiency: the control sample is given by the number of events in which a charged vertex has been reconstructed without any information on the particular final state. Indeed restricting ourselves only to events with a π^0 in the final state the two efficiency are in perfect agreement: the shape and the overall scale of the efficiencies are correctly evaluated, see figure 41.

Having demostrated with the MonteCarlo simulation the reliability of this method for measuring the efficiency, we can proceed in measuring it on data. We used a sample of 210 pb^{-1} and we obtain the distribution shown in figure 42. The agreement between the efficiency evaluated on data and the efficiency evaluated on MonteCarlo data-like is good.

7 Resolution effects

So far we have obtained the proper time distribution and evaluated the efficiency of reconstructing the kaon decay vertex as function of the proper time, for both the methods. In order to perform the exponential fit to the proper time distribution, we need to take into account the resolution effects. Some events in the proper time distribution are generated with a given value but are reconstructed with another one for resolution effects.

We need to evaluate these resolution effects and then we can perform the fit using a function given by the convolution of the exponential decay behavior and the resolution function.

7.1 First method: evaluation of resolution

We have to determine the resolution curves for the signal sample of the first method. These are evaluate with the MonteCarlo simulation and are defined as the difference between the true proper time, see section 4.2, and charged kaon proper time. First of all we have to emphasize that also the resolution curves are functions of the charged kaon proper time. For example the resolution curve for charged kaon proper time between 8 and 10 ns is different from the one for charged kaon proper time between 20 and 21 ns, as shown in figure 43. In order to be less sensitive to the MonteCarlo simulation, we decided to measure the resolution curves directly on data. This is possible using the point of closest approach (PCA) between the kaon track and the charged particle track. The PCA is found minimizing the distance between the helixes built starting from the two tracks and accounting for the energy loss in the DC: the kaon helix is built using the kaon last hit position and momentum, the charged secondary helix is built using its last hit position and momentum. To validate this technique we use the MonteCarlo simulation. We can evaluate with this technique the position and momentum of thekaon at the decay vertex and compare these values with the true ones givenby the simulation. As we can see in

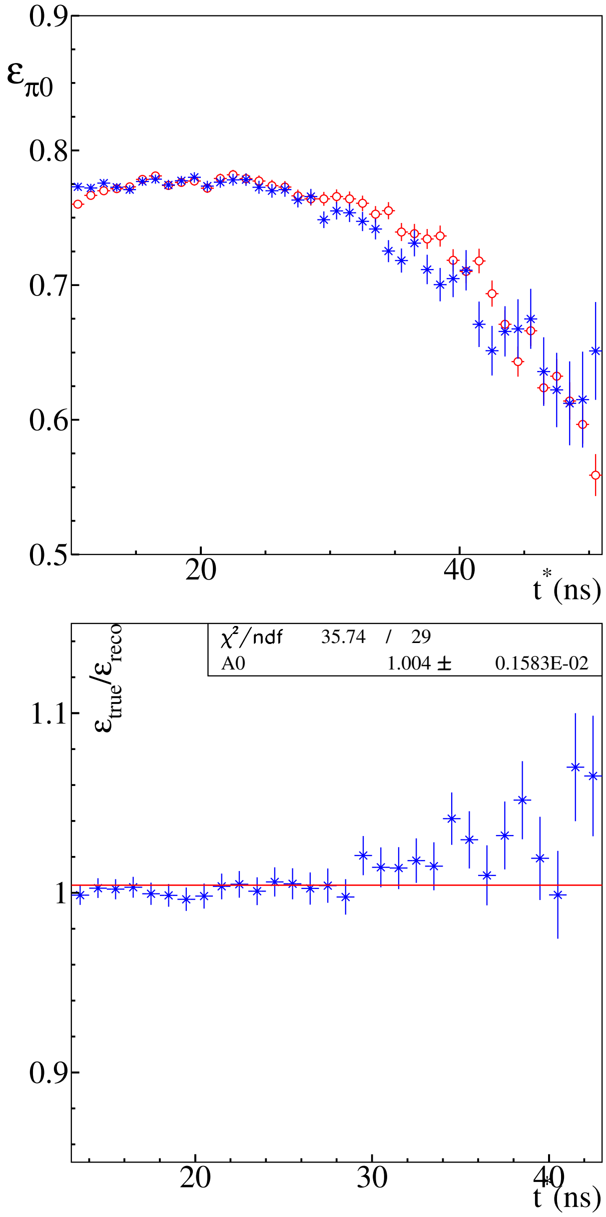

Figure 41: Above: the comparison the π^0 reco efficiency (blue) and the π^0 true efficiency (red) as function of the charged kaon proper time, restricting ourselves to events with a π^0 in the final state for the normalizations. Below: the ratio of the π^0 true efficiency over the π^0 reco efficiency, both normalized to events with a π^0 in the final state.

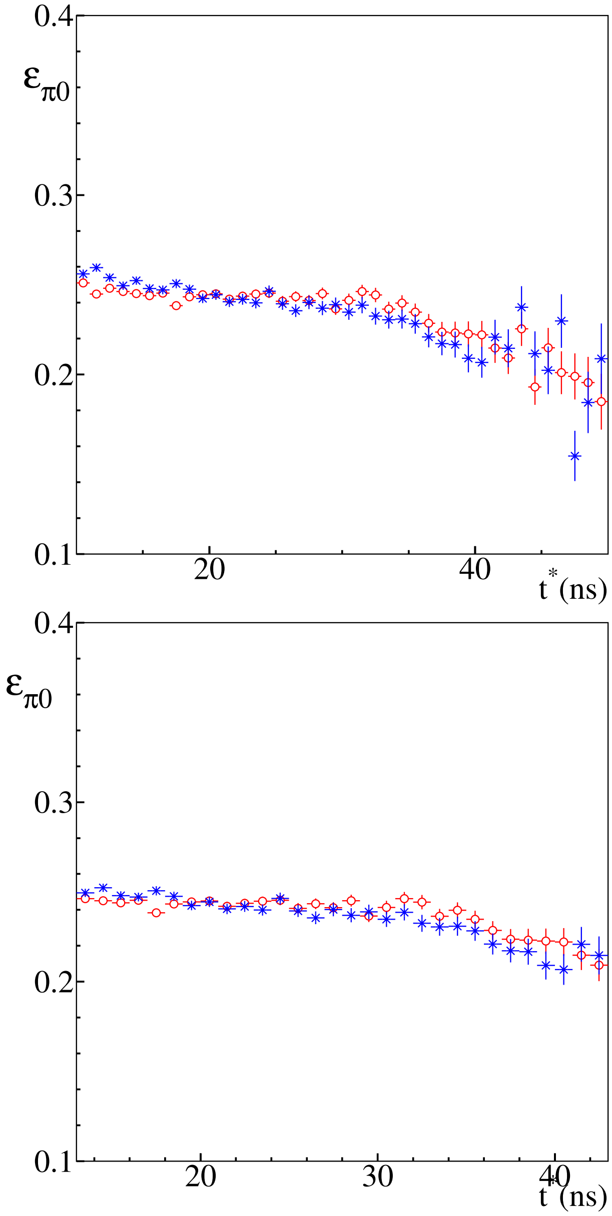

Figure 42: Comparison the π^0 reco efficiency of reconstructing the $\pi^0 \to \gamma\gamma$ vertex evaluated on data (blue) and on MonteCarlo data-like (red) as function of the charged kaon proper time.

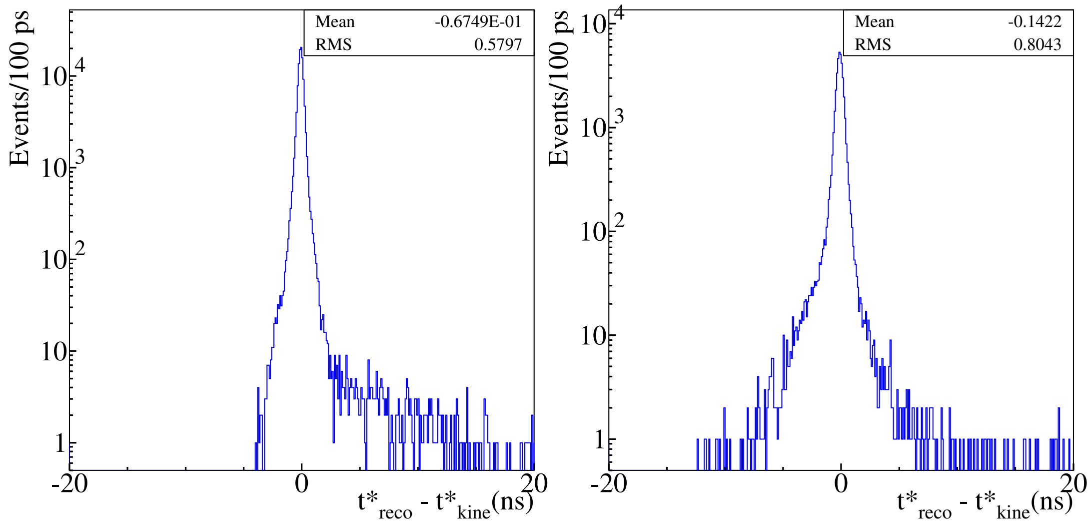

Figure 43: Left. Resolution curve for charged kaon proper time between 8 and 10 ns. Right. Resolution curve for charged kaon proper time between 20 and 22 ns.

the figures 44 and45, we obtain very good results. Therefore we can estimate the charged kaon proper time using the stepping procedure, from the IP to the point of closest approach between the kaon and the charged secondary tracks, and taking into account the energy loss given by the Bethe-Bloch formula. The proper time resolution curve is then defined as the distribution given by the difference between the charged kaon proper time estimated using the point of closest approach and the one obtained using the reconstructed decay vertex in the DC. We obtain the distribution shown in the figure 46. For each bin of the $K^{\pm}$ proper time a different resolution curve is measured.
It 's important to emphasize that this technique can be used also on data and the obtained distribution is shown in figure 47. We can also compare the proper time resolution curves obtained for data and MonteCarlo data-like samples, the results is shown in figure 48. For the fit to the proper time distribution we use the true resolution functions corrected by the ratio of the resolution function obtained with the PCA technique evaluated on data and on MC data-like:

$$Res_{\rm data} = Res_{\rm true} \times \frac{Res_{\rm PCA}(data)}{Res_{\rm PCA}(MC)}. \tag{68}$$

7.2 Second method: evaluation of resolution

As for the first method the resolution functions depend on the charged kaon proper time, see figure 49. The peaks visible at ± 2.7 and ± 5.4 ns are due to wrong determinations of the bunch giving the global T^0_ϕ of the event, that gives a wrong value

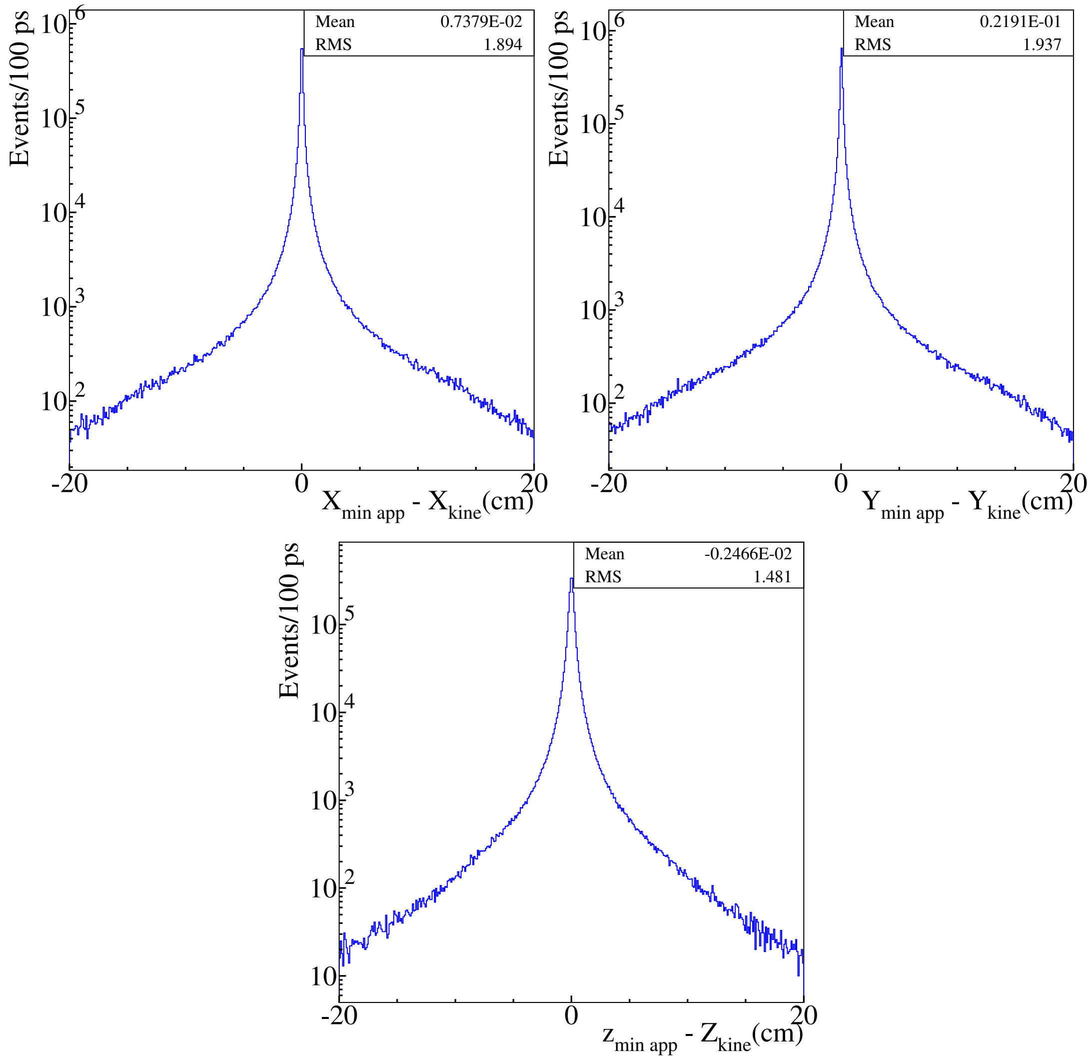

Figure 44: Resolution curves given by the minimum approach technique for charged kaon position along the x, y and z axis.

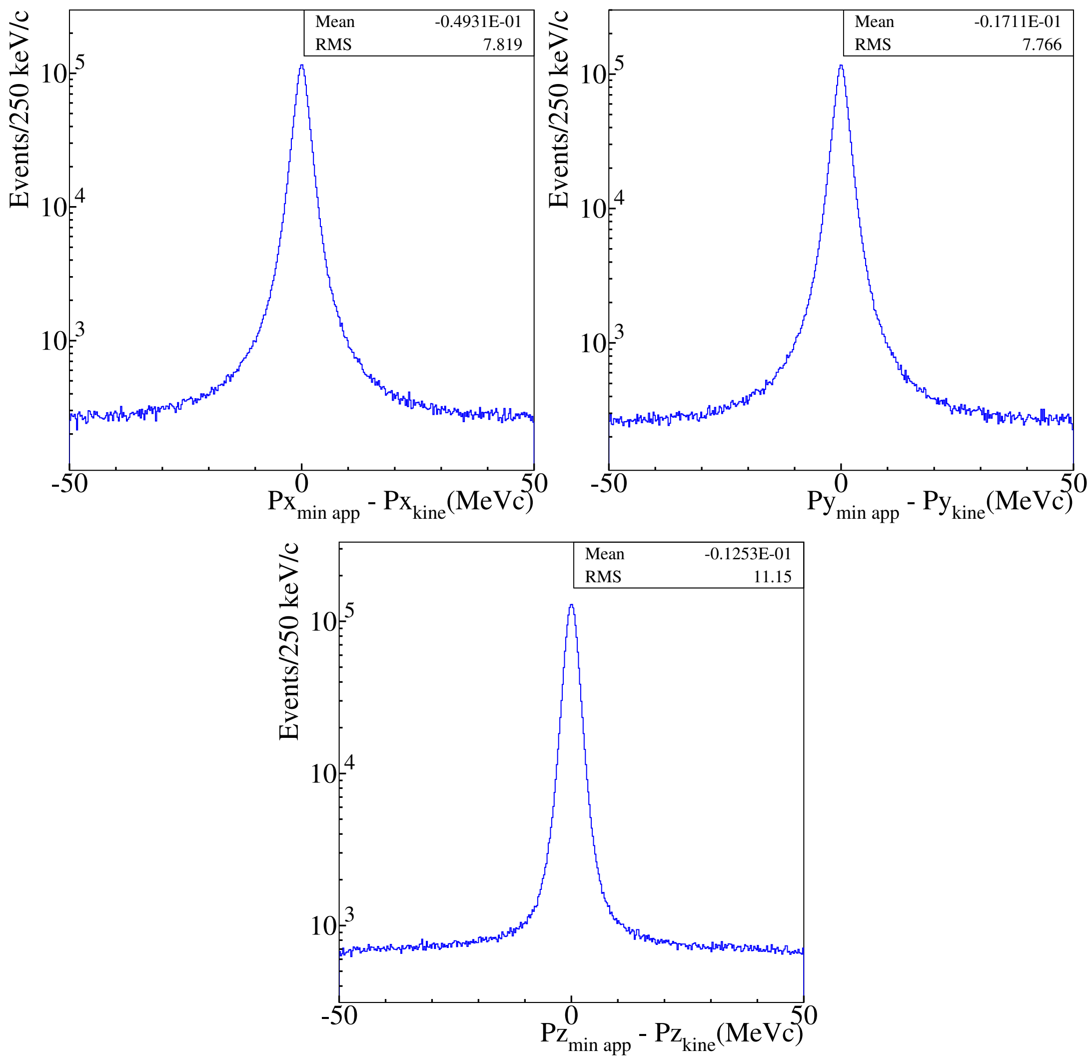

Figure 45: Resolution curves given by the minimum approach technique for charged kaon momentum along the x, y and z axis.

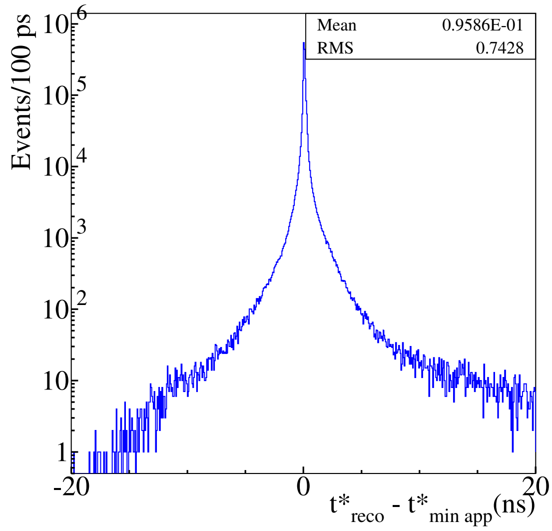

Figure 46: Proper time resolution curve given by the minimum approach technique evaluated on MonteCarlo data-like.

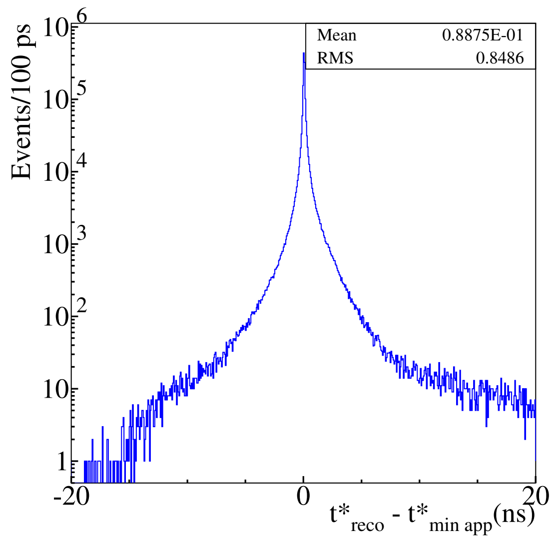

Figure 47: Proper time resolution curve given by the minimum approach technique on data.

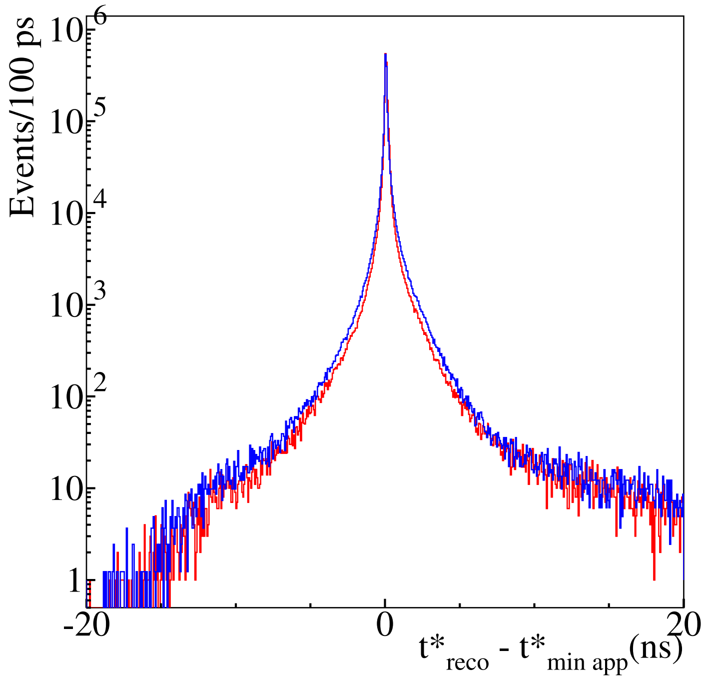

Figure 48: Comparison of the proper time resolution curves obtained by the minimum approach technique from data (blue) and from MonteCarlo (red) compared.

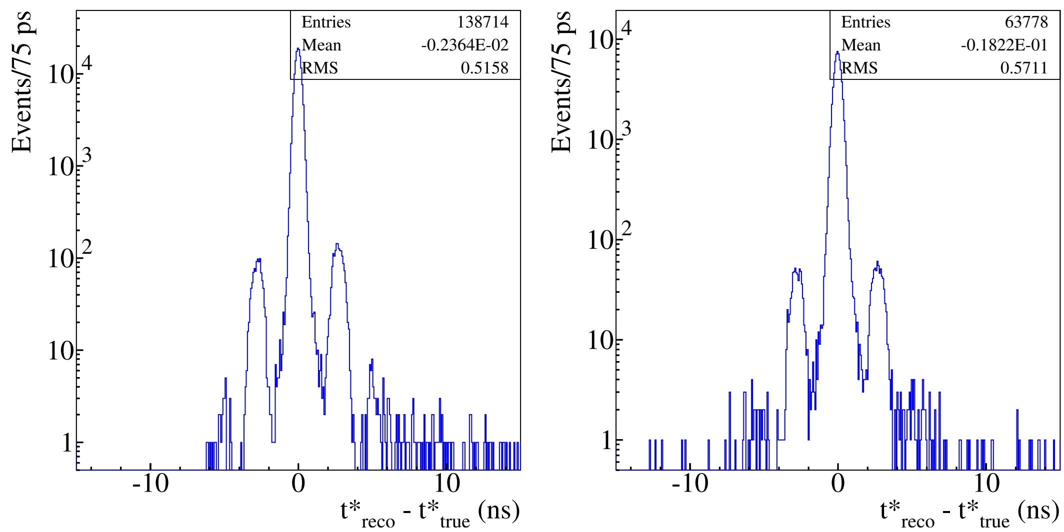

Figure 49: Left. Resolution curve for charged kaon proper time between 10 and 12 ns. Right. Resolution curve for charged kaon proper time between 20 and 22 ns.

of the ϕ meson decay time. Also for this method, in order to be less sensitive to the MonteCarlo simulation, we implemented a technique to smear by data the resolution functions evaluated using the MonteCarlo simulation. We define the $\gamma\gamma$ resolution curves, shown in figure 50, as the difference between the charged kaon time of flight given by the two photons:

$$\Delta t = (t_{cl_1} - \frac{\Delta x_1}{c}) - (t_{cl_2} - \frac{\Delta x_2}{c}) \tag{69}$$

where t_{cl_i} is the time of the cluster and Δx_i is the distance between the neutral cluster and the kaon decay vertex. These resolution functions can be evaluated on MonteCarlo data-like and on data. As it can be seen in figure 50, the $\gamma\gamma$ resolution curves are not able to take into account the resolution effects due to a wrong ϕ decay time, which is common to all time measurements in the event and cancels out exactly in the difference.

In order to evaluate also this effect we estimate the difference, $t^*_{\pi^0} - t^*_{cv}$, between the proper time given by the charged vertex technique and the proper time given by the $\pi^0 \to \gamma\gamma$ vertex technique, figure 51, on data and on MonteCarlo data-like.

The proper time given by the last technique is obtained from EMC information, which are dependent on the ϕ meson decay time, while the proper time given by the charged vertex technique is obtained from DC information which is not dependent on ϕ decay time.

On data we correct the true resolution functions core by the ratio of the $\gamma\gamma$ resolution curves evaluated on data over the $\gamma\gamma$ resolution curves evaluated on MonteCarlo data-like; we correct the peaks at ± 2.7 and ± 5.4 ns by the ratio of $t^*_{\pi^0} - t^*_{cv}$ resolution curves evaluated on data over $t^*_{\pi^0} - t^*_{cv}$ resolution curves evaluate on MC data-like:

$$Res_{\text{data}} = Res_{\text{true}} \times \frac{Res_{\gamma\gamma}(data)}{Res\gamma\gamma(MC)} + Res^{t\phi}_{true} \times \frac{t^*_{\pi^0} - t^*_{cv}(data)}{t^*_{\pi^0} - t^*_{cv}(MC)}, \tag{70}$$

where Res_{true} are the resolution functions given by the MonteCarlo true, defined as the difference between the charged kaon proper time evaluated on MonteCarlo data-like and the charged kaon proper time given by the MonteCarlo true; $Res_{\gamma\gamma}(data)$ and $Res_{\gamma\gamma}(MC)$ are the $\gamma\gamma$ resolution curves evaluated on data and on MonteCarlo data-like respectively; $t^*_{\pi^0} - t^*_{cv}(data)$ is the difference between the proper time given by the $\pi^0 \to \gamma\gamma$ vertex technique and the proper time given by the charged vertex technique evaluated on data and $t^*_{\pi^0} - t^*_{cv}(MC)$ is the same difference evaluated on MonteCarlo data-like.

8 The fit of the proper time distribution

The last step is to obtain the charged kaon lifetime fitting the proper time distribution. For both the methods we use a function given by the convolution of the exponential decay function and the resolution function, estimated bin by bin. We

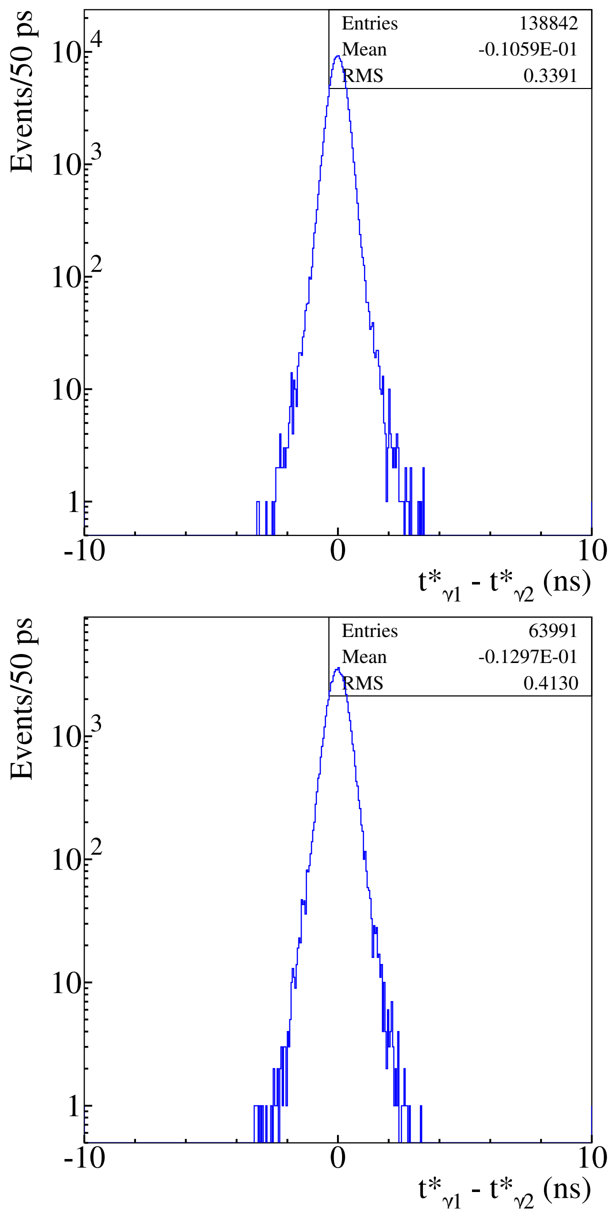

Figure 50: Left. $\gamma\gamma$ resolution curve for charged kaon proper time between 10 and 12 ns. Right. $\gamma\gamma$ resolution curve for charged kaon proper time between 20 and 22 ns.

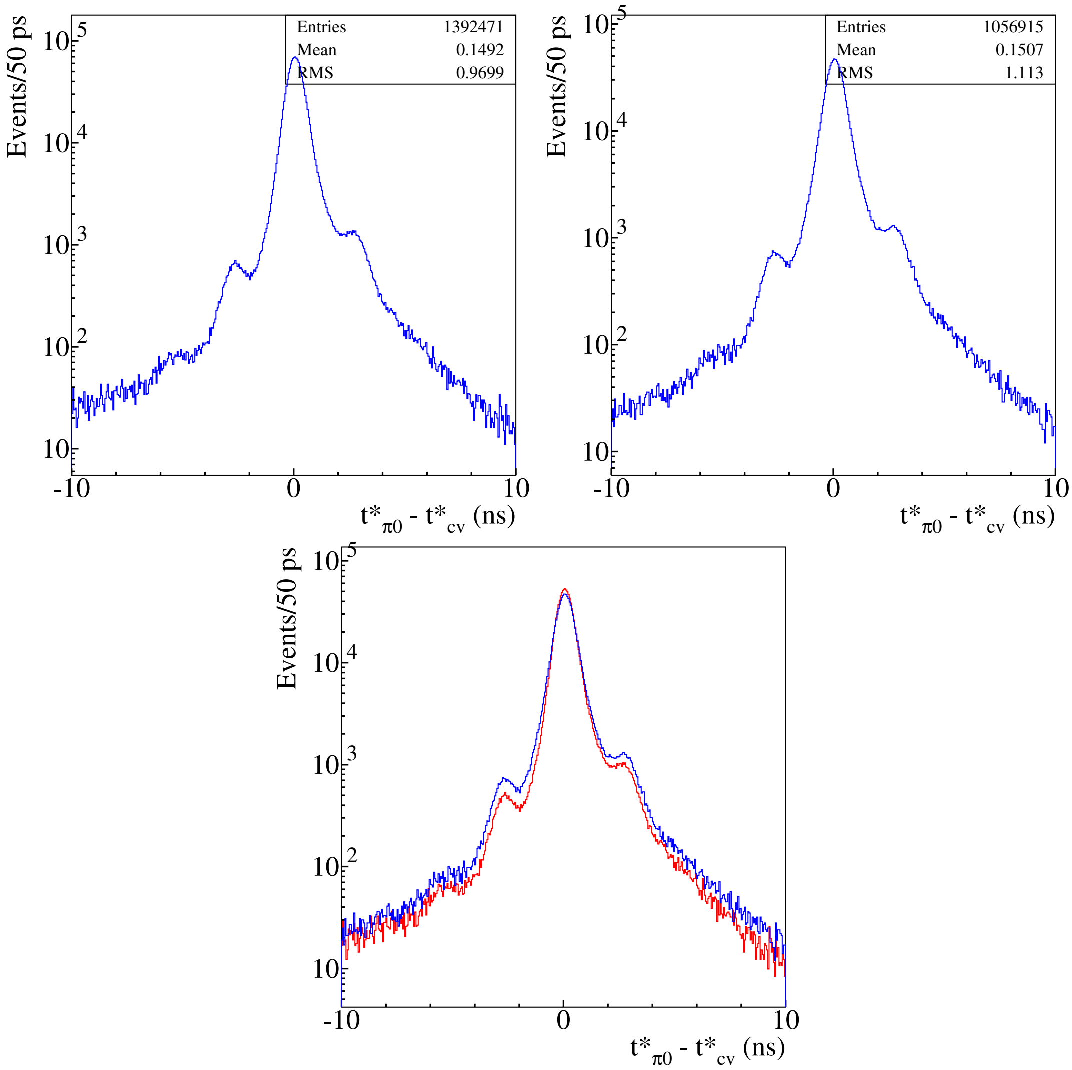

Figure 51: $t^*_{\pi^0} - t^*_{cv}$ resolution curves, evaluated on MonteCarlo data-like, above on the left. $t^*_{\pi^0} - t^*_{cv}$, resolution curves evaluated on data, above on the right. Comparison between data (blue) and MonteCarlo (red).

notice anyhow that the measured distributions, corrected bin by bin for the efficiency exhibits a nicely exponential behavior, even with no smearing correction for both the methods (see figures 52 and 53). To fit to the proper time distribution, obtained on MonteCarlo data-like or on data, we use an histogram, the *expected* histo. This is built in the following way. The number of entries in each bin of the *expected* histo is given by the integral of the exponential decay function, which depends on one parameter only, the lifetime, and corrected for the efficiency curve and for all the corrections to the efficiency curve, self trigger tag efficiency or MonteCarlo true vs MonteCarlo reco correction. Then a smearing matrix accounts for the effect of the resolution. For each bin, j, we obtain a χ^2-like variable which is so defined:

$$\chi_j^2 = \frac{(N_j^{observed} - N_j^{expected})^2}{(\sigma_j^{fit})^2} \tag{71}$$

where $N_j^{observed}$ is the number of entries in the j-th bin of the proper time histogram, $N_j^{expected}$ is the number of entries in the j-th bin of *expected* histo and σ_j^{fit} is the statistic fluctuation in the j-th bin of the *expected* histo. The χ^2 variable to be minimized is:

$$\chi^2 = \sum_{j=1}^{Nbins} \chi_j^2 \ . \tag{72}$$

We can build our *expected* histo in the more convenient range, given by the one in which we have a good agreement between the true and the reco efficiencies. To take into account the resolution effects, we have allowed the migration from/to the bins used in the fit for a slightly larger range.

The range have to be divided in slices of the order of few nanoseconds in which we evaluate the resolution functions. The choice of the bin size is done in order to reduce the statistical fluctuation of the resolution measurement.

Using these resolution functions we can build the $n \times n$ smearing matrix, S_{nn}, with n equal to the number of bins in which we have divided the proper time distribution. Each element of S_{nn}, s_{ji}, gives the fraction of events generated in the i-th bin but reconstructed in the j-th bin. Therefore the content of the j-th bin of the *expected* histo, ($N_j^{expected}$), is:

$$N_j^{expected} = \sum_{i=1}^{Nbins} s_{ji} \times \epsilon_i \times \epsilon_i^{corr} \times N_i^{theo}, \tag{73}$$

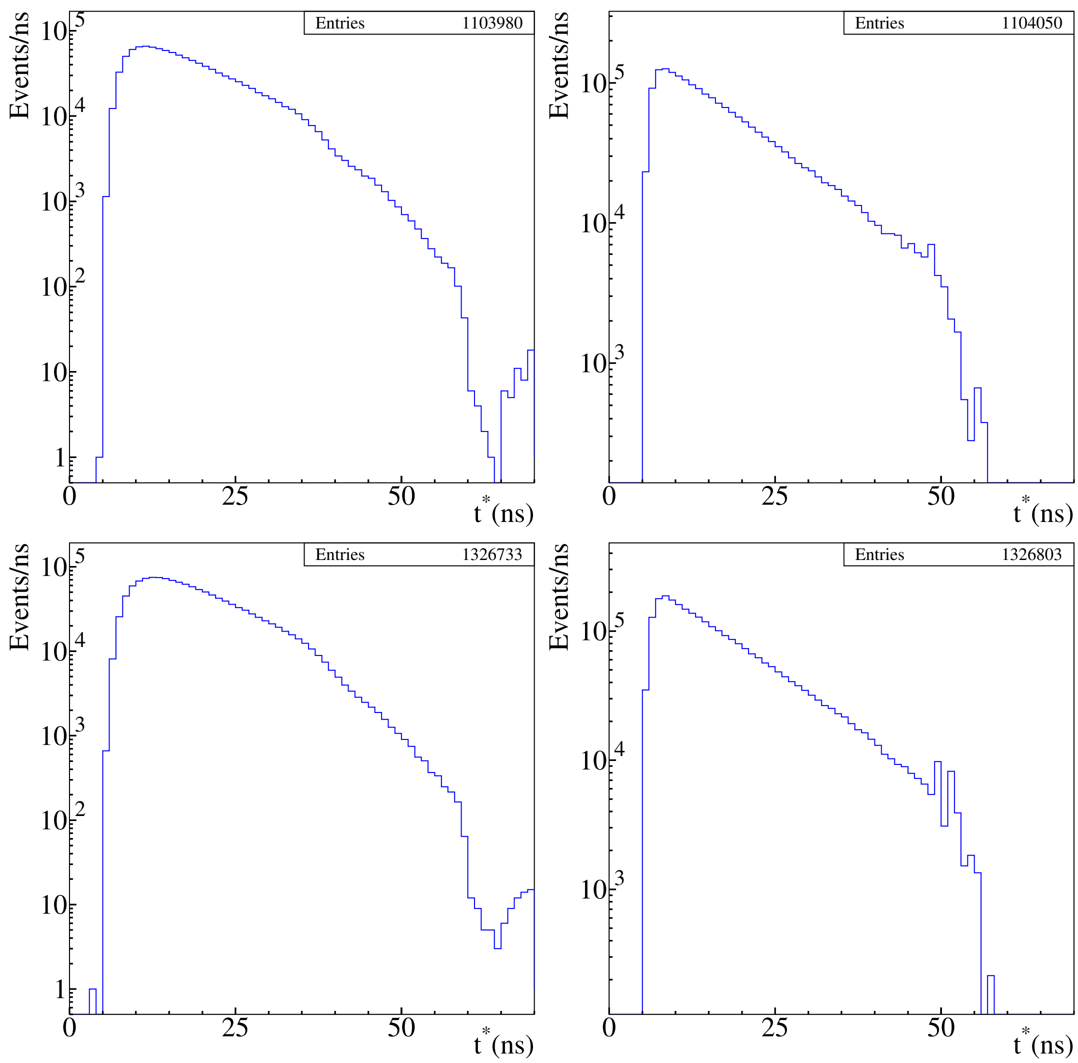

Figure 52: First method:above on the left the proper time distribution in logarithmic scale, evaluated on a MonteCarlo data-like; above on the right the same distribution divided, bin by bin, by its efficiency evaluated on a MonteCarlo data-like sample; below on the left the proper time distribution in logarithmic scale, evaluated on a data sample; below on the right the same distribution divided, bin by bin, by its efficiency curve evaluated on a data sample.

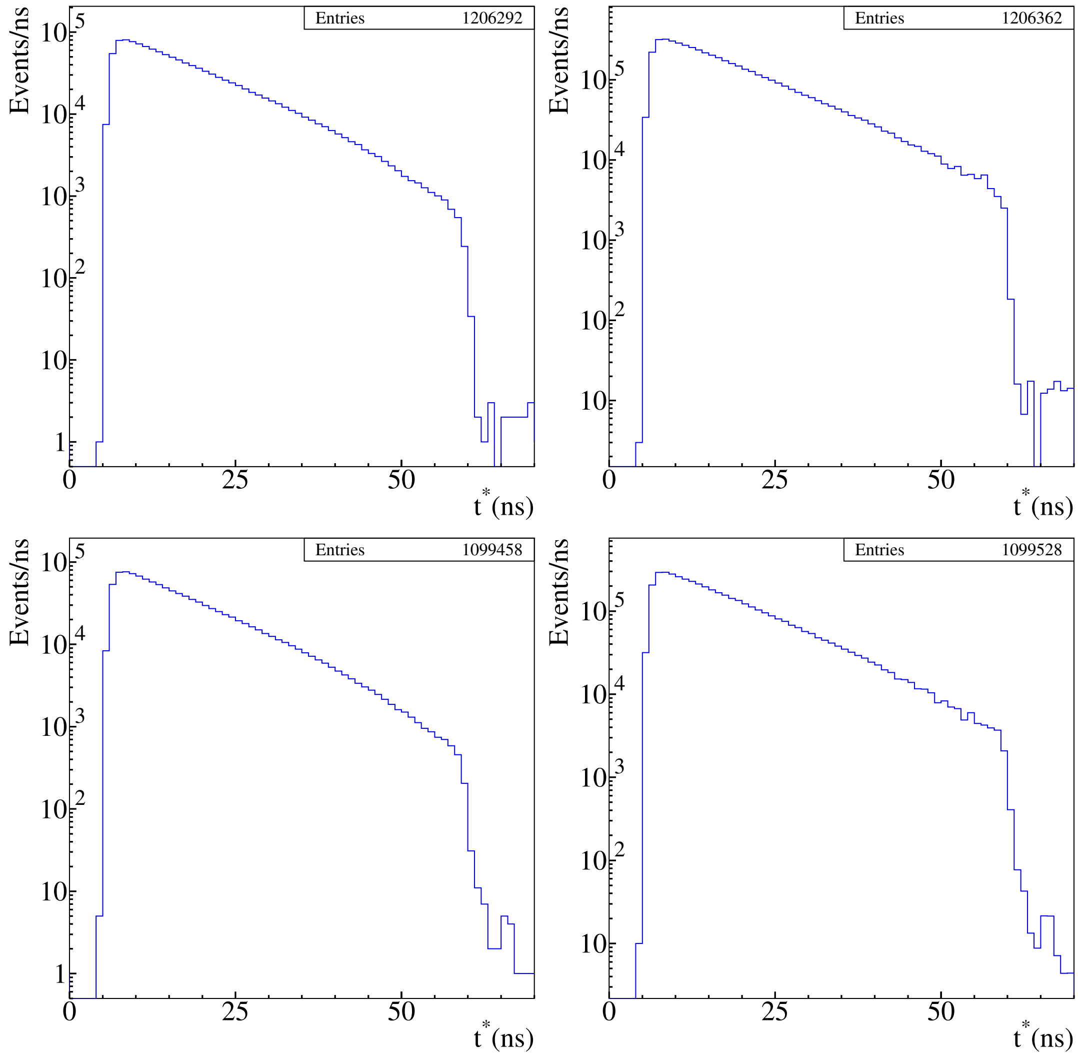

Figure 53: Second method:above on the left the proper time distribution in logarithmic scale, evaluated on a MonteCarlo data-like; above on the right the same distribution divided, bin by bin, by its efficiency evaluated on a MonteCarlo data-like sample; below on the left the proper time distribution in logarithmic scale, evaluated on a data sample; below on the right the same distribution divided, bin by bin, by its efficiency curve evaluated on a data sample.

where ϵ_i is the measured reconstruction efficiency and ϵ_i^{corr} the tiny correction of O(10^{-3}) to be applied to the efficiency accounting for the ratio between the MonteCarlo data-like and MonteCarlo true efficiencies. The statistical fluctuations of the *expected* histo are given by the sum of the statistical fluctuation of the efficiency, the statistical fluctuation of its correction and the poissonian fluctuation of the *expected* histo:

$$\sigma_j^{fit} = \sqrt{\sum_{i=1}^{Nbins} (s_{ji} \times \sigma_{\epsilon_i} \times \epsilon_i^{corr} \times N_i^{theo} \oplus s_{ji} \times \epsilon_i \times \sigma_{\epsilon_i^{corr}} \times N_i^{theo}) \oplus \sqrt{N_j^{expected}}}. \tag{74}$$

Now we are ready to fit the proper time distribution, for both the methods. We use a bin size of 1 ns in order to reduce the statistical fluctuations and the relative importance of the smearing corrections. We perform the fit on a MonteCarlo data-like sample to check the reliability of the procedure.

8.1 Fit of the proper time distribution obtained from the kaon decay length

We build the *expected* histo in the region between 12 and 40 ns.
The fit range has been divided in resolution bins of the order of 1 ns for a total of 28 different resolution functions.
On MonteCarlo data-like we made the fit in the region between 15 and 35 ns and we obtained:

$$\tau^+ = (12.39 \pm 0.04)\ \text{ns} \qquad \chi^2/\text{ndf} = 0.46 \qquad \text{P}_{\text{chi}^2} = 97.5\%\ . \tag{75}$$

For the K^-, in the region between 15 and 35 ns, we obtained:

$$\tau^- = (12.36 \pm 0.04)\ \text{ns} \qquad \chi^2/\text{ndf} = 0.85 \qquad \text{P}_{\text{chi}^2} = 63.5\%\ . \tag{76}$$

These values have to be compared with the one used by the simulation $\tau^\pm$ =12.36 ns. As shown in the previous figures 54 and 55 the agreement between data-like distribution and *expected* histo distribution is very good for both the charges and the values obtained are in agreement with the MonteCarlo simulation input.
It is interesting to look at the plot of the residuals and of the normalized residuals, fig 56. The first ones are defined as the bin by bin differences between the entries of the proper time histogram and the entries of *expected* histo, the second ones are the residuals divided by σ^{fit}. As shown in the previous figures 56 and 57, fitting

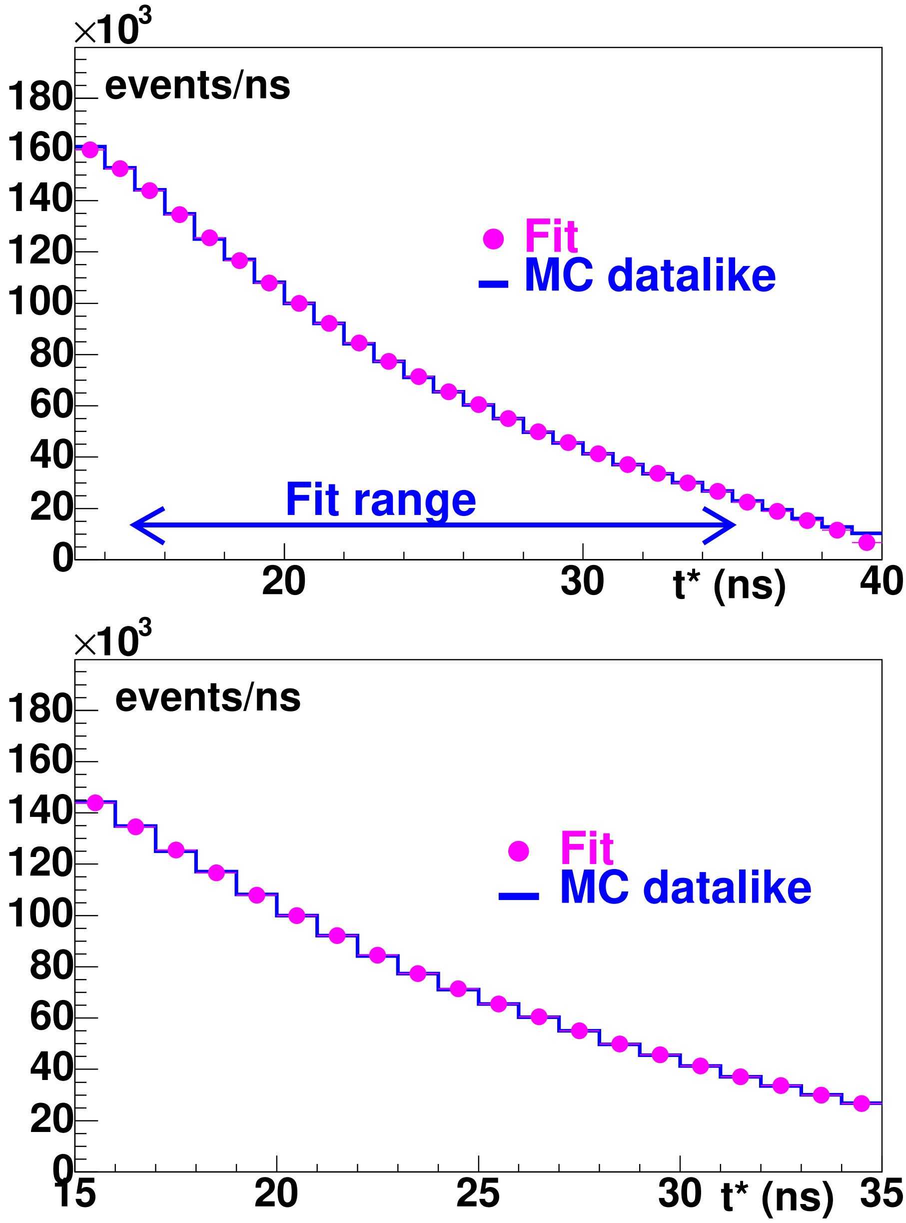

Figure 54: Fit to the K^+ proper time distribution: in blue the MonteCarlo data-like distribution, in pink the *expected* histo distribution.

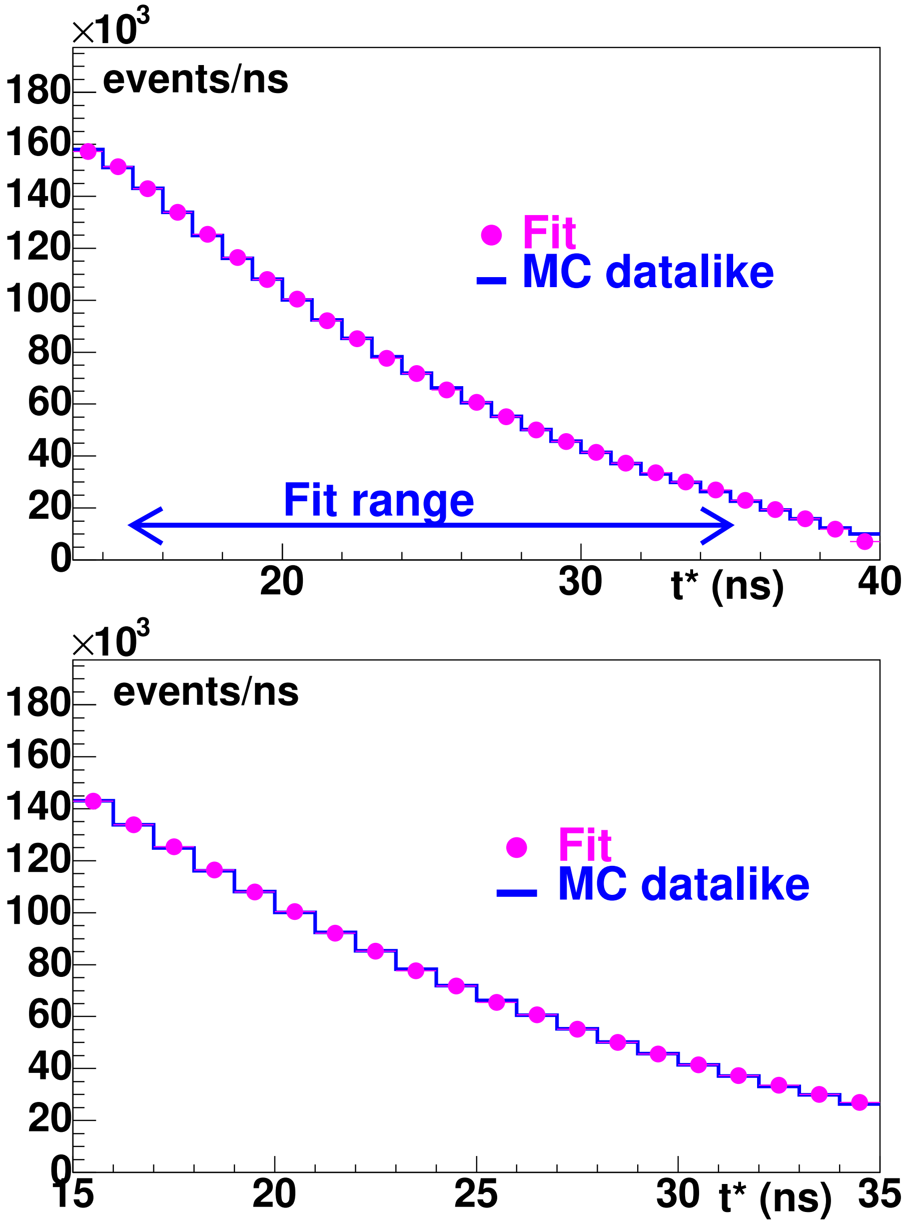

Figure 55: Fit to the K^- proper time distribution: in blue the MonteCarlo data-like distribution, in pink the *expected* histo distribution.

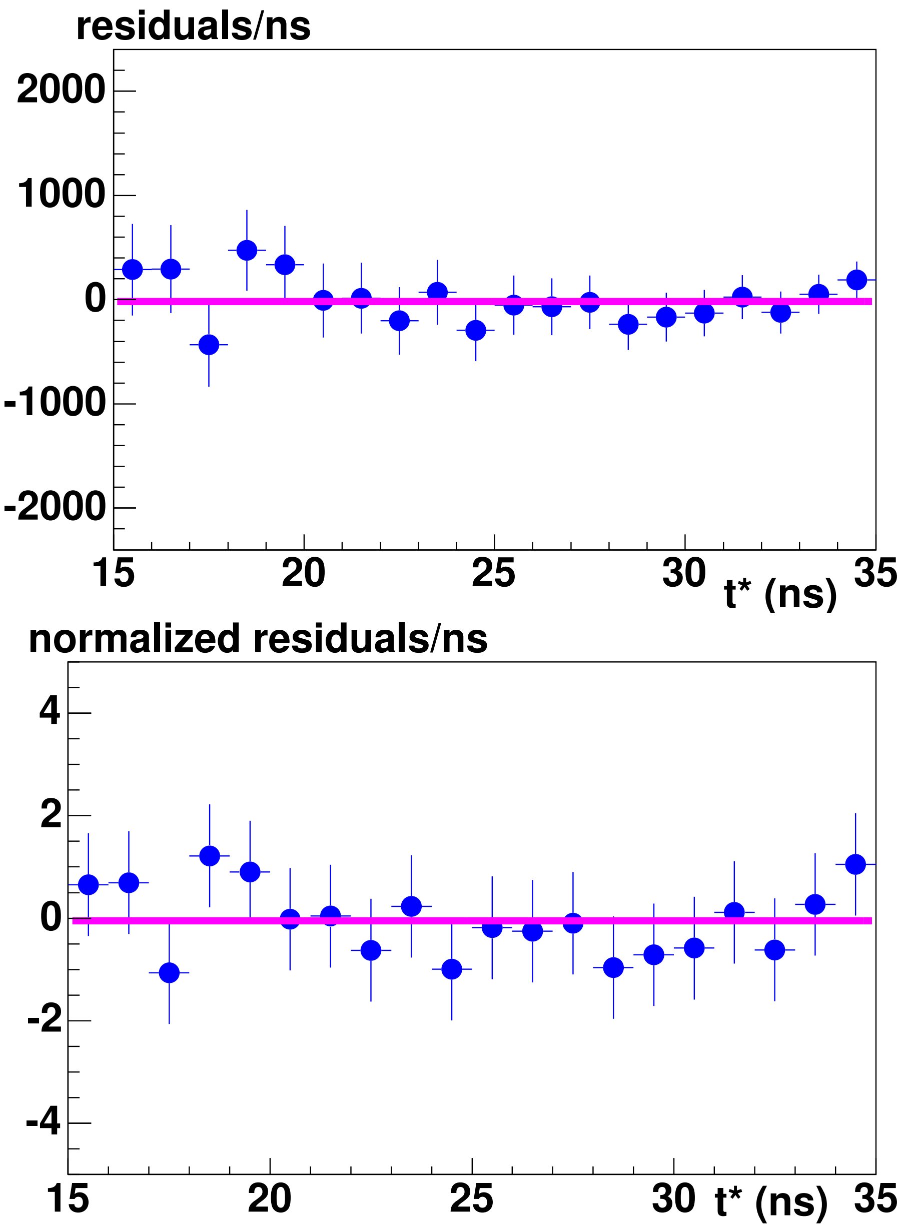

Figure 56: K^+ residuals and the normalized residuals, in the region between 15 and 35 ns, fitted with a constant, are shown.

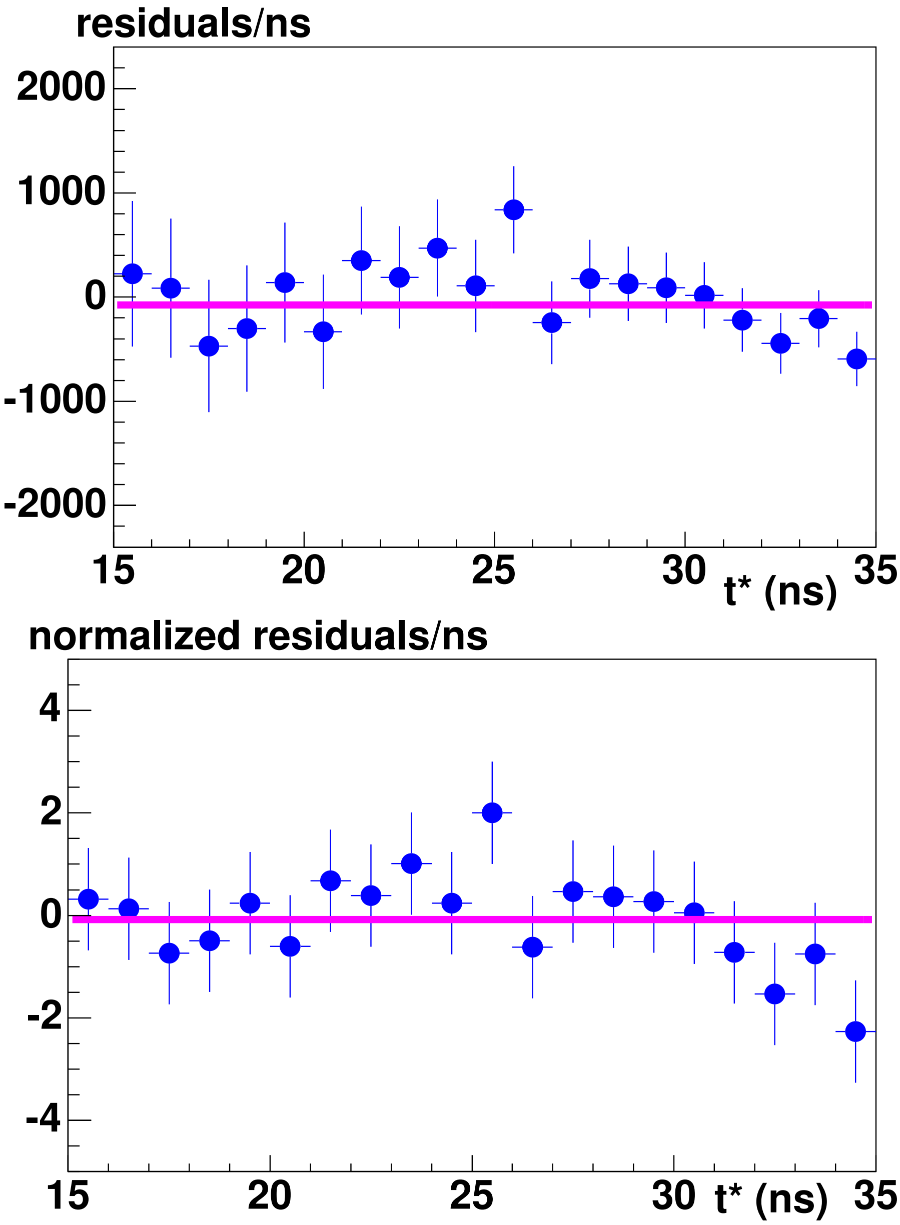

Figure 57: K^- residuals and the normalized residuals, in the region between 15 and 35 ns, fitted with a constant are shown.

the residuals and the normalized residuals plots with a constant function we obtain a value compatible with zero:

$$const^{+}_{\text{res}} = -19. \pm 60. \qquad P_{\chi^2} = 97\% \tag{77}$$
$$const^{+}_{\text{norm res}} = -0.05 \pm 0.22 \qquad P_{\chi^2} = 97\% \tag{78}$$
$$const^{-}_{\text{res}} = -75. \pm 88. \qquad P_{\chi^2} = 68\% \tag{79}$$
$$const^{-}_{\text{norm res}} = -0.08 \pm 0.22 \qquad P_{\chi^2} = 64\%. \tag{80}$$
$$\tag{81}$$

We also use a toy MonteCarlo to generate data with different lifetimes for both the charges. In particular we generate about 60 pb$^-$1 of MonteCarlo data-like with lifetimes equal to 11, 12, 13 and 14 ns.
Fitting the histograms obtained with these MonteCarlo data-like samples, the results are:

$$\tau^{+}_{11} = (10.98 \pm 0.08) \text{ ns} \tag{82}$$
$$\tau^{-}_{11} = (11.02 \pm 0.08) \text{ ns} \tag{83}$$
$$\tau^{+}_{12} = (11.98 \pm 0.09) \text{ ns} \tag{84}$$
$$\tau^{-}_{12} = (12.02 \pm 0.09) \text{ ns} \tag{85}$$
$$\tau^{+}_{13} = (12.97 \pm 0.09) \text{ ns} \tag{86}$$
$$\tau^{-}_{13} = (13.02 \pm 0.09) \text{ ns} \tag{87}$$
$$\tau^{+}_{14} = (13.97 \pm 0.10) \text{ ns} \tag{88}$$
$$\tau^{-}_{14} = (14.01 \pm 0.10) \text{ ns} \tag{89}$$
$$\tag{90}$$

These are indicator of the goodness of our method and make us confident about its application for the fit of the proper time distribution obtained on data. On data, concerning the K^+ lifetime, we made the fit in the region between 15 and 35 ns and we obtained:

$$\tau^{+} = (12.338 \pm 0.042) \text{ ns} \qquad \chi^2/\text{ndf} = 1.01 \qquad \text{P}_{\chi^2} = 44.7\% \;. \tag{91}$$

While for the K^- we fit in the range between 15 and 35 ns and we obtained:

$$\tau^{-} = (12.395 \pm 0.045) \text{ ns} \qquad \chi^2/\text{ndf} = 1.42 \qquad \text{P}_{\chi^2} = 10.8\% \;. \tag{92}$$

As shown in the previous figures 58 and 59 the agreement between data distribution and *expected* histo distribution is very good for both the charges.
For both the charges the distribution of residuals and of the normalized residuals is

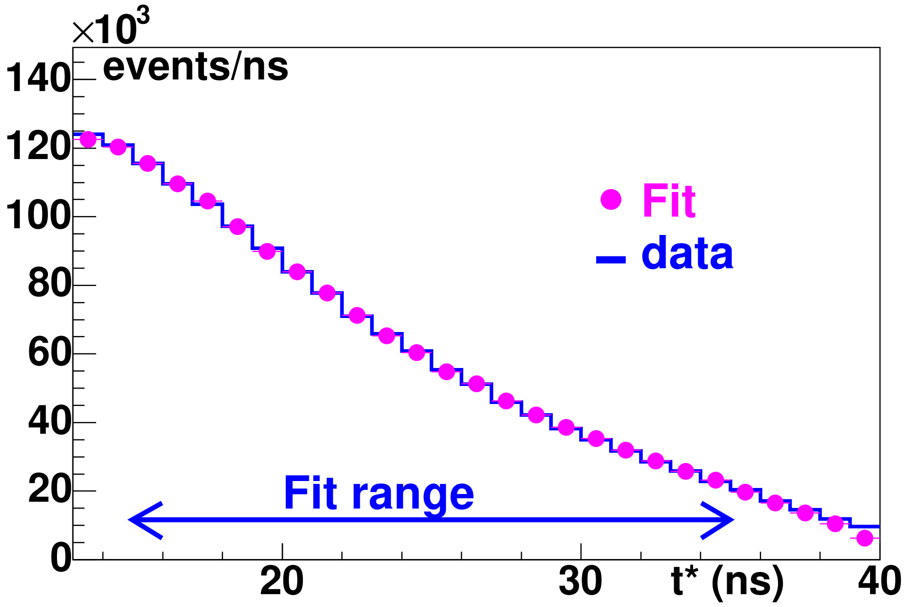

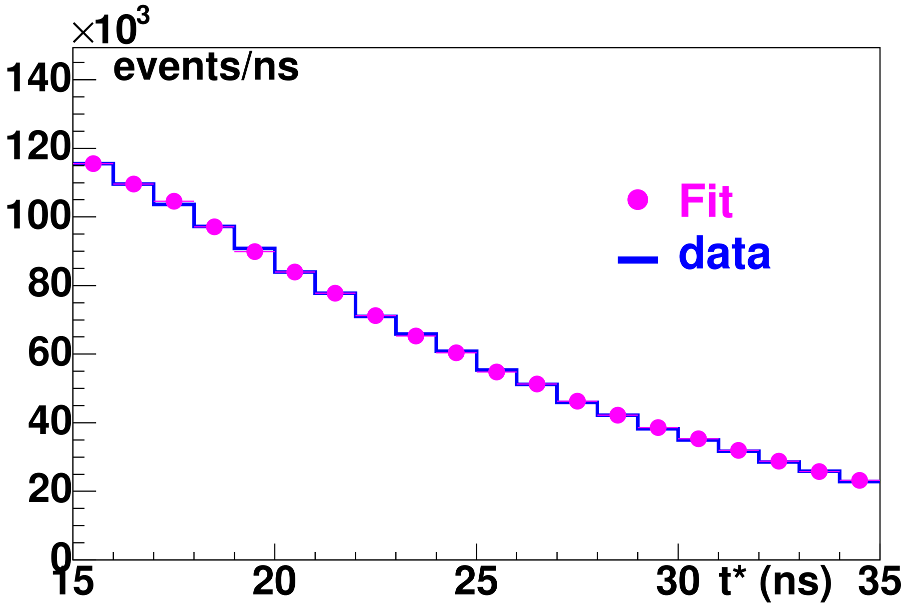

Figure 58: Fit to the K^+ proper time distribution: in blue the data distribution, in pink the *expected* histo distribution.

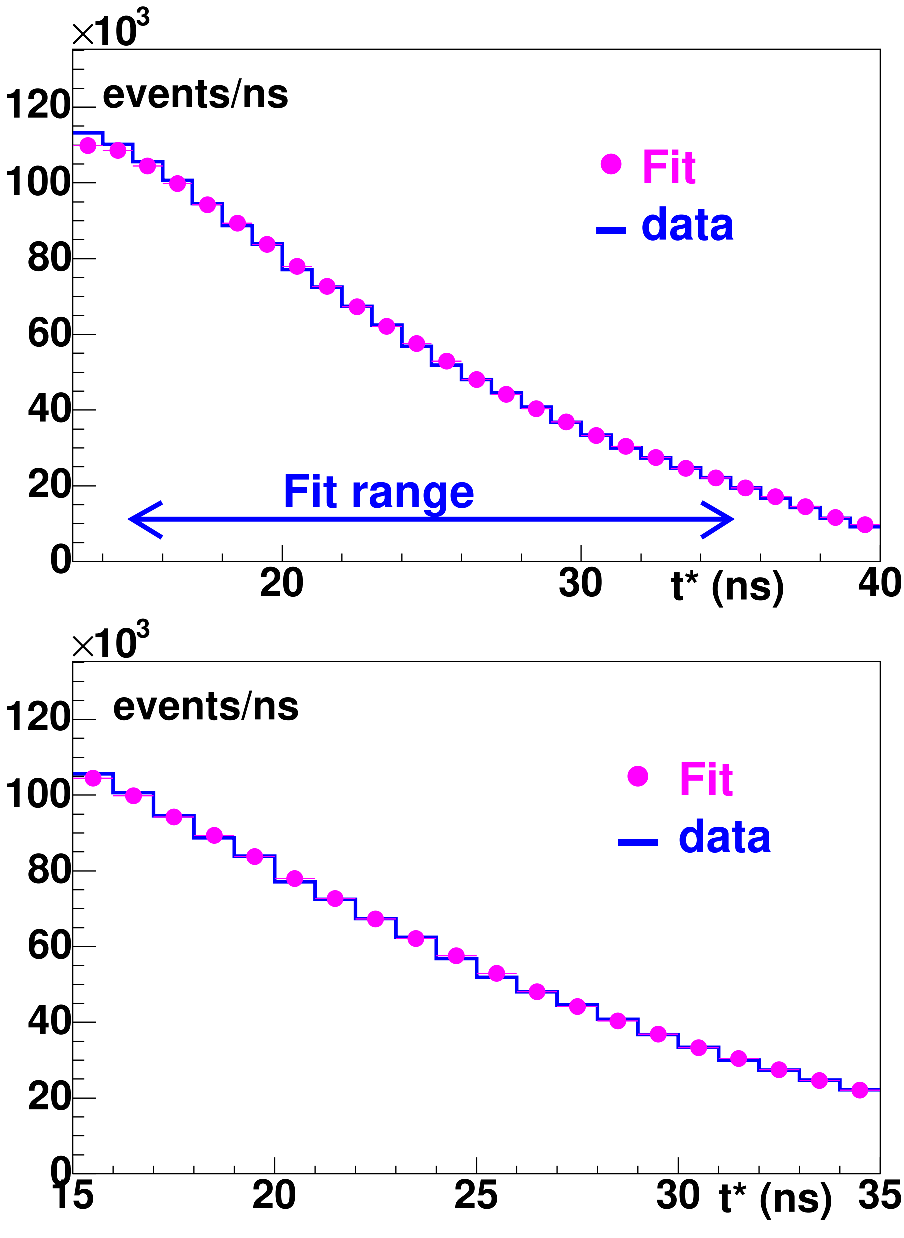

Figure 59: Fit to the K^- proper time distribution: in blue the data distribution, in pink the *expected* histo distribution.

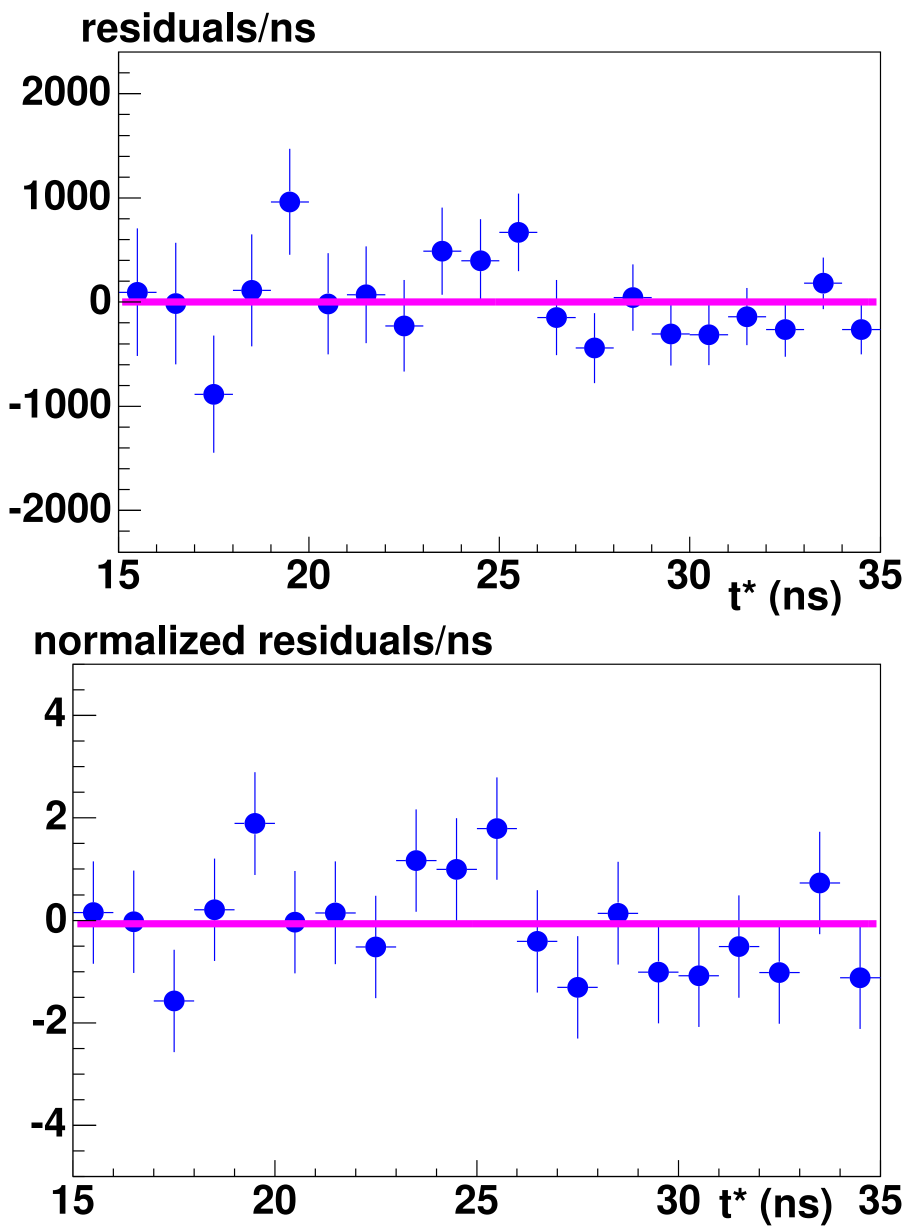

Figure 60: K^+ residuals and the normalized residuals, in the region between 15 and 35 ns, fitted with a constant.

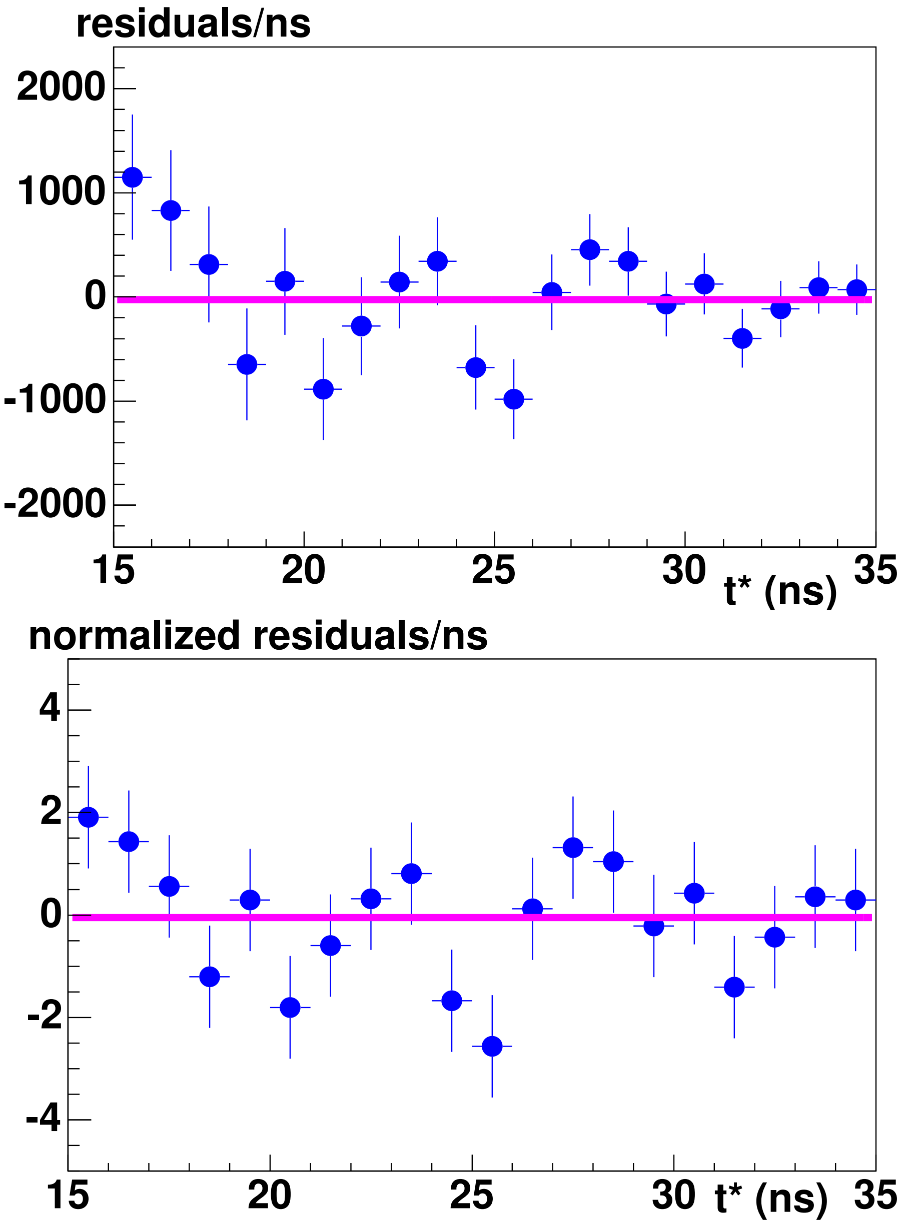

Figure 61: K^- residuals and the normalized residuals, in the region between 15 and 35 ns, fitted with a constant.

very good and compatible with a constant function equal to zero. As shown in the previous figures, fitting the residuals and the normalized residuals with a constant the values obtained are in agreement with zero:

$$const^{+}_{\text{res}} = 0.0 \pm 1.4 \qquad P_{\chi^2} = 45.\% \tag{93}$$
$$const^{+}_{\text{norm res}} = -0.06 \pm 0.22 \qquad P_{\chi^2} = 45.\% \tag{94}$$
$$const^{-}_{\text{res}} = -25. \pm 80. \qquad P_{\chi^2} = 11.\% \tag{95}$$
$$const^{-}_{\text{norm res}} = -0.05 \pm 0.22 \qquad P_{\chi^2} = 11.\%. \tag{96}$$
$$\tag{97}$$

The measurements obtained for the different charges are in agreement with each other. Their weighted mean is:

$$\tau = (12.364 \pm 0.031) \text{ ns}. \tag{98}$$

8.2 Fit to the proper time distribution obtained from the kaon decay time

We build the *expected* histo in the region between 10 and 50 ns.
The fit range has been divided in bins of the order of few nanoseconds for a total of 17 different resolution functions. In particular the interval between 10 and 40 ns has been divided in bins of 2 ns. The last two resolution functions have been obtained in the intervals between 40 and 45 ns and between 45 and 50 ns.
On MonteCarlo data-like we made the fit in the region between 13 and 40 ns and we obtained as best value:

$$\tau^{+} = (12.39 \pm 0.04) \text{ ns} \qquad \chi^2/\text{ndf} = 0.43 \qquad \text{P}_{\chi^2} = 99.4\%. \tag{99}$$

For the K^{-}, in the region between 12 and 40 ns, we obtain as best value:

$$\tau^{-} = (12.30 \pm 0.04) \text{ ns} \qquad \chi^2/\text{ndf} = 0.81 \qquad \text{P}_{\chi^2} = 73.\%. \tag{100}$$

As shown in the previous figures 62 and 63 the agreement between data-like distribution and *expected* histo distribution is very good for both the charges and the values obtained are in agreement with the MonteCarlo simulation input, $\tau^{\pm}$ =12.36 ns.

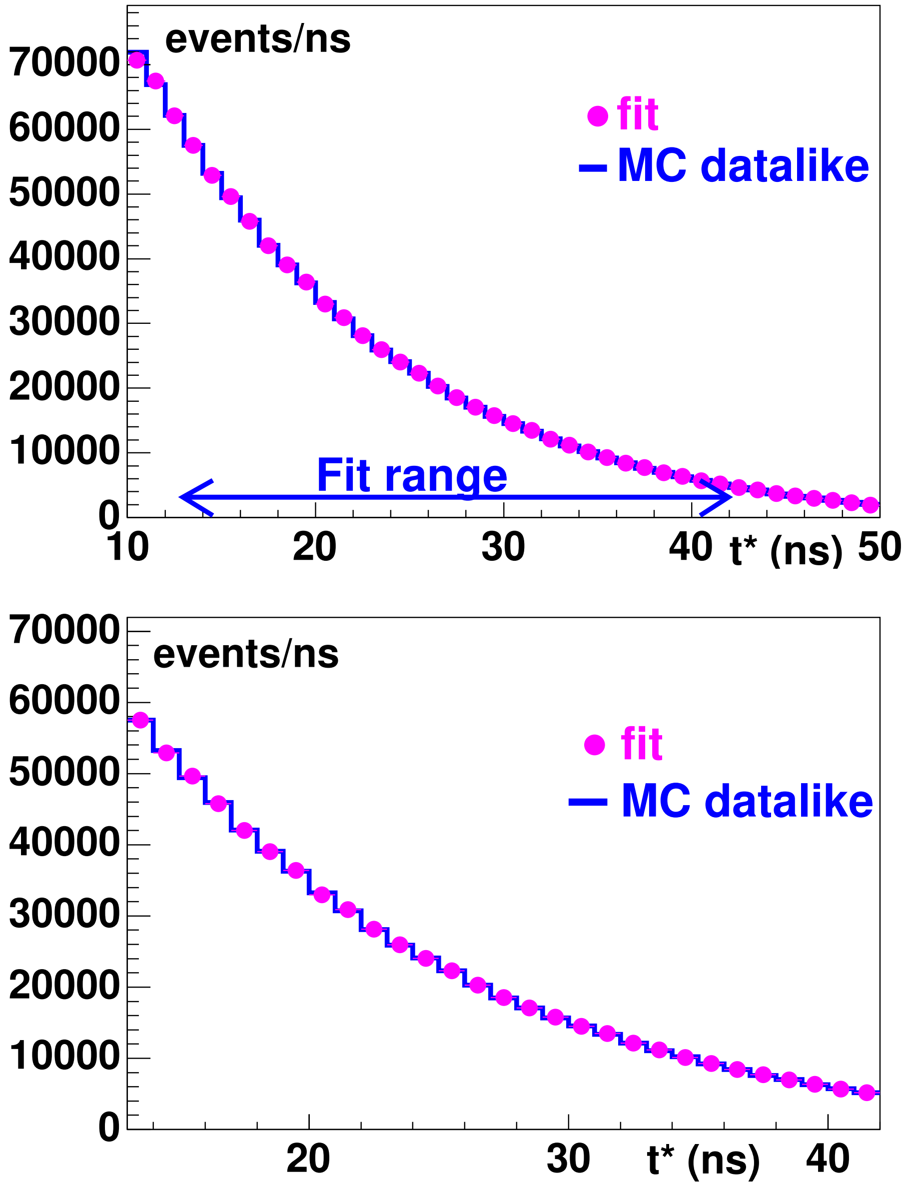

Figure 62: In the picture the fit to the K^+ proper time distribution is shown: in blue the MonteCarlo data-like distribution, in pink the *expected* histo distribution.

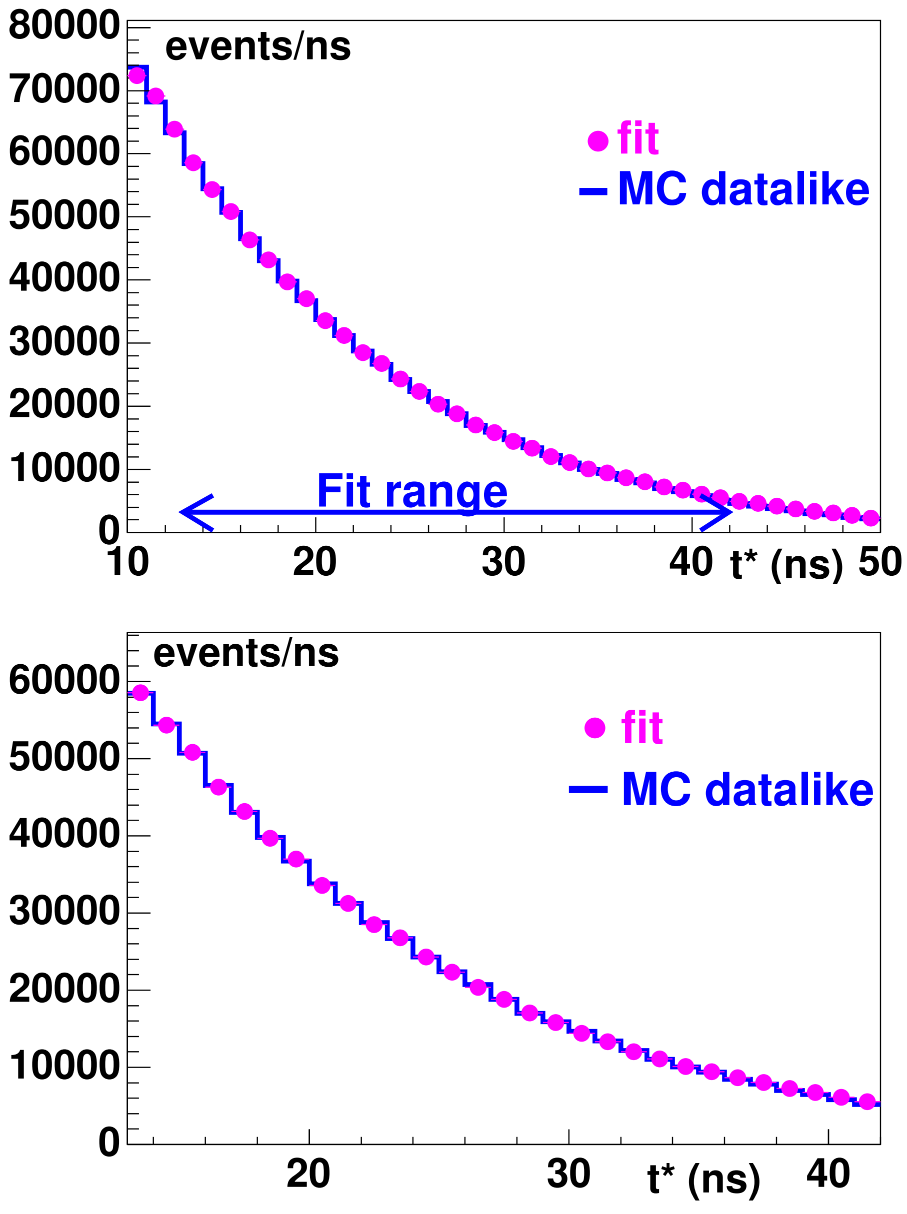

Figure 63: In the picture the fit to the K^- proper time distribution: is shown in blue the MonteCarlo data-like distribution, in pink the *expected* histo distribution.

Fitting with a constant the residuals and the normalized residuals, figures 64 and 65, we obtain values compatible with zero:

$$
\begin{aligned}
&const^{+}_{\mathrm{res}} = -15. \pm 28. && P_{\chi^2} = 99.\% && (101)\\
&const^{+}_{\mathrm{norm\ res}} = -0.06 \pm 0.19 && P_{\chi^2} = 99.\% && (102)\\
&const^{-}_{\mathrm{res}} = -37. \pm 39. && P_{\chi^2} = 77.\% && (103)\\
&const^{-}_{\mathrm{norm\ res}} = -0.08 \pm 0.19 && P_{\chi^2} = 73.\%. && (104)\\
& && && (105)
\end{aligned}
$$

Also for this method, looking at the MonteCarlo data-like results, we are confident about its application for the fit of the proper time distribution obtained on data. On data, concerning the K^+ lifetime we made the fit in the region between 13 and 42 ns and we obtained:

$$\tau^+ = (12.315 \pm 0.042)\ \mathrm{ns} \qquad \chi^2/\mathrm{ndf} = .98 \qquad \mathrm{P}_{\chi^2} = 49.\%. \tag{106}$$

Also for the K^- we fit in the range between 12 and 42 ns and we obtain as best value:

$$\tau^- = (12.360 \pm 0.043)\ \mathrm{ns} \qquad \chi^2/\mathrm{ndf} = 0.85 \qquad \mathrm{P}_{\chi^2} = 69.\%. \tag{107}$$

As shown in the figures 66 and 67 the agreement between data distribution and *expected* histo distribution is very good for both the charges.
For both the charges the distributions of residuals and of the normalized residuals is very good and compatible with a constant function equal to zero. Fitting the residual plots and the normalized residual plots with a constant the value obtained are in agreement with zero:

$$
\begin{aligned}
&const^{+}_{\mathrm{res}} = (0. \pm 7.) \times 10^{-7} && P_{\chi^2} = 49.\% && (108)\\
&const^{+}_{\mathrm{norm\ res}} = -0.07 \pm 0.18 && P_{\chi^2} = 50.\% && (109)\\
&const^{-}_{\mathrm{res}} = -19. \pm 32. && P_{\chi^2} = 70.\% && (110)\\
&const^{-}_{\mathrm{norm\ res}} = -0.06 \pm 0.12 && P_{\chi^2} = 69.\%. && (111)\\
& && && (112)
\end{aligned}
$$

The measures obtained for the different charges are in agreement with each other. Their weighted mean is:

$$\tau = (12.337 \pm 0.030)\ \mathrm{ns}. \tag{113}$$

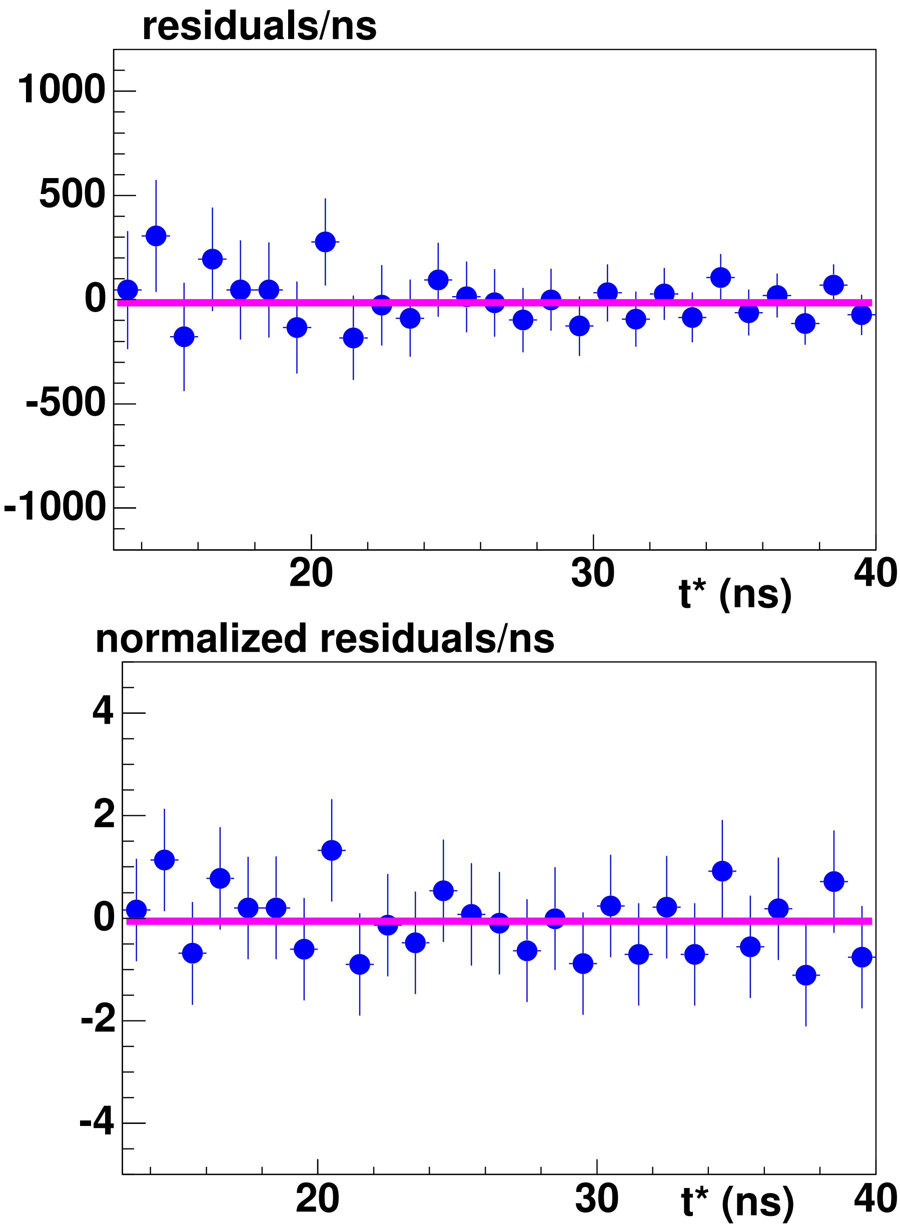

Figure 64: The K^+ residuals and the normalized residual plots, in the region between 13 and 40 ns, fitted with a constant are shown.

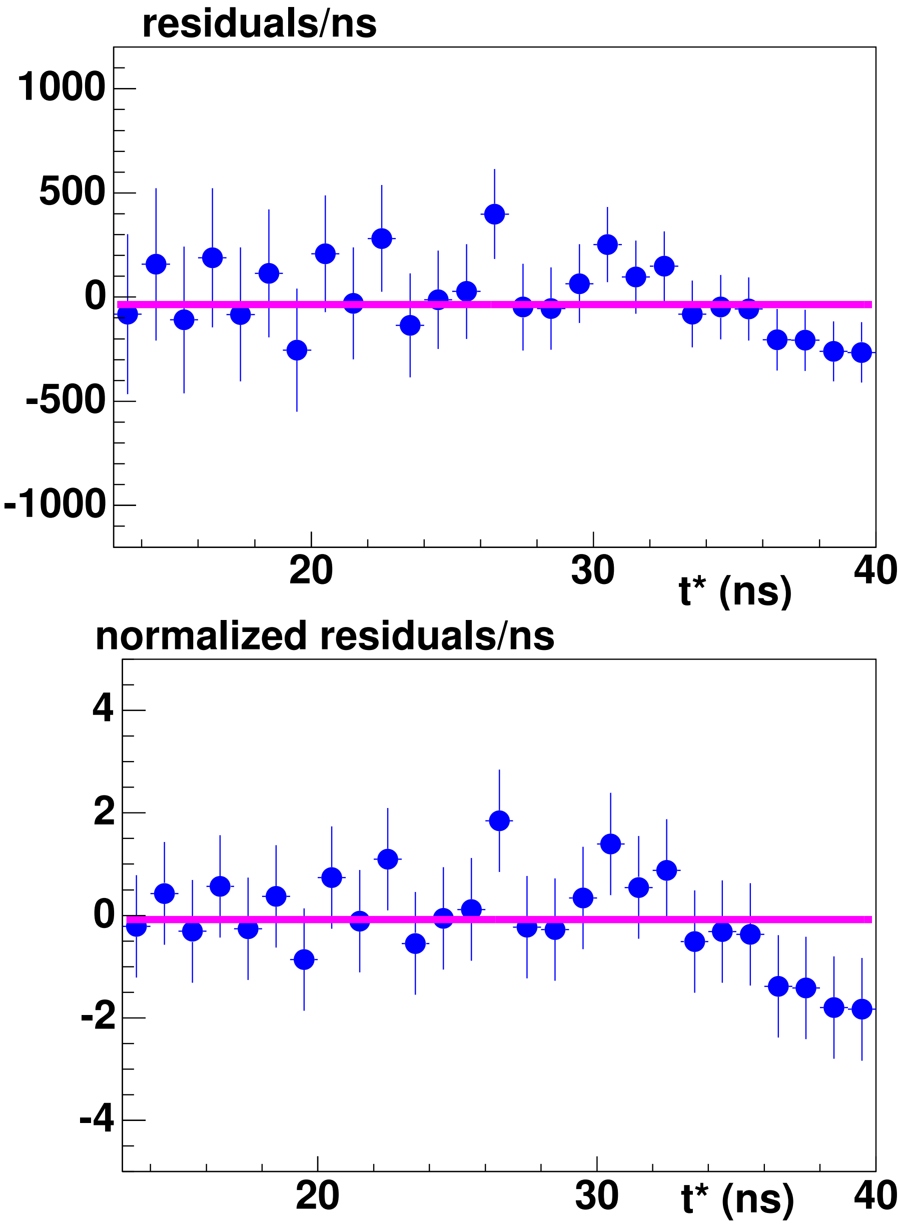

Figure 65: The K^- residuals and the normalized residuals, in the region between 13 and 40 ns, fitted with a constant are shown.

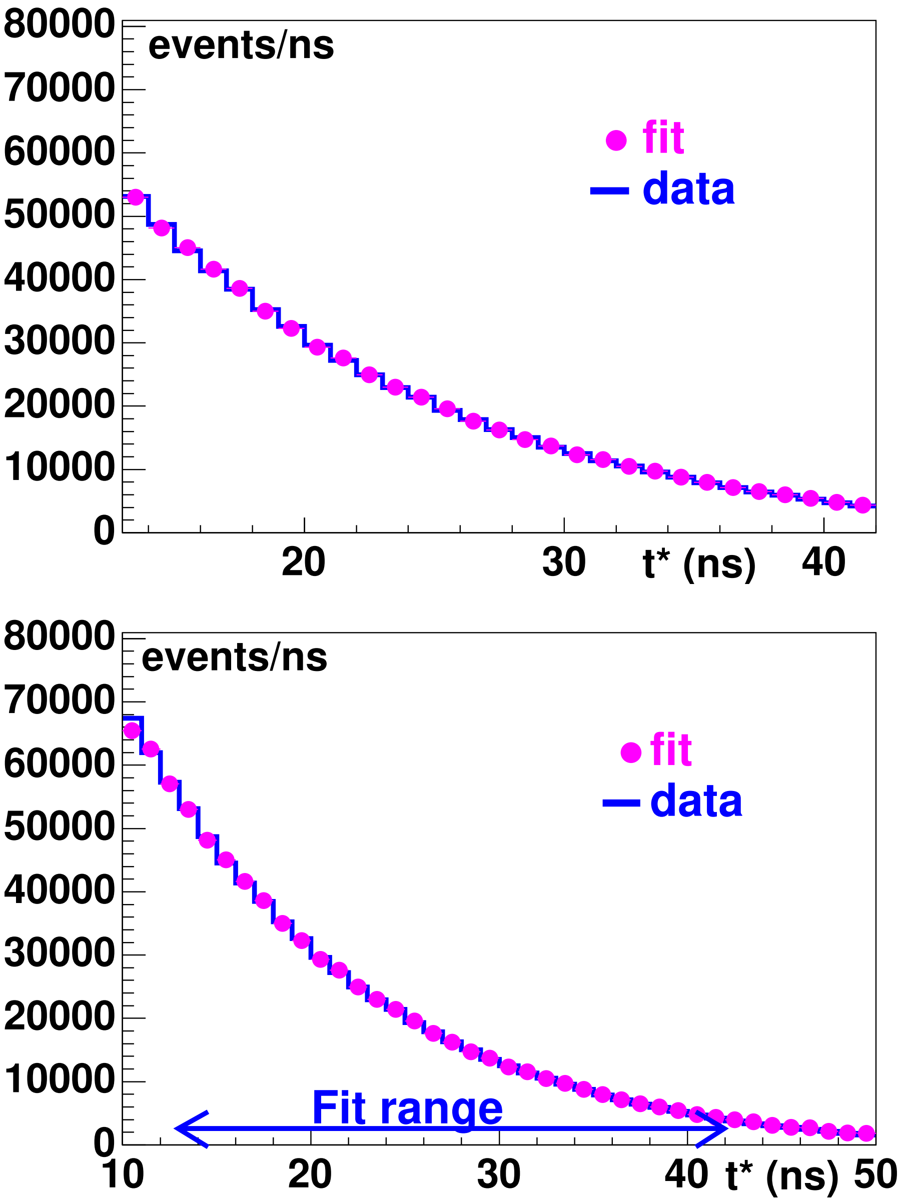

Figure 66: Fit to the K^+ proper time distribution: in blue the data distribution, in pink the *expected* histo distribution.

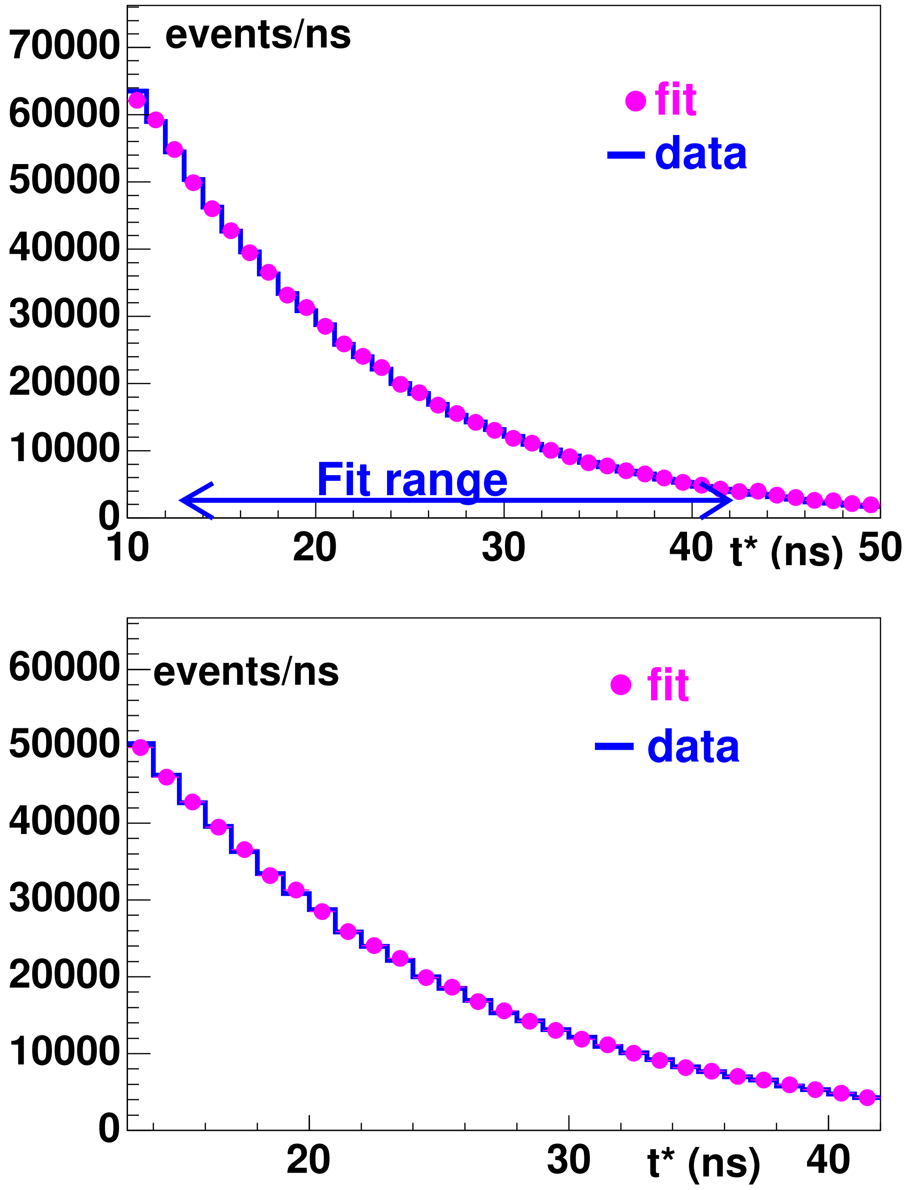

Figure 67: Fit to the K^- proper time distribution: in blue the data distribution, in pink the *expected* histo distribution.

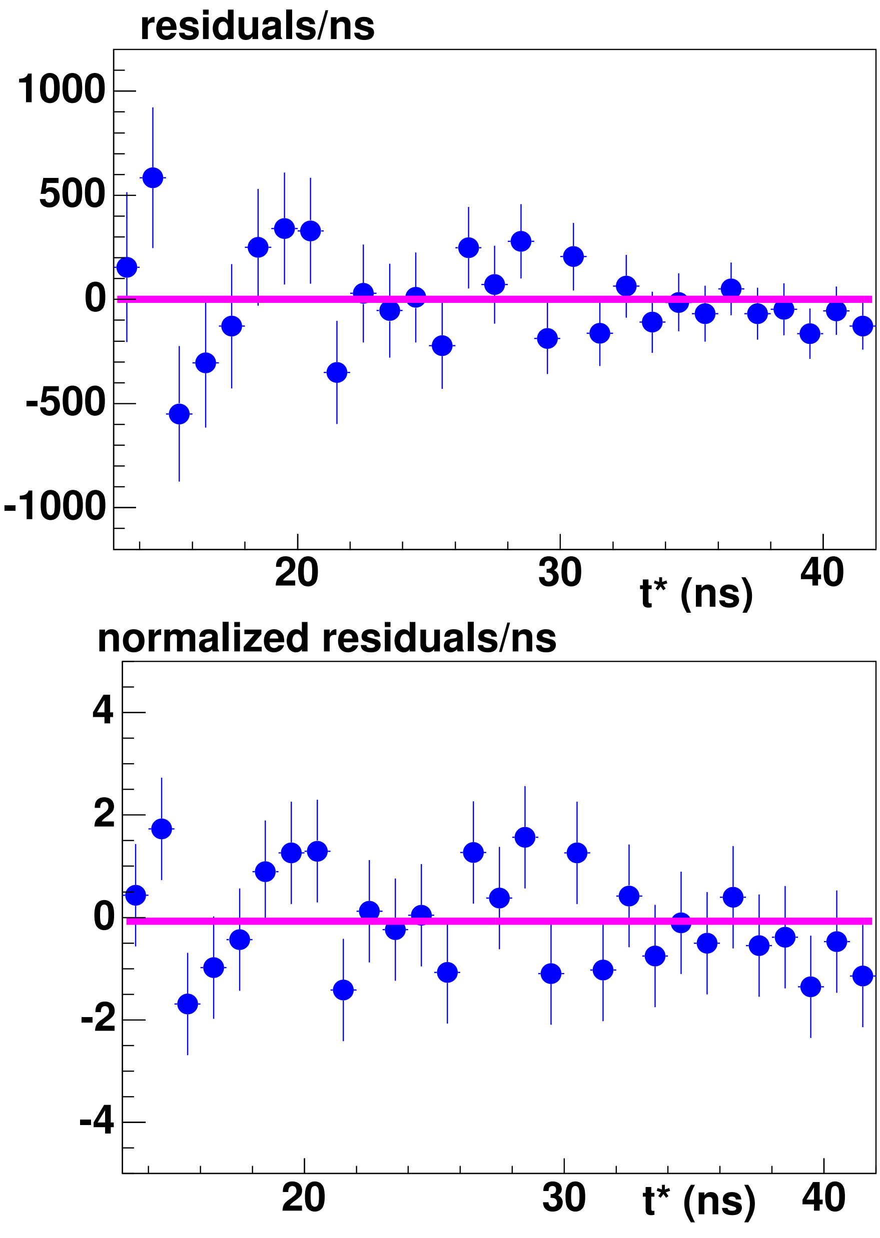

Figure 68: K^+ residuals (up) and the normalized residuals (down), in the region between 12 and 42 ns, fitted with a constant.

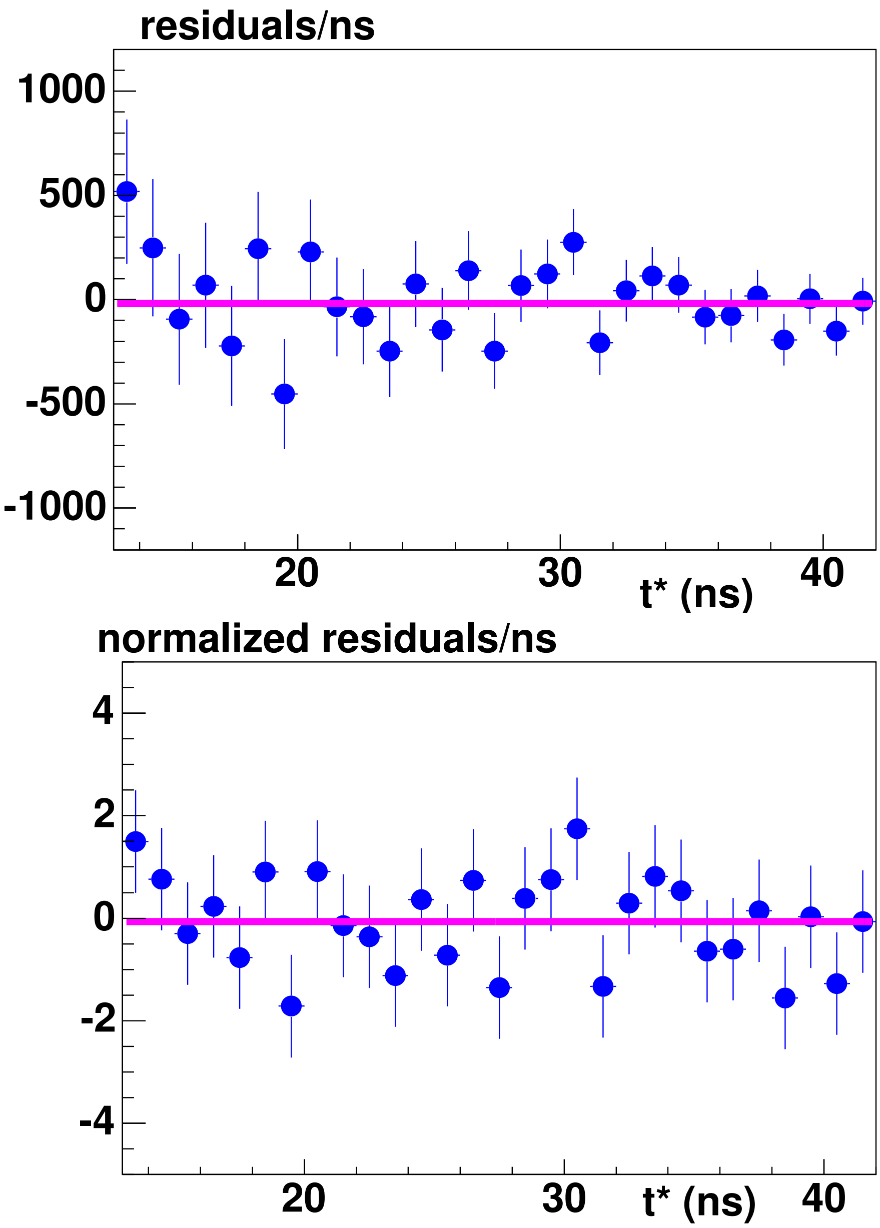

Figure 69: K^- residuals (up) and the normalized residuals (down), in the region between 12 and 42 ns, fitted with a constant.

9 Study of the systematics

For both the methods we used the same data sample for the evaluation of the reconstruction efficiency of the kaon decay vertex and for the evaluation of the proper time distribution. In order to determinate any possible correlation between the measurement of the efficiency and the proper time distribution we divided the data sample into two subsamples. For both these subsamples we evaluate the reconstruction efficiency of the kaon decay vertex and the proper time distribution.
We measured the charged kaon lifetime for the four possible combinations (1-1, 1-2, 2-1, 2-2) for the two different methods. Results do not change using the proper time distribution evaluated in the first (second) subsample and the efficiency evaluated in the same subsample or in the other.
We can say that no one correlation is introduced by the use of the same data sample for the evaluation of the reconstruction efficiency of the kaon decay vertex and for the evaluation of the proper time distribution.
In order to check the goodness of the equation 74, used for the evaluation of the statistical fluctuations of the *expected* histo, we developed a MonteCarlo toy. For each bin j we generate poissionian random numbers with mean given by:

$$N_j^{rnd} = \sum_{i=1}^{Nbins} s_{ji} \times \epsilon_i^{rnd} \times \epsilon_i^{corr\ rnd} \times N_i^{theo}, \tag{114}$$

where ϵ_i^{rnd} is a random number generated using a gaussian whose mean and sigma are the value of the reconstruction efficiency, ϵ_i, and its error, σ_{ϵ_i}, evaluated in the i-th bin respectively; $\epsilon_i^{corr\ rnd}$ is a random number generated using a gaussian whose mean and sigma are the value of the correction to the reconstruction efficiency, ϵ_i^{corr}, and its error, $\sigma_{\epsilon_i^{corr}}$, evaluated in the i-th bin respectively.
For each bin j the Root Mean Square of the random poissionian numbers generated with mean N_j^{rnd} are used as statistical fluctuations of the *expected* histo. The result of the fit using this formula for the error doesn't change.

9.1 Length measurement

We have studied the following sources of systematic uncertainties for the:

1. fit stability as a function of the range used;
2. fit stability as a function of the bin used for the proper time distribution;
3. fit stability as a function of the efficiency correction;
4. correction due to a not correct evaluation of the Beam Pipe and DC walls thicknesses;

5. fit stability as a function of the p_K^* cut.

A more detailed discussion of the systematics studiy follows.

9.1.1 Fit range

We fitted the distribution using various different ranges in the *golden* region between 15 and 35 ns. The maximum fluctuation of the results is about 10 ps, which we take as systematic uncertainty.

9.1.2 Binning

We made the fit also using a bin size of 500 and 250 ps (one half and one third of the nominal bin size respectively). The maximum fluctuation of the result is of the order of 10 ps for both the charges which we take as systematic uncertainty.

9.1.3 Efficiency correction

We made the fit also without the efficiency correction. The maximum fluctuation of the measure is of the order of 15 ps for both the charges. Therefore we conservatively estimate the systematic error given by the efficiency correction to be about 15 ps .

9.1.4 Beam Pipe and DC wall thicknesses

We evaluate the proper time distribution without taking into account the energy loss in the Beam Pipe and in the DC walls. The maximum fluctuation of the result is of the order of 100 ps for the Beam Pipe and 150 ps for the DC walls. But the uncertainty on the Beam Pipe and DC walls thicknesses is about 10%. Therefore we conservatively estimate the systematic error given by uncertainty on the Beam Pipe thickness to be about 10 ps and the one given by uncertainty and DC wall thickness to be about 15 ps.

9.1.5 P_K^* cut

We made the fit with different p_K^* cuts between 50 and 150 MeV/c. The maximum fluctuation of the measure is of the order of 15 ps for both the charges. Therefore we conservatively estimate the systematic error given by the efficiency correction to be about 15 ps .

9.2 Total systematic uncertainty

The total systematic uncertainty evaluated is of the order of 31 ps.

$$\tau = (12.364 \pm 0.031_{stat} \pm 0.031_{syst}) \text{ ns.} \tag{115}$$

Sources of systematic uncertainties	Systematic uncertainties (ps)
Fit range	$\pm$ 10
binning	$\pm$ 10
efficiency correction	$\pm$ 15
Beam Pipe thickness	$\pm$ 10
DC wall thickness	$\pm$ 15
P^*_K	$\pm$ 15

Table 2: Sources of systematic uncertainties evaluated.

9.3 Time measurement

We have studied the following sources of systematic uncertainties on the measured branching ratio:

1. fit stability as a function of the range used;
2. fit stability as a function of the bin used for the proper time distribution;
3. fit stability as a function of the efficiency correction;
4. correction due to a not correct evaluation of the Beam Pipe and DC walls thicknesses;
5. fit stability as a function of the efficiency cuts;
6. fit stability as a function of the T^0_ϕ;

A detailed discussion of the systematic studies follows.

9.3.1 Fit range

We evaluated the fit in the whole region between 13 and 42 ns. The maximum fluctuation of the measure is of the order of 10 ps for both the charges. Therefore we extimate the systematic error given by the range stability to be about 10 ps.

9.3.2 Binning

We made the fit also using a bin size of 2 ns (two times nominal bin size respectively). The maximum fluctuation of the result is of the order of 10 ps for both the charges which we take as systematic uncertainty.

9.3.3 Efficiency correction

We made the fit also without the efficiency correction. The maximum fluctuation of the measure is of the order of 10 ps for both the charges. Therefore we estimate the systematic error given by the efficiency correction to be about 10 ps.

9.3.4 Efficiency cuts

We made the fit applying different p^*_K cuts to the efficiency, between 50 and 150 MeV/c. The maximum fluctuation of the measure is of the order of 10 ps for both the charges. Therefore we conservatively estimate the systematic error given by the efficiency correction to be about 10 ps

9.3.5 Beam Pipe and DC wall thicknesses

We evaluate that the fluctuation of the measurement, if we assume an uncertainty of the order of 10% on the thicknesses of the Beam Pipe and DC walls, is negligible. This uncertainty is a construction parameter.

9.3.6 $\mathbf{T}^0_\phi$

Using the two different tag, $K \to \mu\nu$ and $K \to \pi\pi^0$, we estimate that fluctuation of the measurement, as a function of the T^0_ϕ is negligible.

9.4 Total systematic uncertainty

The total systematic uncertainties evaluated is of the order of 20 ps.

$$\tau = (12.337 \pm 0.030_{stat} \pm 0.020_{syst}) \text{ ns.} \tag{116}$$

Sources of systematic uncertainties	Systematic uncertainties(ps)
Fit range	± 10
binning	± 10
efficiency correction	± 10
Efficiency cuts	±10

Table 3: Sources of systematic uncertainties evaluated.

10 Correlation and weighted mean

In order to evaluate the weighted mean between the two methods we calculate the statistical correlation between the two methods. Therefore we divide the data sample into five subsamples. For each subsample, and for each method, we evaluate the proper time distribution and its efficiency.
Then we evaluate, for each subsample and for each method, the value of the charged kaon lifetime, see table 4. The correlation is given by:

subsample	length fit(ns)	time fit(ns)
1	12.368	12.307
2	12.393	12.312
3	12.389	12.362
4	12.351	12.301
5	12.330	12.326

Table 4: In the table the weighted mean for the different techniques and for the different subsamples are shown.

$$\rho = \frac{1}{N-1} \frac{\sum_{i=1}^{N} (\tau_l - \tau_l^i)(\tau_t - \tau_t^i)}{\sigma_l \sigma_t} \tag{117}$$

where N is the number of subsample, τ_l^i is the value of the lifetime for the first method evaluated on the i-th subsample, τ_l is the mean of the values of the lifetime for the first method evaluated on the different subsamples, τ_t^i is the value of the lifetime for the second method evaluated on the i-th subsample, τ_t is the mean of values of the lifetime for the second method evaluated on the different samples,σ_l and σ_t are the standard deviation of the measurements evaluated on the five subsample for the first and the second method respectively.
The value of the statistical correlation is:

$$\rho = 0.307\ . \tag{118}$$

The weighted mean between the two methods and its error is given by following equations:

$$\tau = \frac{(\sigma^2_{\mathrm{t\ tot}} - \rho\ \sigma_{\mathrm{t\ stat}} \sigma_{\mathrm{l\ stat}}) \times \tau_l + (\sigma^2_{\mathrm{l\ tot}} - \rho\ \sigma_{\mathrm{l\ stat}} \sigma_{\mathrm{t\ stat}}) \times \tau_t}{\sigma^2_{\mathrm{t\ tot}} + \sigma^2_{\mathrm{l\ tot}} - 2\rho\ \sigma_{\mathrm{t\ stat}} \sigma_{\mathrm{l\ stat}}} \tag{119}$$

$$\sigma_\tau = \sqrt{\frac{\sigma^2_{\mathrm{l\ tot}} \sigma^2_{\mathrm{t\ tot}} - \rho^2 \sigma^2_{\mathrm{l\ stat}} \sigma^2_{\mathrm{t\ stat}}}{\sigma^2_{\mathrm{l\ tot}} + \sigma^2_{\mathrm{t\ tot}} - 2\rho\ \sigma^2_{\mathrm{l\ stat}} \sigma^2_{\mathrm{t\ stat}}}} \tag{120}$$

where $\sigma_{\mathrm{l\ tot}}$ and $\sigma_{\mathrm{t\ tot}}$ are the total errors on the length and the time measurement $\sigma_{\mathrm{l\ stat}}$ and $\sigma_{\mathrm{t\ stat}}$ are the statistical errors on the length and the time measurement, respectively. The corresponding result is:

$$\tau = (12.347 \pm 0.030)\ \mathrm{ns} \tag{121}$$

11 CPT test

The comparison of K^+ and K^- lifetimes is a test of CPT invariance which guarantees the equality of the decay lifetimes for particle and antiparticle.

For the positive kaons the average of the two methods, taking into account the correlation of the statistical errors, and the systematic errors is:

$$\tau^+ = (12.325 \pm 0.038) \text{ ns} \tag{122}$$

and for the negative kaons is:

$$\tau^- = (12.374 \pm 0.040) \text{ ns} \tag{123}$$

From these we obtain:

$$\tau^- - \tau^+ = (49 \pm 50) \text{ ps} \tag{124}$$

$$\frac{\tau^-}{\tau^+} = 1.004 \pm 0.004 \tag{125}$$

The result agrees well with CPT invariance at the 4 per mil level.

References

[1] W.-M. Yao *et al.* (Particle Data Group Collaboration) *Journal of Physics* **G 33, 1** 2006 W. M. Yao *et al.*, J. Phys. G. 33,1 (2006).

[2] F. Lobkowicz *et al.* 1970. Phys.Rev.185:1676-1687,1969.

[3] V. L. Fitch *et al.* Phys. Rev. 140, B1088 - B1091 1965

[4] R.J. Ott *et al.*. 1971. Phys.Rev. D3:52-56,1971.

[5] V.P. Koptev *et al.* 1995. JETP Lett.62:877-881,1995, Pisma Zh.Eksp.Teor.Fiz.61:865-868,1995.

[6] P. Franzini, *Remarks on decay rates and partial decay rates measurements.*, KLOE Memo **299** (2005). http://www.lnf.infn.it/kloe/kloedef.html

[7] M. Adinolfi *et al.*, [KLOE Collaboration] Nucl. Instrum. Meth. A 488, 51 (2002) Y

[8] M. Adinolfi *et al.*, [KLOE Collaboration] Nucl. Instrum. Meth. A 482, 364 (2002)

[9] F. Ambrosino *et al.*, [KLOE Collaboration] Nucl. Instrum. Meth A 534, 403 (2004).

[10] M. Adinolfi *et al.*, [KLOE Collaboration] Nucl. Instrum. Meth. A 492, 134 (2002).

[11] F. Ambrosino, E. De Lucia, P. de Simone, P. Massarotti and V. Patera *Measurement of the reconstruction efficiency of the charged kaon decays.*, KLOE Memo **320** (2005). http://www.lnf.infn.it/kloe/kloedef.html

List of Figures

List of Tables